Aalto University

MASTER THESIS

Hydrothermal treatment of Vinasse

Author: Maria Costa

Supervisor: Mika Järvinen
Instructors: Cataldo De Blasio
and Mohamed Magdeldin

December 7, 2017

AALTO UNIVERSITY
SCHOOL OF ENGINEERING

ABSTRACT OF THE
MASTER'S THESIS

Author: Maria Costa

Title: Hydrothermal treatment of vinasse

Date: November 2017 Language: English

School of engineering (ENG), Department of Mechanical Engineering

Professorship: Thermodynamics and Combustion Technology lab

Supervisor: Prof. Mika Järvinen

Advisors: M.Sc. Mohamed Magdeldin, D.Sc. Cataldo De Blasio

Vinasse is a by-product obtained from the distillation of ethanol from molasses from sugarcane. Due to its characteristics, such as high organic and moisture content, it is a potential source for fuel production. The thesis presents a techno-economic assessment for supercritical water gasification of the vinasse for the production of liquid fuels. The main goals of this work are the process modeling of a complete plant layout on Aspen Plus for supercritical water gasification of vinasse and the evaluation of the economic feasibility and profitability of the process compared to other bio-fuels plants. The process includes four main process blocks: supercritical water gasification, gas cleaning, Fischer-Tropsch process and Product separation. Different scenarios were considered to optimize the heat exchanger network of the plant. The feasibility of the process was then evaluated in terms of thermal efficiency and minimum selling price of the products. The plant recorded a minimum selling price of 360 euro per MWh with a carbon recovery of ~14% in the product and a thermal efficiency of ~21%. What emerges from the study is that the process is energetically self sufficient, although it is not economically feasible due to the high production costs.

Keywords: Vinasse, Supercritical Water Gasification, Fischer-Tropsch, Fractionation, Techno-economic assessment

Acknowledgements

I would first like to thank my thesis supervisor Prof. Mika Jarvinen of the School of Engineering at Aalto University for giving me the chance of fulfilling this experience. The environment in which I had the chance to work in was friendly and stimulating. Secondly, I would like to thank my instructor D.Sc. Cataldo De Blasio for supporting me and giving me the chance to visit the Åbo Akademi laboratories for better understanding my research field.

A special thanks goes to my advisor M.Sc. Mohamed Magdeldin, who was always available and supportive. He was always willing to give me advices and help whenever I ran into a trouble spot or had a question about my research or writing and he steered me in the right the direction whenever he thought I needed it.

Finally I would like to thank the team of the building K4 for their kindness, availability and the nice moments we shared during coffe breaks.

Contents

List of Figures

List of Tables

List of Abbreviations

SCWG	**S**upercritical **W**ater **G**asification
HTL	**H**ydrothermal **L**iquefaction
AGR	**A**cid **G**as **R**emoval
PSA	**P**ressure **S**wing **A**dsorption
RWGS	**R**everse **W**ater **G**as **S**hift
FT	**F**ischer **T**ropsch
FCC	**F**luid **C**atalytic **C**racking
TBP	**T**emperature **B**oiling **P**oint
PEC	**P**urchased **E**quipment **C**ost
TCI	**T**otal **C**apital **I**nvestment
MSP	**M**inimum **S**elling **P**rice
NPV	**N**et **P**resent **V**alue

Chapter 1

Introduction

1.1 Research background

1.1.1 Energy outlook

Nowadays, fossil fuels are the world's primary energy source. Although they have fueled the global economic development over the past century, fossil fuels are a limited source and they also can irreparably damage the environment. Fortunately, sustainable solutions, such as renewable energy, exist. In recent years, especially from 2010, renewable sources consumption has risen, although the largest growth was shown by natural gas, as shown in figure 1.1.

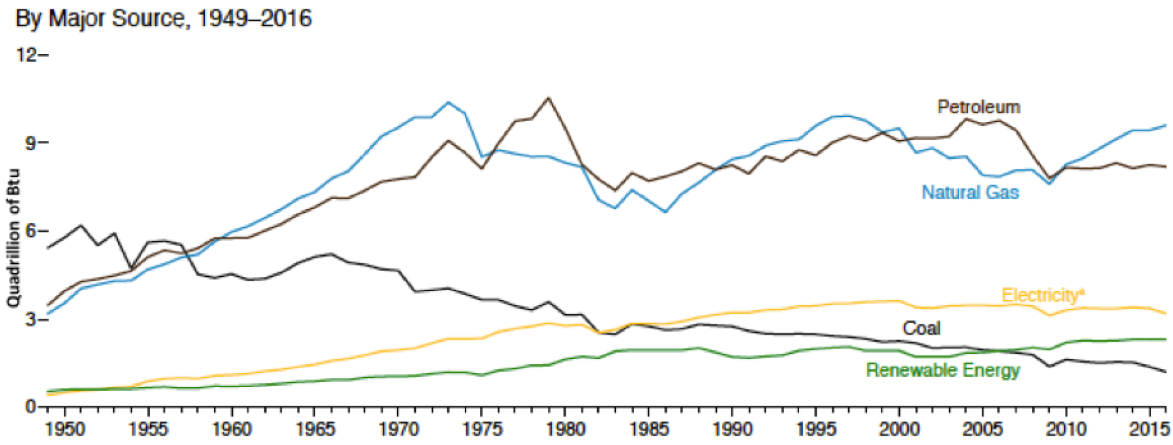

FIGURE 1.1: Energy consumed in the industrial sector [1]

If we focus on the EU members, we can say that the energy produced from renewable sources is higher in the Nordic countries and the highest trends are shown from Sweden and Finland. Concerning other countries, the targets expected for 2020 are still far to reach as shown in figure 1.2.

In the Monthly energy review of July 2017 (U.S. Energy information Administration "Monthly Energy Review" [1]) it is reported the currently quadrillion of Btu consumed in March 2017 for each source (figure 1.3). It is possible to notice that the renewable energy consumption in still largely lower that the petroleum one [1].

The Greenhouse gases (GHG) emitted by the treatment of fossil fuel contribute to climate change. With the use of renewable sources it is possible not only to have a sustainable feedstock, but the emission of pollutants can be largely reduced.

For these reasons, EU countries have agreed new targets and objectives with the aim of achieving a energy system with lower emissions. Thus, the European commission set new targets for 2030: a decrease of greenhouse gas emission of 40%

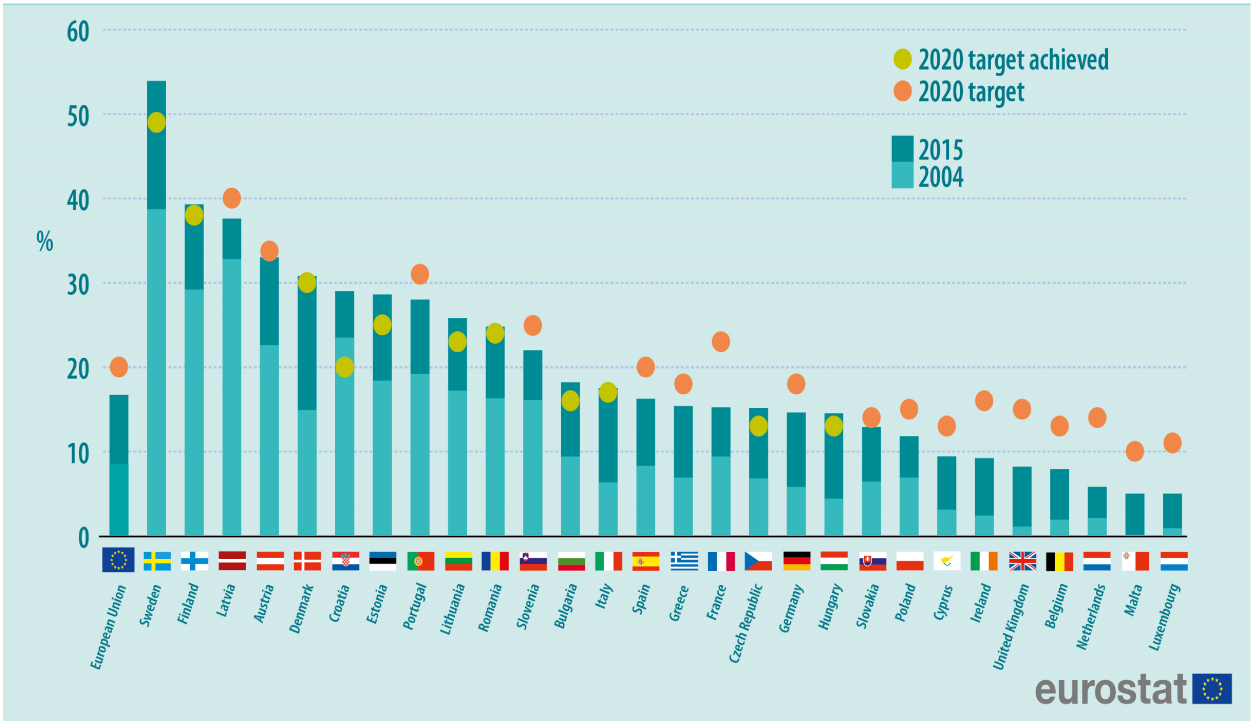

FIGURE 1.2: Share of energy from renewable sources in the EU member states [2]

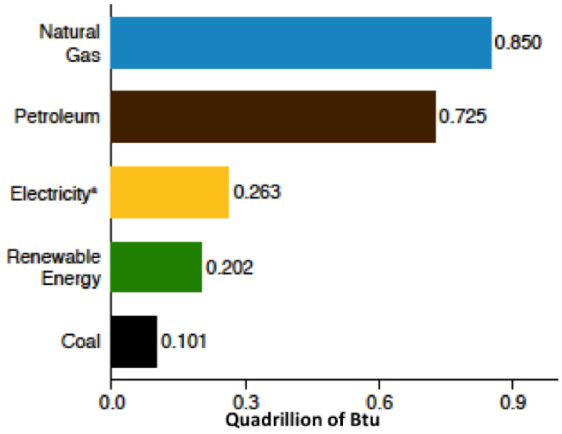

FIGURE 1.3: Energy consumed in the industrial sector for each type of source [1]

compared to the levels in 1990 and also a share of renewable energy consumption at least 27% [3].

The term *biomass* is used to indicate any organic matter, derived from plants or animals, that can be converted into biofuels after treatment, and is therefore regarded as an energy source.

Biomass chemical compositions varies in terms of moisture, ash and organic content based on the feedstock source [4]. It is mostly composed of carbon, hydrogen and oxygen with a minor percentage of other elements such as nitrogen, phosphor, potassium and sulfur, which vary with the origin of the biomass (Ultimate Analysis). From a chemical point of view cellulose, hemicellulose and lignin are found to be the major components of biomass [5].

Cellulose is a polysaccharide with the molecular formula $(C_6H_{10}O_5)_n$ which derives from the condensation of glucose unit.

Hemicellulose is a matrix of polysaccharides, such as arabinoxylans, that exist with cellulose in the plant cell walls. Combined with cellulose, it provides structural strength to the cell wall. Lignin is a complex polymer of aromatic alcohols, insoluble in water and alcohol. Its composition varies from species to species.

Depending on the composition of these compounds and on the extractives, which happens to be one of the minor compound, the elemental analysis varies.

If properly treated, the biomass can be converted into various biofuels (e.g. syngas, bio-oil, bioethanol). Table 1.1 shows current technologies used to obtain energy from biomass and their typical conditions and characteristics.

TABLE 1.1: Current technologies for biomass treating [6]

Process	Type of biomass	Conditions	Features
Combustion	Dry biomass	150-800°C Atmospheric pressure With air	Low energy efficiency (10-30%) Pollutant emissions
Pyrolysis	Dry biomass	350-550°C 10-50 bar Absence of air	Produced bio-oil and gases
Liquefaction	Wet biomass	250-450°C 50-200 bar Absence of air	Transforming biomass to liquid fuel biocrude Without a necessary drying process
Conventional gasification	Dry biomass	800-900°C Atmospheric pressure Limited oxygen	Partial oxidation reaction A gaseous mixture, mainly H_2, CO and CO_2
Anaerobic digestion	Wet biomass	Bacteria, in absence of oxygen, degrade the organic matter	Very slow process A relatively low efficiency It produces methane only, no hydrogen
SCWG	Wet biomass	300-650°C >221 bar Limited oxygen (oxygen coefficient 0-0.25)	Higher gas yields Hydrogen more than 50% on a mole basis, CO_2 about 33%, and others including CH_4 and low CO Low level of residual chars and tars

Traditional gasification technologies have encountered several difficulties, for instance a low quality gas due to higher presence of impurities such as char and tar [6], and the low efficiency at high moisture content. It was demonstrated that through anaerobic digestion or hydrothermal gasification, efficiency does not decrease with moisture content [6].

1.1.2 Vinasse production: the bioethanol plant

Sugarcane production is mostly based on the world demand for sugar, in fact almost the 80% of sugar globally produced comes from sugarcane [7]. The sugar extraction and refining is a process that leads to the recovery of molasses as a byproduct. It is a circular path of washing and heating the cane (and beets also) with hot water. It has a great potential for the production of ethanol through fermentation and distillation. The residue obtained by the fermentation is called vinasse, and it is a feedstock that has potential for fuel production [5].

As illustrated in figure 1.4, vinasse can be produced both from molasses and from the juice and depending on the production process, its properties and characteristics vary [8].

The processing steps in vinasse production could be summarized as [9]:

- Washing and cutting
  The sugar cane stalks are at first subjected to hot water sprays to remove dirt

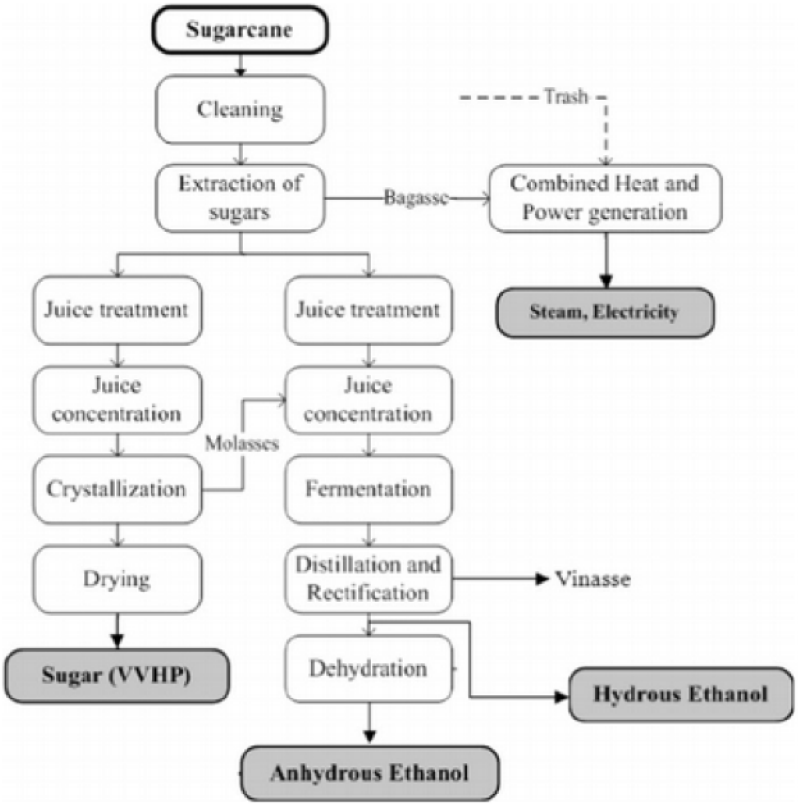

FIGURE 1.4: Vinasse production [8]

and impurities. Then, they are passed under rotating knife blades to reduce the stalks in short pieces.

- Extracting the sugar juice
  Extraction can be realized in two possible ways: diffusion or milling. By the diffusion method, the cut stalks are dissolved in hot water or lime juice. In the milling process, the stalks are passed under several successive heavy rollers, which squeeze the juice out of the cane pulps. Water is sprayed throughout the process to facilitate the dissolving of the juice.

- Clarifying the juice
  The extracted juice is clarified by adding milk of lime and carbon dioxide.

- Evaporating and concentrating the syrup
  The juice is pumped into an evaporator that allows the evaporation of the water present in the juice. The syrup obtained is concentrated through several stages of vacuum boiling at low temperature. Eventually, the sugar crystallizes out of the syrup, creating a substance that is centrifuged to further separate the raw sugar crystals from the syrup. The remaining syrup is called molasses.

The molasses can be fed to a bio-ethanol plant where it is at first diluted with water and then is fed to the fermentation chamber where the fermentation process lasts from 30 to 70 hours based on temperature, yeast and sugar concentration [8]. After that, the process is fed to a distillation still where solid and slurry (the vinasse) is separated leaving a solution of ethanol and water. This solution is then fed to a distillation column which separates the aldehydes on the top, an ethanol mixture from the middle and a water stream at the bottom [8].

Vinasse from molasses generally presents higher values of COD (chemical oxygen demand) and BOD (biochemical oxygen demand) than vinasse from sugarcane juice. This means that the first one has a higher organic content, therefore his potential as fuel is higher [8].

1.1.3 Vinasse characteristics

The word Vinasse comes from the Latin word vinacaeus, and originally it meant wine yeast. It is a residue obtained from alcohol distillation of fermented molasses and if properly treated it can be a source of energy, because it can be converted into a valuable biofuel. It has a light black-reddish color when obtained from sugarcane molasses and it appears as a very viscous liquid. It contains between 50 and 100 g/L of suspended solids [10]. Generally, its pH ranges between 3,5 and 5 and it has a high chemical oxygen demand (COD) [11]. Its density has a value of 1051 kg/m^3 at 20°C [12]. It is a mixture of water, organic and inorganic compounds, and its composition varies because of the different raw materials and different plants used for the ethanol production.

Vinasse is often used for irrigation due to its high organic content, although it needs to be treated before due to the presence of phytotoxic, antibacterial and recalcitrant compounds such as phenols, polyphenols and heavy metals, which cause negative effects on microorganisms and plants [11]. Vinasse is also used in on-site combustion.

Its high moisture content make vinasse a promising feedstock for hydrothermal treatments. In this study the Supercritical Water Gasification (SCWG) of Vinasse will be evaluated. In spite of its large potential, the current studies made on the SCWG of vinasse do not lead to high energy and economic efficiencies, therefore more studies are needed [13].

1.1.4 An overview on Hydrothermal treatments of biomass

The hydrothermal treatment is defined as "reactions occurring under the conditions of high temperature and high pressure in aqueous solutions in a closed system"[14], therefore a pre-drying step is not needed. Those include supercritical and subcritical treatments depending on the conditions of temperature and pressure.

When the process conditions are below the critical point of water (374°C and 22,1 MPa) Hydrothermal Liquefaction is a used to produce bio crude. The reaction is carried out at a temperature that ranges between 280°C and 370°C and a pressure up to 200 bar. Under this conditions organic compounds have high solubility and thus are miscible. The process is essentially pyrolysis in hot water but it does not require a catalyst and the product obtained is a bio-crude. As well as Pyrolysis, the HTL is the thermo-chemical decomposition of organic matter, but the working conditions are different. In the pyrolysis process the feedstock has to be dry (moisture content below 10%), it is treated at moderate temperature (between 350 and 550°C) and atmospheric pressure; on the contrary, HTL is performed in the presence of water, in fact it can convert biomass with high moisture content, at lower temperature and higher pressure[15]. In the HTL process the feedstock is made of wet biomass and water (which needs to be added as auxiliary water in order to reduce the solid content) and the energy consumption in feedstock pre-treatment is limited compared to technologies in which biomass drying is required (pyrolysis). The low energy consumption is due to the possibility to recover the heat when the process is in liquid

form, however in drying, the water is evaporated and the heat is dissipated to the atmosphere.

The product obtained, the bio crude, vary its chemical composition based on the HTL reaction conditions and also on the characteristics of the feedstock.

When the process condition are near and beyond the critical point of water ($374°$C and 22,1 MPa), biomass can be gasified with Supercritical water (SCWG). As a result, the organic constituents of biomass decompose into synthetic gas.

At supercritical conditions the liquid water loses its polarity and its non-polar nature allows a reasonably easy extraction of inorganic or polar constituents. Water under these conditions has high reactivity, and this makes it a good medium to improve the reaction rate. Reaction times are faster compared to other processes such as anaerobic digestion and as a result an optimal conversion of biomass can be achieved [16]. At Lower temperature (from 370 to $550°$C) the tests can be taken both in catalytic and non-catalytic environments; the primary product are water soluble organics when no catalyst is used, while it is observed the release of a carbon rich syngas when a metallic or alkali based syngas is used [16]. At higher temperature (beyond $550°$C) the mainly product is a hydrogen rich syngas due to the endothermic reaction of H_2 generation. According to Le-chatelier's principle when a change in temperature occurs, the system will no longer remain at equilibrium: the reaction will change the direction in order to restore the equilibrium. Effect of change in temperature is related to the nature of reaction whether it is an endothermic reaction or an exothermic reaction [17], consequently along with the hydrogen other compounds are formed.

Through SCWG the biomass is converted into multiple gaseous product such as CO_2, CO, H_2 and CH_4. If the feedstock contains a large percentage of sulfur, the product contains H_2S, so it is necessary to include an acid gas removal step [16].

The syngas, can be produced from the material that contain carbon, so from a great variety of feedstock for example biomass, plastics and coal. The SCWG of biomass is a complex process, but the overall conversion for hydrogen production can be simplified as:

$$CH_xO_y + (2-y)H_2O \leftrightarrow CO_2 + (2 - y + \frac{x}{2})H_2 \tag{1.1}$$

Where x and y indicated the $\frac{H}{C}$ and $\frac{O}{C}$ ratios in the feedstock [18]. Along with this reaction, some others can occur: steam reforming (1.2), water gas shift (1.3) and methanation (1.4) [18].

$$CH_xO_y + (1-y)H_2O \leftrightarrow CO + (1 - y + \frac{x}{2})H_2 \tag{1.2}$$

$$CO + H_2O \leftrightarrow CO_2 + H_2 \tag{1.3}$$

$$CO + 3H_2 \leftrightarrow CH_4 + H_2O \tag{1.4}$$

The methanation is an exothermic reaction while the H_2 formation is endothermic; this is why it is possible to obtain a hydrogen rich syngas at higher temperature [18]. Differently from the thermal gasification, with the supercritical water gasification the syngas has a high content of CO_2. This is caused by both the oxygen present in the biomass and the one in the auxiliary water that allows oxidation.

1.2 Objectives and aim of the thesis

This work focuses on the process design, simulation and technoeconomic evaluation of the supercritical water gasification (SCWG) of vinasse for the production of valuable transportation liquid fuels.

The main goals are:

1. Process modelling of a complete plant layout on Aspen Plus for SCWG of vinasse
2. Evaluation of the economic feasibility and profitability of the process compared to other bio-fuels plants.

1.3 Methods

The complete process layout will be simulated through the commercial software Aspen Plus®V8.8 [19]. The first calculations of solvents and reactants mass flows where evaluated on Microsoft Office Excel and then implemented on Aspen for the model confirmation.

The calculations and the choices made while building the model are illustrated in detail in the chapter 3. Some of the physical parameters cannot be modeled on the software used, so they will be assumed based on the literature data, for instance the reactors working conditions when a catalyst is considered. The scenario was scrutinized with the pinch analysis method to define the auxiliary utility demand and evaluate the overall thermal performance (see section 3.3). Finally, the Techno-Economic Assessment (TEA) establishes the commercial potential of the plant by determining the minimum selling price (MSP) and the net present value (NPV) relative to current commercial and market conditions (see section 3.4).

Chapter 2

Literature review

2.1 Vinasse composition

Vinasse has a high moisture content which ranges between 40% and 50%. The solids include ashes, proteins and carbohydrate. The major compounds found in the Vinasse are Glycerol, Acetic acid and Lactic acid [20]. Akram et al. [21] analyzed sugarcane vinasse behavior during combustion in a fluidized bed combustor. For the study they used a vinasse with a moisture content higher than 50% (table 2.1) and a low Calorific Value (CV) thus they showed the impossibility of combustion without the support of a fuel having a high CV (coal was utilized in the study).

TABLE 2.1: Proximate and ultimate analysis for the vinasse used by Akram et al. [21]

	Coal	Vinasse
Proximate analysis		
Moisture (%)	5.6	58
Ash (%)	4.9	9.7
Volatiles (%)	34.2	32.3
Fixed carbon (%)	55.3	-
Ultimate analysis		
Carbon (%)	74.4	17.3
Hydrogen (%)	4.06	2.11
Oxygen (%)	6.97	8.73
Nitrogen (%)	1.62	2.1
Sulphur (%)	2.01	2.1

One of the possible treatments for vinasse is gasification. It has been widely investigated because of its potential of providing higher efficiency cycles. Wide ranges of biomasses and waste products have been studied as potential fuels [22]. Dirbeba et al. studied the gasification of sugarcane vinasse in CO_2 and the release of ash matters in CO_2 and N_2 atmospheres. As a result, they obtained an ash content on a dry fuel basis of 34.1 %wt on to 67.4%wt dry solids diluted samples of dried vinasse [22]. As said in the previous chapter, one of the uses of vinasse is its combustion on-site. Cortez et al. [23] investigated and developed the basic technology of on-site disposal of vinasse by combustion and they evaluated its heating value, composition, and flame characteristics through combustion tests. They tested the characteristics of the vinasse obtained from the Shepherd Oil Distillery, which has the ultimate analysis reported in table 2.2. In conclusion, even at lowered moisture content the vinasse

combustion remains challenging and not a favorable process due to its low calorific value.

TABLE 2.2: Vinasse composition from Shepherd Oil Distillery on dry basis [23]

C	%	39.72
H	%	8.60
O	%	n.a.
S	%	0.12
N	%	1.65
Ash	%	18.95

2.2 Properties of water: comparison between subcritical and supercritical conditions

A fluid is considered to be in supercritical conditions when the temperature and the pressure of the system are above its critical point. The critical point of water is found at 374°C and 22.1 MPa (shown in figure 2.1 where the water phase diagram is represented). Below that the fluid is considered to be in subcritical conditions. When a fluid is upgraded to supercritical conditions, its properties show important changes and the physical and transport properties are between those corresponding to the gas and the liquid state. The main advantage of reaching supercritical conditions is that the fluid has an optimal heat transfer and also an ideal mass transfer. [24].

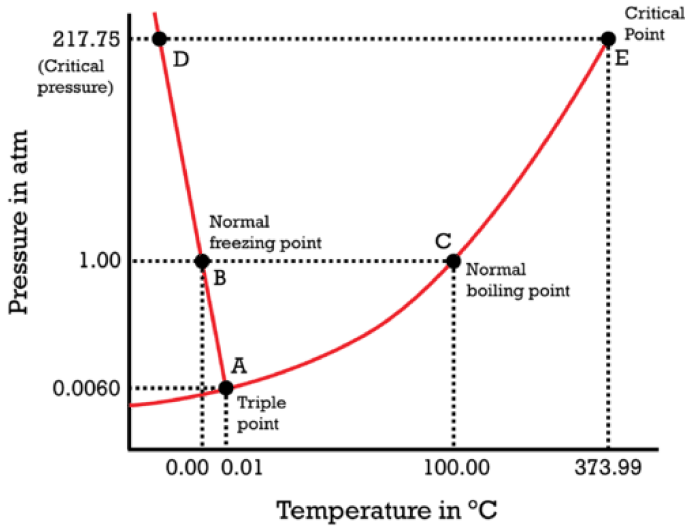

FIGURE 2.1: Water phase diagram [25]

One of the physical properties that can be evaluated is the density which in supercritical conditions is greater than the water vapor. During the transition, it decreases in a similar way as it happens during transition of phase in subcritical conditions, with a smoother reduction as pressure increase above critical point, as shown in figure 2.2. The SCW viscosity coefficient is similar and its diffusion coefficient lies between that of liquid and gas phases [24].

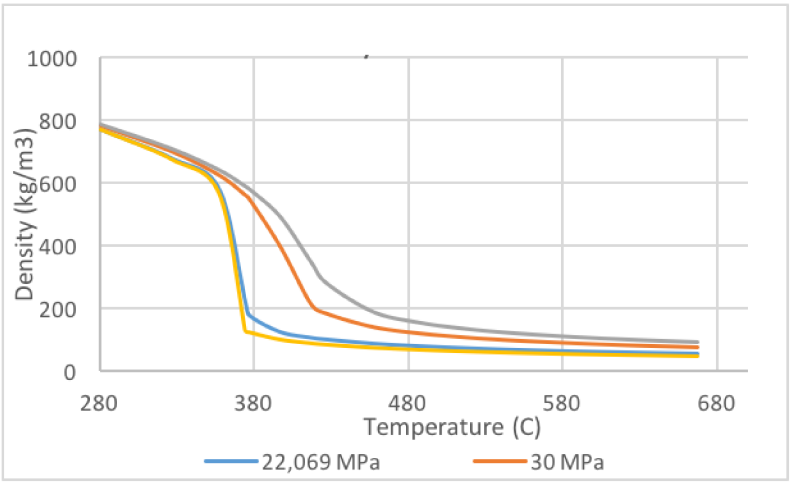

FIGURE 2.2: variation of water density with temperature (diagram realized on excel based on the value of water density taken from the NIST database [26])

When changing the physical conditions, water has different and often anomalous properties, which is due to changes in the hydrogen bonding [27]. As an example, when increasing the temperature, the dielectric constant (ϵ) of water decreases from 80 at standard conditions, to 6 at critical conditions as a result of a decreased effectiveness of hydrogen bonds. Above the supercritical point, the hydrogen bonds break down changing the water properties, which becomes less polar and it behaves more like an organic solvent [27]. The most interesting property of SCW is its low polarity; its high miscibility with gases as well as many organic compounds makes it a great solvent for reactions with organic slurries. The dielectric constant gives a measure of water polarity, as illustrated in figure 2.3. [27]

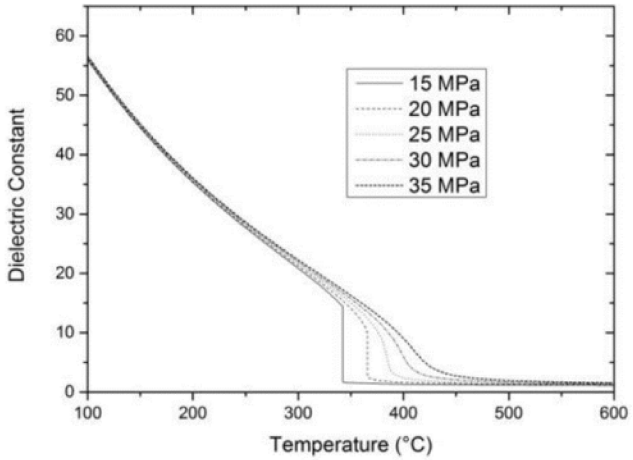

FIGURE 2.3: variation of dielectric constant with temperature [27]

Above 300°C, water starts to behave as a near-critical liquid so the physical properties start to change significantly with the pressure. When the water is heated above 100°C the ionic products increase due to a decrease of its dielectric constant, this indicates that water can act as an acid or a base catalyst [27]. As the temperature raises, the dissociation of water increases into H_3O^+ and OH^- ions. In figure 2.4 is shown how the ionic product changes with temperature. The process is reversible and sufficiently rapid to be considered as an equilibrium reaction. The ionic product of

water is significantly increased in the subcritical and supercritical state of water, and due to this property the supercritical and the subcritical water are highly reactive. This allows high reaction rates and leads to a better conversion and a shorter residence time with economic advantages and lower environmental mark. The amount of ionic products in subcritical conditions increase with the temperature because of the water dissociation, until they reach a maximum before the critical point. After that, the ionic products start to decrease because the decrease of the density of water and also as a result of the solvent change of polarity. With the reduction of ionic products, free radical gas phase reactions are promoted [27].

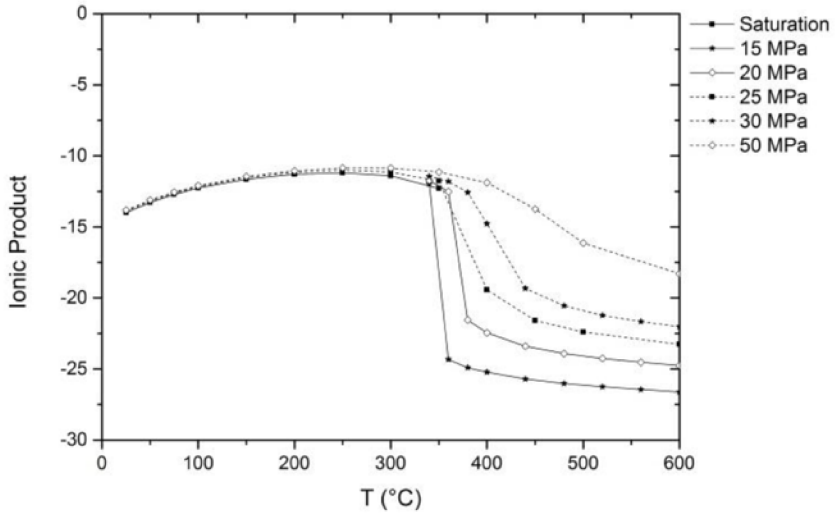

FIGURE 2.4: variation of the ionic product $[log_{10}K_w/mol^2kg^{-2}]$ with temperature [27]

At a fixed pressure, beyond the critical point, the solubility of organic compounds begins to increase quickly around $200°C$ and continues raising as it reaches the critical temperature. On the contrary, the solubility of ionic compounds, such as salts, decrease significantly in supercritical conditions, as it is possible to see in figure 2.5.

To sum up, table 2.3 shows the characteristics of water at different conditions.

TABLE 2.3: Properties of water in various conditions [28]

	Normal water	Subcritical water	Supercritical water
Temperature ($\circ$ C)	25	250 - 350	400
Pressure (MPa)	0.1	5 -25	25-50
Density (g cm^{-3})	1	0.8-0.6	0.17-0.58
Dielectric constant (F m^{-1})	78.5	27.1-14.07	5.9-10.5
Ionic product	14	11.2 -12	19.4-11.9
Dynamic viscosity	0.89	0.11- 0.064	0.03-0.07

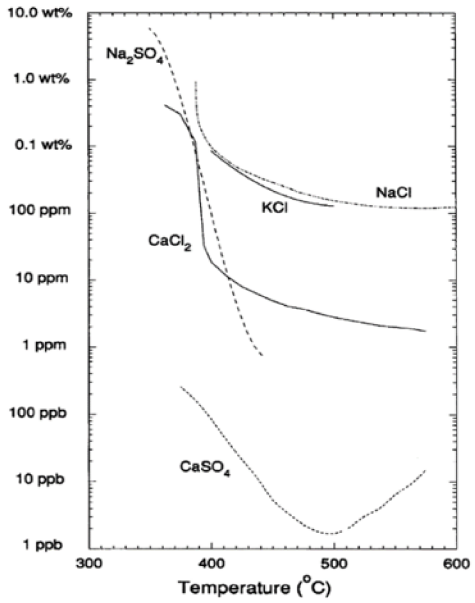

FIGURE 2.5: solubility of various salts at 25 MPa ([27])

2.3 Process designs

2.3.1 SCWG

The SCWG has been widely studied both for coal and for the biomass [16], [29], [24], [30]. Table 2.4 shows an overview of the studies based on SCWG of biomass.

Before modeling the process it is necessary to define the objective, so whether the desired product is a hydrogen rich syngas or a methane rich syngas. This choice allows to determine the optimal working conditions as the two reactions are one exothermic and one endothermic. The biomass feedstock is at first mixed with the solvent, water, which can be fresh or recycled in order to obtain a slurry with a solid content from 10% to 20% depending on the type of biomass. If the solid content is too high, the production of syngas is limited. Furthermore this leads to the possibility of obstructing the pipelines leading to an excessive pressure increase in the system when the solid content is too high.

After mixing, the slurry is pumped to the working pressure (above 221 bar) and it is pre heated. For the pre heating design it is necessary to understand the amount of heat needed and also the amount of heat that is released from the other sections of the plant in order to minimize the hot utility required and so the costs of the plant. This will be analyzed in chapter 3.3.

TABLE 2.4: Overview of SCWG working conditions found in literature

Feedstock	Reactor working conditions	Solid Content	Reference
Algae feedstock	600°C	5%	[16]
49 biomass	600, 700, 800 C	5, 15,25%	[29]
Black liquor	600°C	5%	[24]
Sewage sludge	600°C	20%	[30]

Many useful products can be obtained from the SCWG of biomass: they include syngas, heat and power. These can be further treated to obtain bio-fuels and biochar. Syngas can also be further processed into methanol, dimethyl ether and other chemical feedstocks. An evaluation of the thermal performance of the plant identifies the feasibility and the limitations of the study. Table 2.5 highlights the energetic efficiencies associated to different configurations for SCWG of biomass. Magdeldin et al. [16] studied the SCWG of an algae feedstock with different configurations and different products. What emerges from their study is that the energy efficiency related to the plant is higher in the BioSNG production cases. The thermal efficiency observed for the production of hydrogen is similar to the work of Lu et al. [31] whose study focuses on the thermodynamic analysis of biomass gasification for hydrogen production in supercritical water. Aziz et al. [32] proposed system for SCWG of a spirulina algae feedstock in a catalyzed fluidized bed for power production step in an integrated gasification combined cycle excess power integration configuration. Overall, the thermal efficiency of the plant ranges around the 40% because of the different systems of fluidized beds.

TABLE 2.5: Thermal efficiency associated with SCWG of biomass

Feedstock	Product	Energy efficiency	Reference
Algae feedstock	Hydrogen	42-55%	[16]
Algae feedstock	BioSNG	63-66%	[16]
Lignocellulosis biomass	Hydrogen	55%	[28]
Biomass	Hydrogen	42%	[31]
Spirulina algae	Power production	40%	[32]
Sewage sludge	Hydrogen	56%	[33]
Corn starch and sawdust	Hydrogen and CO	44%	[34]

With the conventional treatments the efficiency decreases with the moisture content, mainly due to the heat load required for the drying step. On the contrary, this characteristic was not observed with SCWG. This makes SCW a good medium for gasification processes for feedstocks with high moisture content [28].

After the SCWG reactor, the water contained in the syngas needs to be romoved along with the acid gas. For this reason, it is necessary a quench step, which allows the water removal, and then an acid gas scrubbing. There are multiple possibilities to quench the gas, for example it can be fed into an heat exchanger, or it can be diluted with cold water[35].

The Acid Gas Removal (AGR) stage is a lot discussed in literature; hydrogen sulfide removal processes can be either physical-chemical or biological [36]. Swanson et al. [35] evaluated the acid gas removal from a syngas through amine scrubbing and subsequent LO-CAT®process. The advantages and disadvantages of the different possibilities for acid gas removal are analyzed in chapter 3, based on the characteristics of the syngas.

As final stage, many solutions are possible. One option is, when obtained a hydrogen-rich syngas, to purify the syngas in order to rich a major content of hydrogen. This can be done through some special filter (Palladium) or with the Pressure Swing Adsorption (PSA), as studied in [16]. This solution could be used for instance for chemical industry and fuel cells, but it is discouraging because it is needed a large scale consumer nearby due to the high transportation costs.

2.3.2 Liquid fuels production

Another possible route is the Fisher Tropsch (FT) process that can be carried out in order to obtain a bio-crude from the syngas, which is comparable with the one produced in hydrothermal liquefaction. The Fischer-Tropsch process allows the conversion of the syngas into liquid fuels. Several articles on the FT have been published from 1980, as shown in figure 2.6. The increase of the studies on the FT process are due to the growth of the oil price, which makes the gas to liquid processes more interesting [37].

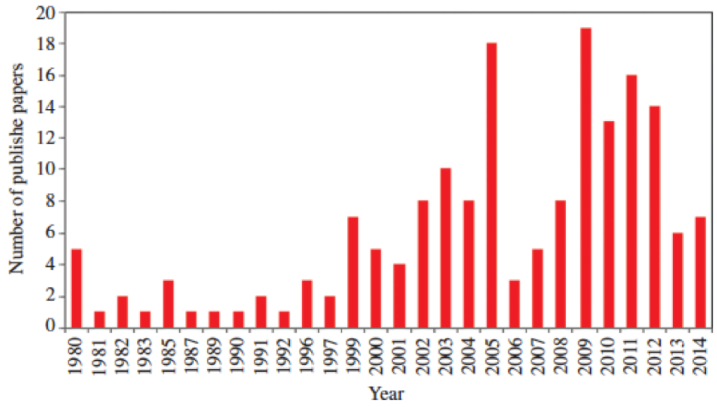

FIGURE 2.6: Number of published papers on the FT process from 1980 to 2014 [37]

The crude obtained from the FT reactor could be the end pipe product of the process, as studied by Pondini et al. [38], but it needs treatments to be used as transportation fuel. Many solutions are possible. For instance, figure 2.7 shows possible routes for fuel production from Fischer Tropsch processes at different working conditions [37].

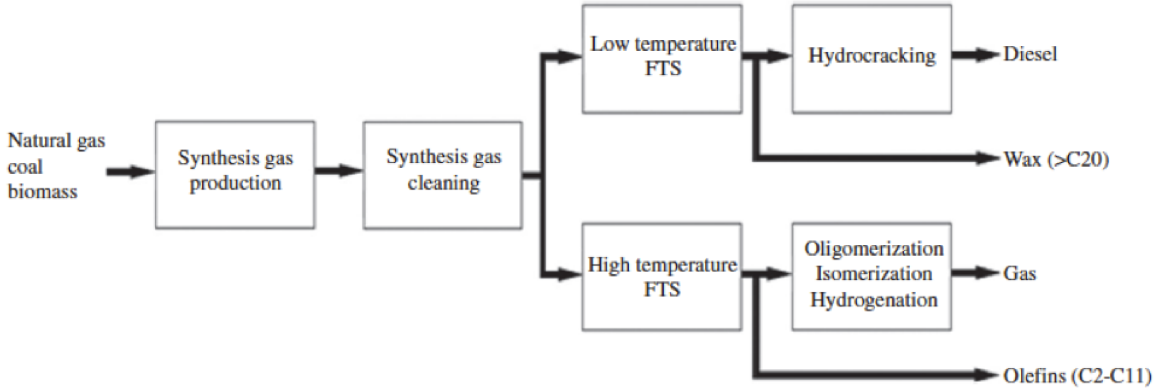

FIGURE 2.7: Processes for fuel production through FT [37]

The commercial FT processes can be carried out at lower or higher temperature. The type of reactor and the catalysts mostly depend on the working condition selected. Dancuart et al. [39] studied the development of the FT industry and their commercial expansion before 2007. In this paper is given a general information (see table 2.6) on the commercial processes for FT at different temperature (data referred

to Sasol plants, which represent the most significant example of commercialized FT synthesis in the world).

TABLE 2.6: General information about the LTFT and HTFT processes of Sasol [39]

FT processes	Low Temperature (LTFT)	High Temperature (HTFT)
Temperature	220-260°	320-350°
Catalyst	Fe/Co	Fe
Traditional reactor	ARGE	Synthol
Type	Tubular	Circulating Bed
Advanced reactor	Sasol slurry phase distillate (Sasol SPD)	Sasol advanced synthol (SAS)
Type	Slurry (three-phase)	Fluidixed bed

To adjust the CO-H_2 ratio entering the Fisher-Tropsch, it is possible to design a reverse water gas shift process block that allows the production of carbon monoxide from CO_2 and H_2. Saeidi et al. [40] studied the CO_2 hydrogenation to hydrocarbons. The FT process was thus preceded by a Reverse Water Gas Shift. The RWGS reaction is unclear and extensive studies have been performed to understand the RWGS reaction mechanism along with the characterizations techniques of the catalyst. The effect of catalyst types on RWGS reaction were evaluated along with the selectivity through CO, methane and methanol. Porosoff et al. [41] studied the catalytic reduction of CO_2 evaluating the conditions for synthesis of CO, methanol and hydrocarbons. Each catalyst has different selectivity to the products, and therefore with the appropriate catalyst it is possible to pursue the required route.

As shown in figure 2.7 the FT crude is not a transportation liquid fuel, consequently it has to be upgraded. Due to his characteristic and composition, the crude can be fractioned in a similar way as for the crude oil. Several studies are currently available on the fractionation of the crude oil. Haydary et al. [42] evaluated the separation of the crude oil into the different fractions with the use of Aspen Plus®. This unit allows the fractionation of the crude into Naphtha, Kerosene and Diesel. The Residuum of the fractionation step is the process by-product. As an alternative it can be treated through Fluid catalitic cracking (FCC) riser reactor, as studied by Mahfud [43].

2.4 Technical analysis in literature

There are several method for a techno-economic evaluation of the plant. Generally, the capital investment and the present value of the plant is determined by finding all equipment costs and operating costs for the construction and operation a plant for 20 years. Total capital investment is based on the total equipment cost with the additional installation costs and indirect costs (such as engineering, construction, and contingency costs) [35]. Generally, the costs related hydrothermal treatments are higher than other major biomass conversion technologies, such as pyrolysis or indirectly-heated gasification.

Magdeldin et al. [44] studied the Hydrothermal liquefaction of lignocellulose residues. They obtained a minimum selling price of the crude which varies from 94 to 169 €/MWh depending on the study case. The production cost obtained from a study on the bio-oil integrated gasification and Fischer-Tropsch [45] is ~75 €/MWh.

Hence, it is possible to notice that the minimum selling price related to the gasification and subsequent FT process is lower than the Hydrothermal liquefaction case.

Biocrude yield is one of the most important factors driving economics of the HTL plant. A maximum yield of 45% is thought to be achievable, therefore the motivation for this research is to look into the SCWG with 98% carbon recovery into the syngas compared to the liquefaction route with only 45% and even lower.

Hrncic et al. [46] gave an overview of the current high pressure processes for treatment of biomass for production of energy and chemicals. They made an analysis of the economic viability of hydrothermal processes. Table 2.7 shows the economic evaluation of scale up hydrothermal processes reported in ref [46].

TABLE 2.7: Economic evaluation of hydrothermal processes [46]

Process	Capacity (t/h)	Feedstock	Total Capital Investment (TCI) (M€)	Product cost (€/Gj)	Environmental impact
HT carbonization				Hydrochar	
Plant 1	5.7	Empty fruit branches	9.01	9.67	Carbon neutral
Plant 2	13.8	Empty fruit branches	16.47	7.49	Carbon neutral
Plant 3	48.6	Waste food	20.719	5.27	Carbon neutral
HT liquefaction				Biofuel	
Plant 4	0.468	Microalgae	1.6	65.9	Carbon neutral
Plant 5	83.3	Microalgae	468	/	Carbon neutral
HT gasification				Syngas	
Plant 6	5	Sewage sludge	2.915	7.1	Carbon neutral

What emerges from the table is that the production cost related to the HT liquefaction is higher that the other hydrothermal processes. The capacity of the plants shown in table 2.7 varies from 0.468 t/h up to 83.33 t/h depending on the feedstock type and operating conditions. As illustrated in the table, the main advantage of these processes is that they have a low environmental impact due to the fact that they are carbon neutral [46]. Generally in a hydrothermal industrial plant the reactor represents between 8.5 and the 21.3% of the total capital investment (TCI) of the plant depending on plant capacity and feedstock used [46]. The cost cost contribution of the reactor to the TCI may vary significantly with increasing the plant capacity and with a hypothetical product upgrading. The design of a product upgrading requires a higher number of equipments and therefore a greater TCI. The competitiveness of the process can be assessed in comparison to conventional technologies of hydrogen production based on the techno-economic assessments reported in literature [30]. The working conditions of the equipments effect the investment cost of the plant, hence materials with suitable characteristics are required.

The current technology based on biomass to liquid production through the Fischer Tropsch processes are based on the treatment of a syngas obtained from conventional gasification. Trippe et al. [47] carried out a techno-economic assessment of Fischer Tropsch synthesis as alternative process steps within biomass-to-liquid production. They concluded that the production costs related to biomass fuels are higher than the current price markets (between 76 and 93%). However, this technologies are close to becoming competitive to conventional refineries since the production costs are slightly higher than the current production costs when coal is used as main feedstock (between 7 and 18%) [47]. A similar approach was carried out by Meerman et al. [48]; they evaluated the economic potential of integrated gasification co-generation facilities with carbon dioxide capture and storage. As a result they obtained that the current production costs of transportation fuels are above market prices, nevertheless, future improvements and plant upgradings could make gasification facilities economical. The main process blocks for the biomass to liquid conversion of their review are shown in figure 2.8.

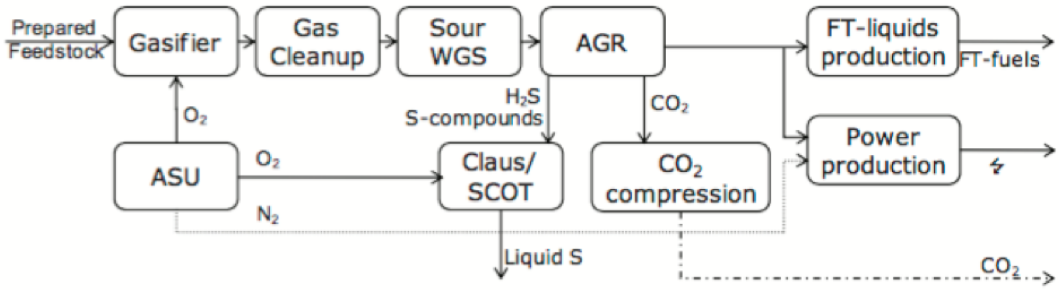

FIGURE 2.8: Biomass to liquid production through FT in ref [48]

As the reader can see, the conventional gasification happens though addiction of auxiliary O_2 to the biomass feddestock differently from SCWG where the auxiliary feedstock is pure water. In both cases, however, the syngas obtained contains impurities, and therefore is needs to be purified (figure 2.8).

As far as vinasse is concerned, it was not possible to find in literature values of the minimum selling price of the bio crude produced from it.

2.5 Experimental set-up in Åbo Akademi

Currently, experiments are being carried out in the Åbo Akademi which include the Supercritical water gasification of model compounds for vinasse. In particular glycerol, which is used in small quantities to study the production of syngas. The experimental set up is shown in figure 2.9.

FIGURE 2.9: SCWG reactor in Åbo Akademi

The core of the experimental set-up is a tubular reactor which works as a semi-batch. This type of reactor was chosen to simulate an industrial plant, where feed is sent continuously. In the laboratory scale, reactor dimensions are limited in order to reduce costs and increase safety, because of use of high temperatures and pressures. However its dimensions are enough to understand SCWG potentiality. Nitrogen is fed first to pressurize the reactor and the temperature is reached and maintained

by a tubular oven, made of insulation material and heated by electrical resistors. There are then three thermocouples to control the temperature inside the reactor. Feedstock does not actually pass directly into the pump in order do avoid corrosion problems, but it is stored into a cylinder put between pump outlet and reactor. At the end products are cooled down and thanks to a apposite valve the products are collected to be analyzed. The experiments were conducted with two different types of reactors: one in Stainless steel and one in Inconel.

The solid content used is around 10% in order to avoid the obstruction of the piping system leading to an excess increase of the pressure. Some of the data obtained from the experimental plant in Åbo Akademi have been used as input for modeling the system. Further information are given in chapter 3.

Chapter 3

Modeling

3.1 Introduction to the software Aspen Plus

The process was modeled and simulated on the commercial software Aspen Plus®V8.8 [19]. It is a broadly used program to simulate chemical process utilizing the thermodynamic and mathematical models contained in its databases and compounds data banks to predict the processing conditions based on energy and mass balances.

The equation of state selected for this study is the Peng Robinson Boston and Mathias (PR-BM). However, for gas cleaning step and for the units containing aqueous solutions the ENRTL-RK was chosen due to its ability to predict the behavior of aqueous electrolytes [49]. For the fractionation and product separation step the BK10 method was used because it is strictly applicable to heavy hydrocarbon systems[19].

3.2 Process design

The flowsheet of the plant is reported in apendix B. The amount of vinasse that arrives to the plant was chosen by literature data as 230 ton per day. This value was obtained considering that the amount of vinasse generated by the bioethanol production plant is around 23 kg per L of ethanol. Moreover it was considered that on an industrial scale the capacity of the ethanol plant is around 10 m^3 of ethanol per day [50].

To model the behavior of the vinasse, three model compounds were selected: Lactic Acid, Acetic Acid and Glycerol [12] and their concentrations were calculated as average of the values found in literature [21], [22], [23], [12] for vinasse from sugarcane.

As Lactic Acid, Acetic Acid and Glycerol are found to be the major compounds but not the only ones, a non conventional compound (CHOSN) was defined for modeling purposes to balance the organic content which was evaluated through an iterative calculation. Knowing the molecular weight of Lactic Acid, Acetic Acid and Glycerol and their amount contained in the vinasse, the moles of Carbon, Hydrogen and Oxygen were calculated. Based on the average of the elemental analysis of the vinasse found in literature [21], [22], [23], [12], it was evaluated the quantity of C, H and O needed in the non-conventional compound in order to compensate the quantity left, and therefore to simulate the presence of other compounds other than Lactic Acid, Acetic Acid and Glycerol.

The solid components (Ash and organic content) were defined as non-conventional compounds and from a thermodynamic point of view they were simulated based on the built-in enthalpy and density coal correlations, HCOALGEN and DCOALGEN, respectively. Table 3.1 shows the composition of the feedstock.

TABLE 3.1: Concentration of compounds in the feedstock (Vinasse) for Aspen simulation

Compound	%wt
Glycerol	6.46
Lactic acid	14.44
Acetic acid	4.87
Ash	15,33
Moisture	49.16
$C_vH_wO_xN_yS_z$	9.75

As previously said, the elemental analysis used for the simulation was defined as average between all the values reported in literature for vinasse from sugarcane.

The Heating value of the biomass was evaluated through the Boie correlation (equation 3.1) based on its elemental composition.

$$\Delta H = 100(a_1x_C + a_2x_H + a3x_S + a_4x_O + a_5x_N) + a_6 \tag{3.1}$$

The values of the constants of Boie correlation are shown in table 3.2.

TABLE 3.2: Constants of Boie correlation [51]

Constant	Btu/lb	kJ/kg
a_1	151,2	351,69
a_2	499,77	1162,46
a_3	45,0	104,67
a_4	-47,7	-110,95
a_5	27,0	62,80
a_6	-189,0	-439,61

Therefore the estimated higher heating value of the biomass was 14,66 MJ/kg on dry basis.

The process modeled can be divided in five main sections (figure 3.1 shows a block diagram of the process):

- Super critical water gasification (SCWG) (1)
- Gas cleaning (2)
- Fischer Tropsch process (3)
- Product separation (4)
- Utility (5)

For each unit of the process, a parametric analysis has been made in order to find the optimal working conditions. Figure 3.1 shows the Block diagram of the process (the numbers on the streams are used to direct the reader to the focus streams in appendix B). The utility unit will be explained in section 3.3.

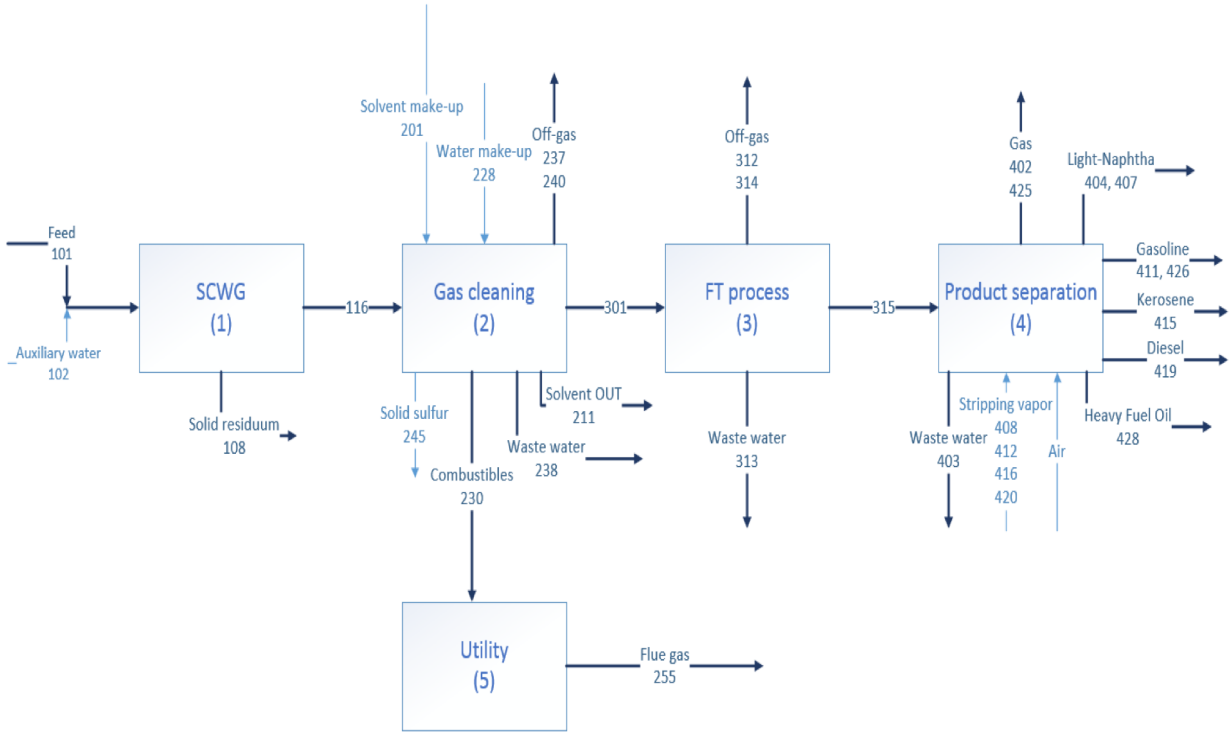

FIGURE 3.1: Block Diagram of the plant (the thicker line shows the Carbon Input and output)

3.2.1 Supercritical water gasification

This step has the objective of converting the solid biomass into a syngas through reactions 1.1, 1.2, 1.3 and 1.4. The main parameters that affect the yield and the characteristics of the product required are temperature, pressure and solid content. These conditions were selected based on the actual experiments that were carried out on SCWG of model compounds for vinasse in the Åbo Akademi in Turku with the aim of producing hydrogen. The solid content can vary between 5 and 40 wt%. For this study a value of 10% of solid content has been selected; in this way the probability of obstructing the inlet pipe is limited. If the pipe is blocked from the biomass entering the system, this can lead to an excessive pressure buildup and consequently to an unsafe and dangerous environment.

Before entering the reactor, the water can be preheated and pumped before being mixed with the biomass feedstock, or it can be upgraded to supercritical conditions after being mixed with the biomass. For this study the solution preferred was the second one, therefore the feedstock is mixed with the water and then pumped and heated to enter the reaction system. This decision was made to reduce the risk of obstructing the pipe with the solid biomass. Figure 3.2 shows the flowsheet of the SCWG unit.

The mixing step was modeled in Aspen Plus®as a Mixer. Afterwards, for the overall plant evaluation, an agitated tank is designed. The designing specifications are reported in appendix A. The reactor temperature selected was 600°C because in the experiments carried out in the laboratory in Åbo Akademi has been detected that the yield at this temperature is comparable to the one at 700°C, therefore it is preferred due to the lower heating load required. In each section of the plant the heating system was at first simulated with HEATER; afterwards an energy analysis has been

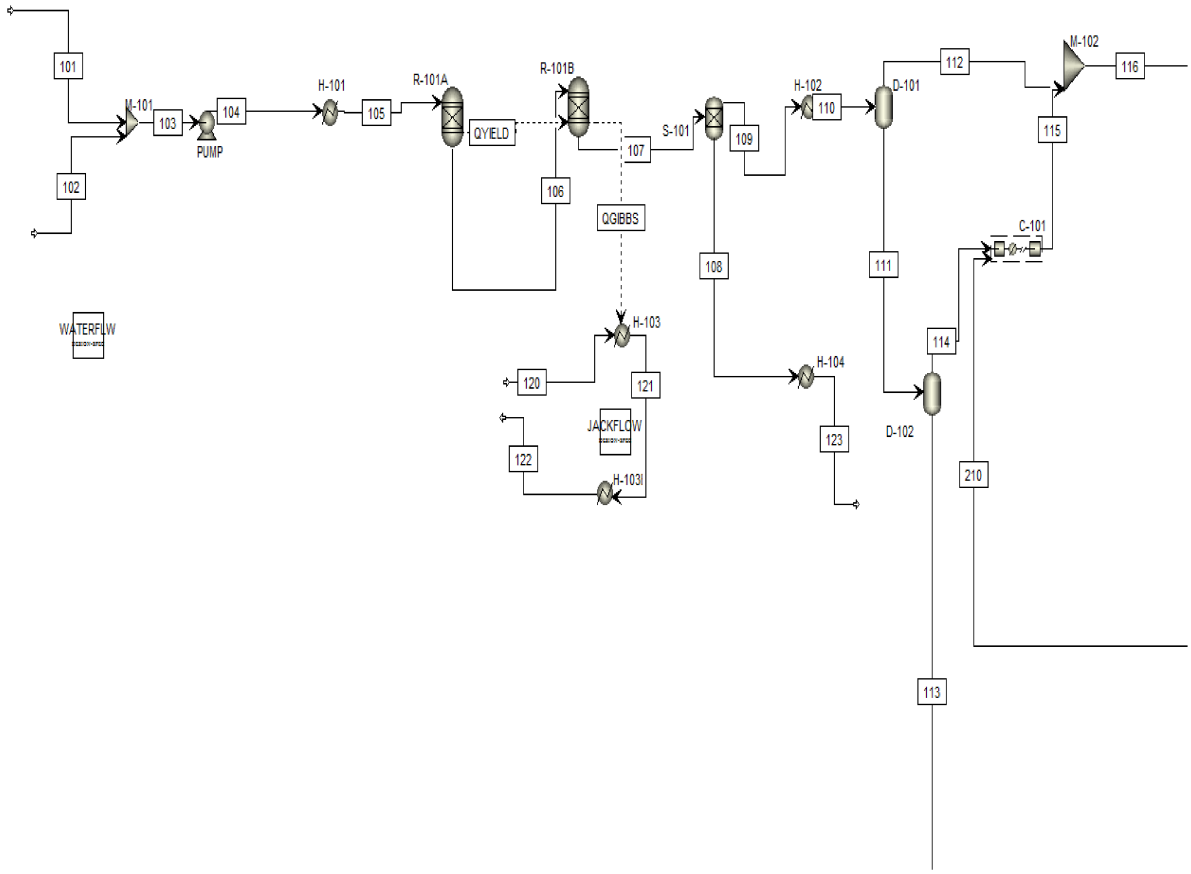

FIGURE 3.2: Snapshot for the SCWG section on Aspen Plus®

made with Aspen Energy Analyzer and will be explained in section 3.3. The SCWG system has been modeled in two subsequently steps: a yield reactor (RYIELD) to decompose the slurry into its elemental constituents and a Gibbs reactor (RGIBBS) which calculates the product component formation. This design simulates an hydrolysis, which allows the cleavage of chemical bonds, and subsequent reactions (1.1, 1.2, 1.3, 1.4) [16].

The RYIELD reactor has the purpose to give as output the elemental analysis of the vinasse reported in table 3.3. The yields in the reactor have been evaluated considering the elemental analysis and a solid content of 10%. Therefore the values inserted in the Aspen plus®simulation are shown in 3.4.

The Gibbs Reactor calculates the formation of the products: hydrogen, methane, carbon dioxide, carbon monoxide water, hydrogen sulfide and ammonia. It was assumed that 98% of the Carbon is transformed into products, thus the remaining 2% leaves the plant with the Ashes. The working temperature of the reactor is fixed, thus a heating jacket needs to be considered in order to keep the temperature at a constant value. For modeling purposes the jacket was designed as two HEATER (H-103A and H-103B) that simulate the cooling of the auxiliary vapor through the heat load of the reactor.

TABLE 3.3: Elemental analysis of Vinasse for the simulation compared to the literature data

C	18.86%	17.3%	14.6%	16.92%
H	2.58%	2.11%	3.16%	2.62%
O	20.86%	8.73%	11.38%	13.65%
N	0.57%	2.10%	0.61%	1.09%
S	1.55%	2.10%	0.04%	1.23%
Ash	22.98%	9.79%	13.31%	15.33%
Moisture	32.60%	58.00%	56.90%	49.16%
Reference	[22]	[21]	[23]	Model

TABLE 3.4: Yields of the RYIELD reactor (%) for the decomposition of the vinasse into its elemental analysis

C	4.22
H	0.60
O	2.26
N	0.18
S	0.20
Ash	2.54
H_2O	90

The reactor outlet is fed to a Cyclone to separate the solid residue from the syngas. It was assumed that all of the solid residue exits within this step. As no information about the particles dimension were detected, a simple SEP was used assuming a complete solid removal. The specific design of the Cyclone was not considered in this study. The solid exiting the separator needs to be cooled from $600°C$ to ambient temperature.

The Syngas obtained is at first cooled to $90°C$ and then fed to a Flash separator for water removal (working pressure is 30 bar). The working conditions of this flash depend on the subsequent gas treatment. In table 3.5 is reported the composition of the syngas after water removal.

TABLE 3.5: Syngas composition (%) after removal of 99.98% of water

Compound	Volume%
H_2O	2.34
H_2	56.09
CO_2	21.96
CO	0.75
CH_4	18.69
H_2S	0.09
NH_3	0.09

From the composition of the dry syngas it is possible to notice that the working conditions selected allow the production of hydrogen as main product, with a lower production of carbon dioxide and methane. At this point of the process, it is important to focus on the acid gas content of the syngas and its removal. As shown in 3.5 the H_2S content is not negligible, therefore it needs to be removed.

3.2.2 Gas cleaning

This section was designed to lower the amount of H_2S entering the FT block, because its presents limit the activity of the catalyst and it is the cause of its deactivation. Before modeling, a research on the current technologies used was made.

Overview on acid gas removal technologies

Various solutions are possible to remove the H_2S and the CO_2.

- Claus process

  This process is mainly used in oil and natural gas refining and it allows the H_2S removal by oxidizing it to elemental sulfur. It can be treated with different configurations, leading to a removal efficiency that ranges between 95% and 98% depending on the reactor configuration.

  The main reactions that take place in the catalytic reactors are the following:

$$H_2S + \frac{3}{2}O_2 \leftrightarrow SO_2 + H_2O \tag{3.2}$$

$$2H_2S + SO_2 \leftrightarrow 3S + 2H_2O \tag{3.3}$$

$$H_2S + \frac{1}{2}O_2 \leftrightarrow S + H_2O \tag{3.4}$$

  The Claus process is most effective in streams that contain a large amount of H_2S, greater than 15% [52].

  Hence this solution was not modeled in this study because the H_2S content is lower (table 3.5).

- Chemical oxidants

  Mainly used in wastewater treatment plants, they allow controlling both odor and toxic potential of H_2S. The most widely used chemical oxidation system is a combination of sodium hydroxide (NaOH) and sodium hypochlorite (NaOCl), which are selected for their low cost, availability, and oxidation capability [52].

- Caustic scrubber

  It works similarly to the chemical oxidation system, with the difference that caustic scrubbers are equilibrium limited. This means that if caustic is added, H_2S is removed, and if the pH decreases, H_2S is produced [52].

- Adsorption

  With the adsorption process, the molecules of the compound that has to be removed are captured to the surface of an adsorbing material. This process can continue until the surface of the material is covered and then the material must be regenerated. The most common material used for adsorption is the activated carbon [52].

- Amine absorption

  Amines have the ability to absorb acid gases due to their chemical structure [53]. They are able to remove H_2S by absorbing it and dissolving it into an aqueous amine stream. The desorbing of the acid components through a heating system allows the regeneration of the stream. Therefore, the acid gas absorption in amine solution is conducted using a two-column operation: the first column is used to absorb the acid gas into the absorbent amine, and the second column is used to regenerate the amine [53].

  When H_2S is exposed to an aqueous amine, or any alkaline solution, it dissociates into the bisulfide ion, SH^-, by a proton-transfer reaction (equation 3.5) [54].

$$H_2S + amine \leftrightarrow (H : amine)^+ + SH^-1 \tag{3.5}$$

  The H_2S reacts almost instantaneously with the amines by proton transfer (equation 3.6).

$$CO_2 + H_2S + amine \leftrightarrow [amine]COOH^+ + OH^- \tag{3.6}$$

$$CO_2 + H_2O + R_2NCH_3 \leftrightarrow R_2NCH_4^+ + HCO_3^- \tag{3.7}$$

  CO_2 reacts with primary and secondary amines to form a carbamate (3.7) [54].

  Amines that are commonly used are monoethanolamine (MEA), diethanolamine (DEA), and methyldiethanolamine (MDEA).

MEA
It is an organic compound with the formula $HOCH_2CH_2NH_2$ generally used as a 10 to 20 weight % solution in water. Due to corrosion problems, the acid gas loading is usually limited to 0,3 to 0,35 moles acid gas per mole of amine for carbon steel equipment [36].

Since MEA is a primary amine, it has a high pH which enables MEA solutions to produce a sweetened gas product [36].

DEA
It is an organic compound with the formula $HN(CH_2CH_2OH)_2$ commonly used in the 25 to 35 weight % range. The total acid gas loading for DEA is also limited to 0,3 to 0,35 mole/mole for carbon steel equipment. The degradation products of DEA are much less corrosive than those of MEA [36].

Since DEA is a secondary alkanolamine, it has a reduced affinity for H_2S and CO_2, although it is selective to H_2S under specific conditions [36].

MDEA
It has the formula $CH_3N(C_2H_4OH)_2$. MDEA is commonly used in the 20 to 50%wt range. Solutions with lower content of MDEA are typically used in very low pressure, high selectivity applications. Due to considerably reduced corrosion problems, acid gas loadings as high as 0,7 to 0,8 mole/mole are suitable in carbon steel equipment.

The main advantage of this amine is its selectivity towards H_2S and CO_2. The higher selectivity of MDEA for H_2S results from the inability of tertiary amines to form a carbamate with CO_2, in fact MDEA does not have a hydrogen attached to the nitrogen and therefore it cannot react directly with CO_2 to form carbamate. The reaction can only take place after the dissolution of CO_2 in the water where it forms a bicarbonate ion [55].

The following chemical reactions occur in an aqueous MDEA solution when CO_2 and H_2S are present:

$$CO_2 + H_2O \leftrightarrow HCO_3^- + H^+ \tag{3.8}$$

$$HCO_3^- \leftrightarrow CO_3^{2-} + H^+ \tag{3.9}$$

$$H_2O \leftrightarrow OH^- + H^+ \tag{3.10}$$

$$RR'R'NH^+ \rightarrow RR'R'N + H^+ \tag{3.11}$$

$$H_2S \rightarrow HS^- + H^+ \tag{3.12}$$

$$HS^- \rightarrow S^{2-} + H^+ \tag{3.13}$$

Where R (3.11) represents a methyl group and R' an ethanol group [55].

The AGR through amine scrubbing allows a H_2S removal until 4 ppm, so if some other phases of the plant require a lower value of ppm, a second step of AGR has to be evaluated. If the Fischer Tropsch process follows, the H_2S content needs to be reduced below 1 ppm [35].

- Zinc Oxide Guard

  Used to remove trace amounts of H_2S from gases at high temperatures (from $200°$C to $400°$C). Zinc oxide catalyst is used as a mixture of ZnO and alumina as a binder in addition to some fillers or binder materials. In general, 90%wt of ZnO is quite acceptable.

  The main reaction in this process is:

$$ZnO + H_2S \rightarrow ZnS + H_2O \tag{3.14}$$

  The quantity of hydrogen sulfide being adsorbed by zinc oxide depends on its value in the feed and on the degree of contact between it and the ZnO bed [56].

Maximum sulfur loading is typically in the range of 30-40 kg sulfur/100 kg sorbent. When the zinc oxide reacts with the H_2S an insoluble layer of zinc sulfide is formed and approximately 40% of the H_2S is converted [52], [57].

- LO-CAT®process

  It is a process commercially used and it allows the conversion of the gas into solid sulfur. It is patented process that consists in a wet scrubbing, liquid redox system that uses a chelated iron solution to convert H_2S to solid sulfur. It mainly consists in the oxidation of the H_2S and it can be divided in five steps.

  1. Absorption of H_2S
  2. Ionization of H_2S

$$H_2S \leftrightarrow H^+ + HS^{\smile} \tag{3.15}$$

  3. Sulfide Oxidation

$$HS^{\smile} + 2Fe^{+++} \leftrightarrow S^{\circ} + 2Fe^{++} + H^+ \tag{3.16}$$

  4. Absorption of Oxygen
  5. Iron Oxidation

$$\frac{1}{2}O_2 + H_2O + 2Fe^{++} \leftrightarrow 2OH^- + 2Fe^{+++} \tag{3.17}$$

  Overall, the reaction can be expressed as:

$$H_2S + \frac{1}{2}O_2 \leftrightarrow H_2O + S^{\circ} \tag{3.18}$$

  This process, carried out at ambient working conditions (25°C and 1 bar) allows the conversion of the 99,99% of H_2S into solid sulfur [58].

Design

The Gas cleaning was consequently designed: it is composed of four main sections, as illustrated in figure 3.3.

Therefore the main sections are:

1. Amine scrubbing, to reduce the H_2S content in the gas fed to the FT;
2. Pressure Swing Adsorption (PSA), in order to obtain a high purity hydrogen stream to send to the reactor;
3. CO_2 recovery, to reduce the carbon losses of the plant;
4. LO-CAT®process, to further reduce the amount of H_2S.

Figure 3.4 shows the flowsheet of the gas cleaning unit.

1. **Amine scrubbing**: This step was evaluated in order to reduce the H_2S and CO_2 content before the gas enters the Fischer Tropsch reactor because the content of sulfur tolerated by the FT catalyst is lower than 1 ppm [59].

   The AGR was made through a MDEA absorption with a 30%wt MDEA solution. The MDEA is able to remove 0,4 mol of acid gas per mol of amine

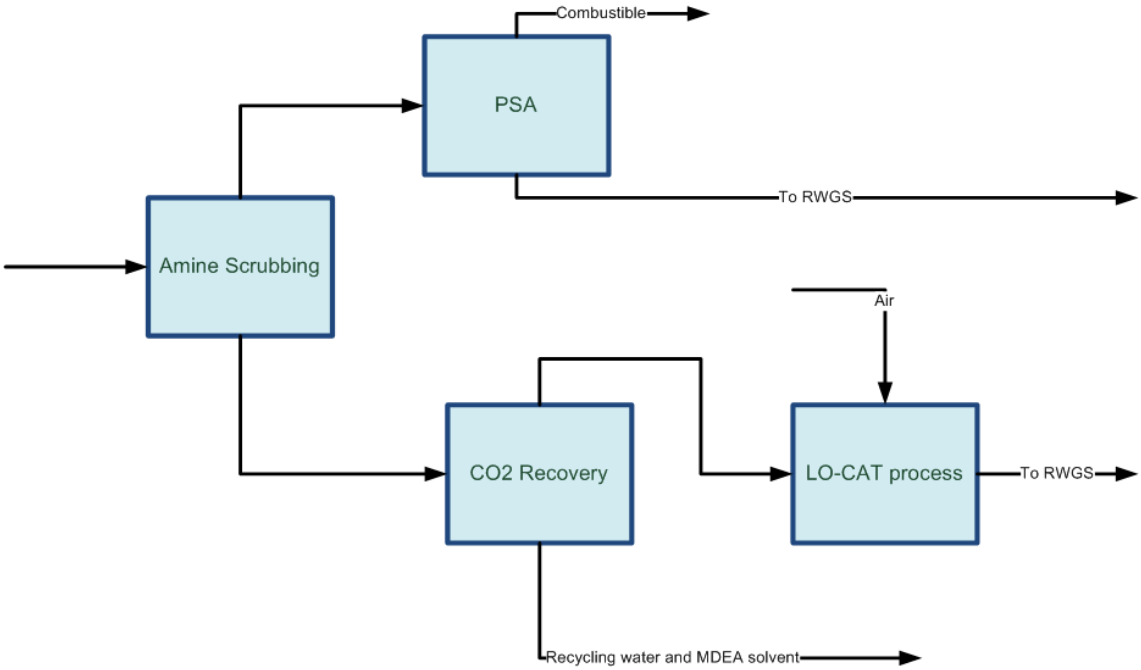

FIGURE 3.3: Block diagram of the Gas cleaning unit

[38]. The amount of solution needed was thus evaluated. At first attempt, the stages needed for the extraction were evaluated with a simplified calculation on Excel for an ideal system. The design is reported in appendix C. The main assumption that has been made in the first extractor design is constant flow rates entering and exiting the extractor. With this, an iterative calculation has been carried out until the H_2S content was reduced below 4 ppm. The results obtained from the excel calculation were then simulated in Aspen Plus®and adjusted using a RADFRAC with 4 stages without a boiler nor a condenser. A sensitivity analysis allowed the evaluation of the optimal working conditions which were $90°$C and 30 bar with a solvent mass flow of 67 ton/hr.

2. **Pressure Swing Adsorption**: Due to the composition of the sweet gas (table 3.6) a pressure swing adsorption step was evaluated in order to recover H_2 stream with high purity for the RWGS step leaving a combustible stream (*219*) that has a potential as hot utility for the plant (composition is shown in table 3.7) .

TABLE 3.6: Sweet gas molar composition (stream 204 in figure 3.4)

Compound	%
H_2	80
N_2	2
CH_4	18

Pressure swing adsorption (PSA) processes are generally used for the production of high purity hydrogen. It is technology based on a physical binding of gas molecules to adsorbent material. The separation effect is based on differences in binding forces to the adsorbent material. The adsorption step works at high pressure typically in the range between 10 to 40 bar until the equilibrium loading is reached. In this condition, the maximum adsorption capacity

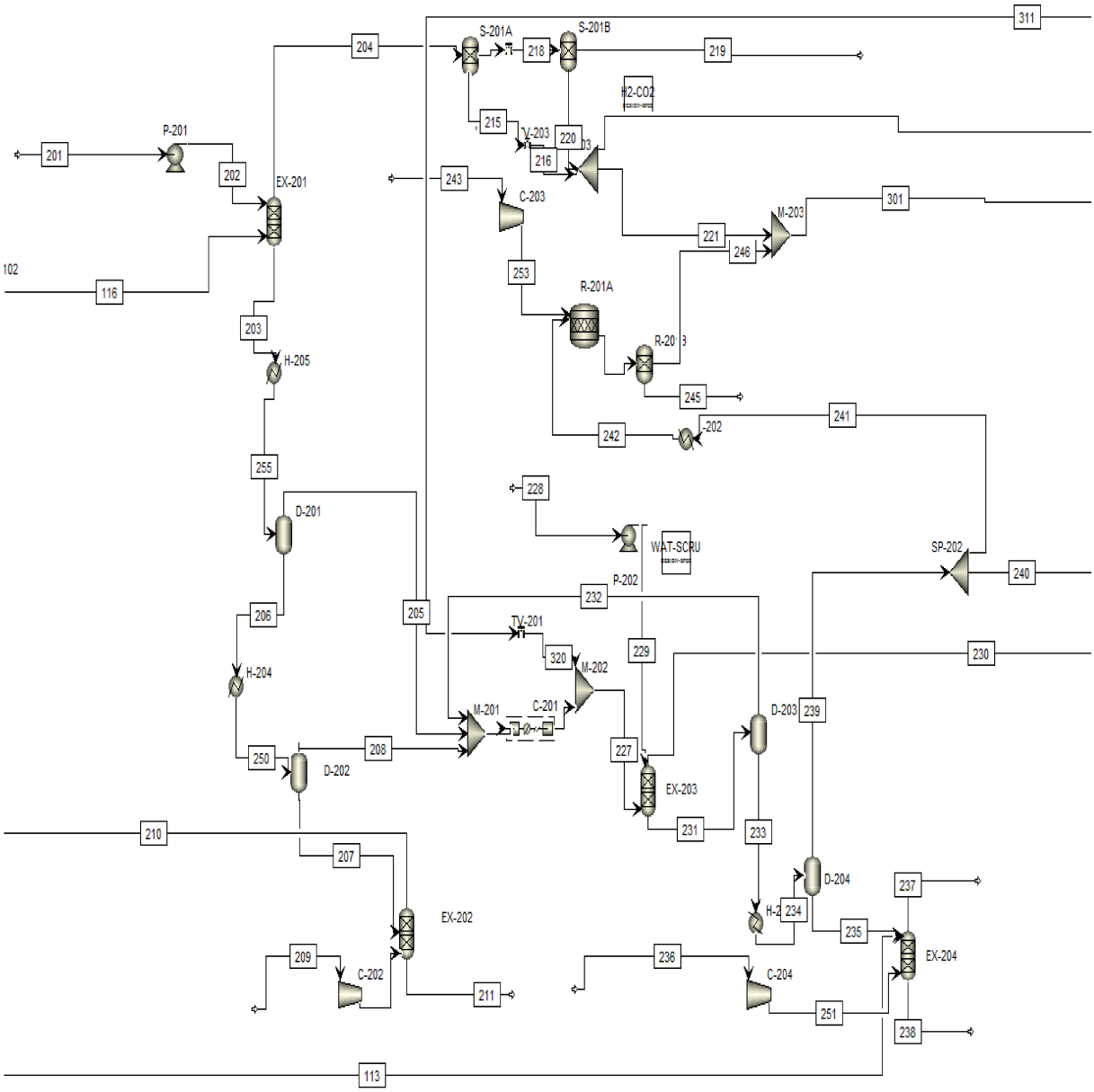

FIGURE 3.4: Snapshot of Gas Cleaning unit

TABLE 3.7: Major compounds in stream 219 (shown in figure 3.4)

Compound	vol%
H_2	39
N_2	5
CO	0.4
CH_4	54

is reached, and the adsorbent material needs to be regenerated. This is done by lowering the pressure resulting in a respective decrease in equilibrium loading [60].

The PSA unit was modeled as a two-stage separation with a recovery of 80% of H_2 for each step. This two stages allow the recovery of a 99.99% H_2 purity

stream wich is fed to the RWGS reactor.

3. CO_2 **recovery** : The solvent exiting the block *EX-201* needs to be recovered, to reduce the MDEA make up along with the cost of the plant. It is therefore possible to recover the CO_2 that can be used for the RWGS step. The CO_2 recovery can be divided in two steps:

   - Solvent recovery
   - Water scrubbing

   As a result the CO_2 (~83%) rich stream exiting this step contains a high amount of sulfur content, thus a LO-CAT®was modeled.

Solvent recovery
The solvent exiting the extractor (stream *203*) was fed to a FLASH unit (block D-201) working at 1 bar and 25°C: this allows the recovery of the 99,99% of MDEA in the liquid stream, although a high amount of CO_2 (~95% of it) exits with the liquid stream. This (stream *206*) is heated to 45°C and fed to a second Flash step (Block D-202) where ~81% of the CO_2 is removed from the liquid stream (*207*). Stream *207* is then fed to a desorption system were the 99% of CO_2 and H_2S are recovered in the top stream through the air fed to the block. The gaseous stream (*210*) is then recirculated to the MDEA adsorption unit in order to reduce the carbon losses. The liquid stream (*211*) is composed by almost the 30%wt of MDEA and around 70% of Water (some impurities are present), therefore it could be recycled to the extractor lowering the solvent make-up (in the simulation the MDEA stream was simulated as pure solvent). Figure 3.5 shows a simplified block diagram of the solvent recovery step. Stream *210* is recycled to the amine adsorption due to its high content of H_2S (~4%).

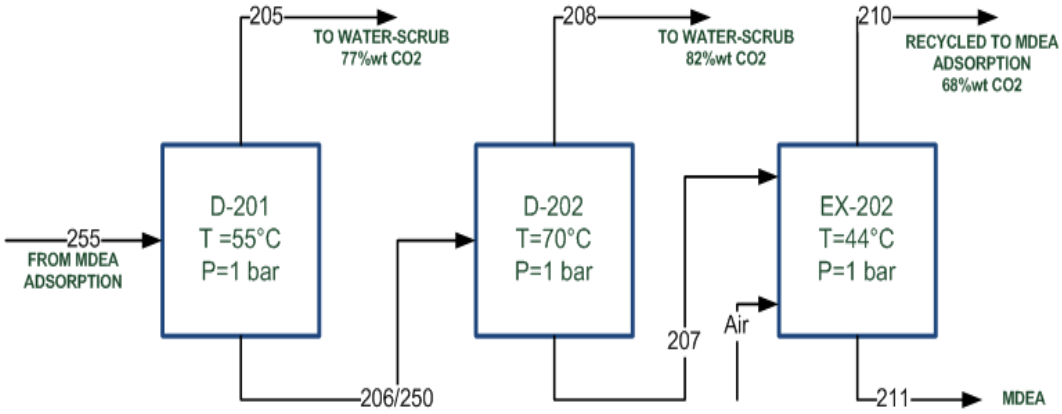

FIGURE 3.5: Block diagram of solvent recovery step

Water scrubbing
The water scrubbing was evaluated due to the high content of methane present in the gaseous streams. This step allows the separation of methane from CO_2. The methane stream (*230*) is mainly composed of combustible compounds (table 3.8 shows its composition), therefore it was evaluated as potential hot utility for the plant (more detailed explanation in chapter 3.3).

TABLE 3.8: Major compounds of the combustible stream (*230*, shown in figure 3.4) (%wt)

Compound	%
H_2O	0,19
H_2	4,07
N_2	13,84
CO_2	0,19
CO	35,14
CH_4	37,53
O_2	4,91
C_2H_6	0,45
C_2H_4	0,23
C_3H_8	0,86
C_3H_6	0,39
C_4H_{10}	1,19
C_4H_8	0,46
C_5H_{12}	0,31
C_5H_{10}	0,16

A water scrubber is a physical scrubber that uses the property of carbon dioxide to have higher solubility than methane in water. The carbon dioxide is separated from the gas and dissolved into the water in the absorption column by using a pressure between 6 and 10 bar, consequently it is released from the water in the desorption column by addition of air at atmospheric pressure (schematic illustration in figure 3.6) [61].

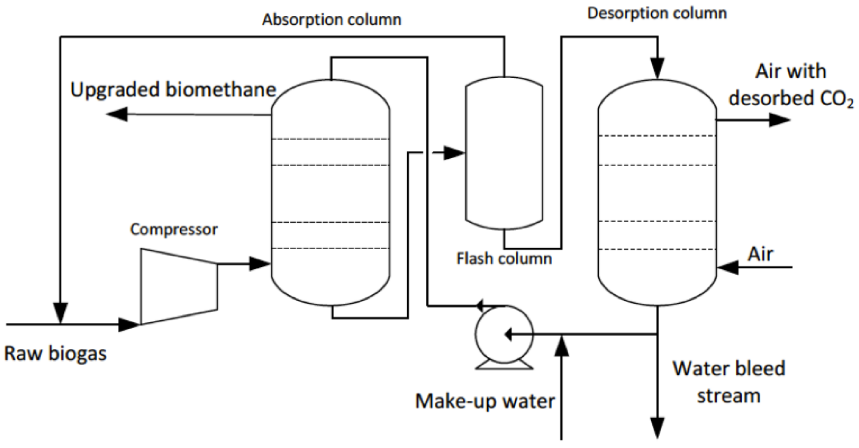

FIGURE 3.6: Schematic illustration of a common water scrubber [61]

In this study, the water scrubbing was modeled in four blocks: as a

- Adsorption column (block EX-203), where the separation of the CH_4 stream happens;
- Flash column (block D-203), where the water is separated from the gas and the gas is recycled to the adsorption column;
- Gas-separation column (block D-204), for the separation of the remaining CO_2 from the water;

- Desorption (block EX-204), for the recovery of high purity water in the bottom and off-gas in the top.

The adsorption step was modeled at 6 bar and the desorption step was simulated as atmospheric a flash (block D-204) for the separation of CO_2 from the water. The optimal working conditions (3 bar and 75°C) were selected based on the H_2S content in the gaseous stream (*239*). Hence, the recovery of CO_2 is limited by the content of H_2S. This configuration allows the recovery of the ~99,5% of water in the bottom stream, and the of ~70% of CO_2 in the top stream. The stream fed to the LO-CAT®reactor is thus mainly composed of CO_2 (~92%wt). Therefore differently from what reported in figure 3.6 in this study a second flash was modeled because of the high sulfur content which limits the amount of CO_2 that can be recovered.

4. **LOCAT®process**: The LO-CAT®process for sulfur removal was selected to remove the H_2S content because compared to the Zinc Oxide guard, it allows higher conversions and therefore a lower H_2S content in the stream fed to the FT step. For modeling purposes, it was used a RSTOIC to model the conversion to elementary sulfur with a 99.99% of conversion and a separator to simulate the total separation of the solid sulfur from the gas stream. Air is fed to the reactor at stoichiometric conditions so that the equation 3.18 occurs. The possibility of feeding a stream with only O_2 was evaluated, but the fraction of N_2 that remains in the process after the LO-CAT ®reactor was considered acceptable (below 1%). As a result, the ppm of H_2S leaving the unit are ~0.19.

3.2.3 RWGS and Fischer Tropsch

Figure 3.7 shows the flowsheet of the RWGS and FT unit.

RWGS

The ratio required from the Fischer Tropsch reactor is adjusted through a Water Gas Shift (1.3) or a Reverse Water Gas Shift (3.19) depending on the stream composition. In this study the RWGS reactor was modeled for this purpose.

The ratio of H_2/CO happens to be high (~84), for this reason a reverse water gas shift is needed (equation 3.19).

$$CO_2 + H_2 \leftrightarrow CO + H_2O \qquad (\Delta H = 41160 J/mol) \tag{3.19}$$

The reaction is mildly endothermic and therefore favored at higher temperature. It is necessary to select an efficient catalyst capable of bearing high temperatures and being selective to CO during the RWGS reaction.

The possibility of the formation of side products have been evaluated: with the same reactants it is possible the synthesis of methane (equation 3.20) and methanol (equations 3.21 and 3.22).

$$CO_2 + 4H_2 \leftrightarrow CH_4 + 2H_2O \qquad (\Delta H = -164.9 KJ/mol) \tag{3.20}$$

For this study the side reactions were not considered due to the catalyst selected.

$$CO + 2H_2 \leftrightarrow CH_3OH \qquad (\Delta H(298K) = -21.7 kcal/mol) \tag{3.21}$$

$$CO_2 + 3H_2 \leftrightarrow CH_3OH + H_2O \qquad (\Delta H(298K) = -11.9 kcal/mol) \tag{3.22}$$

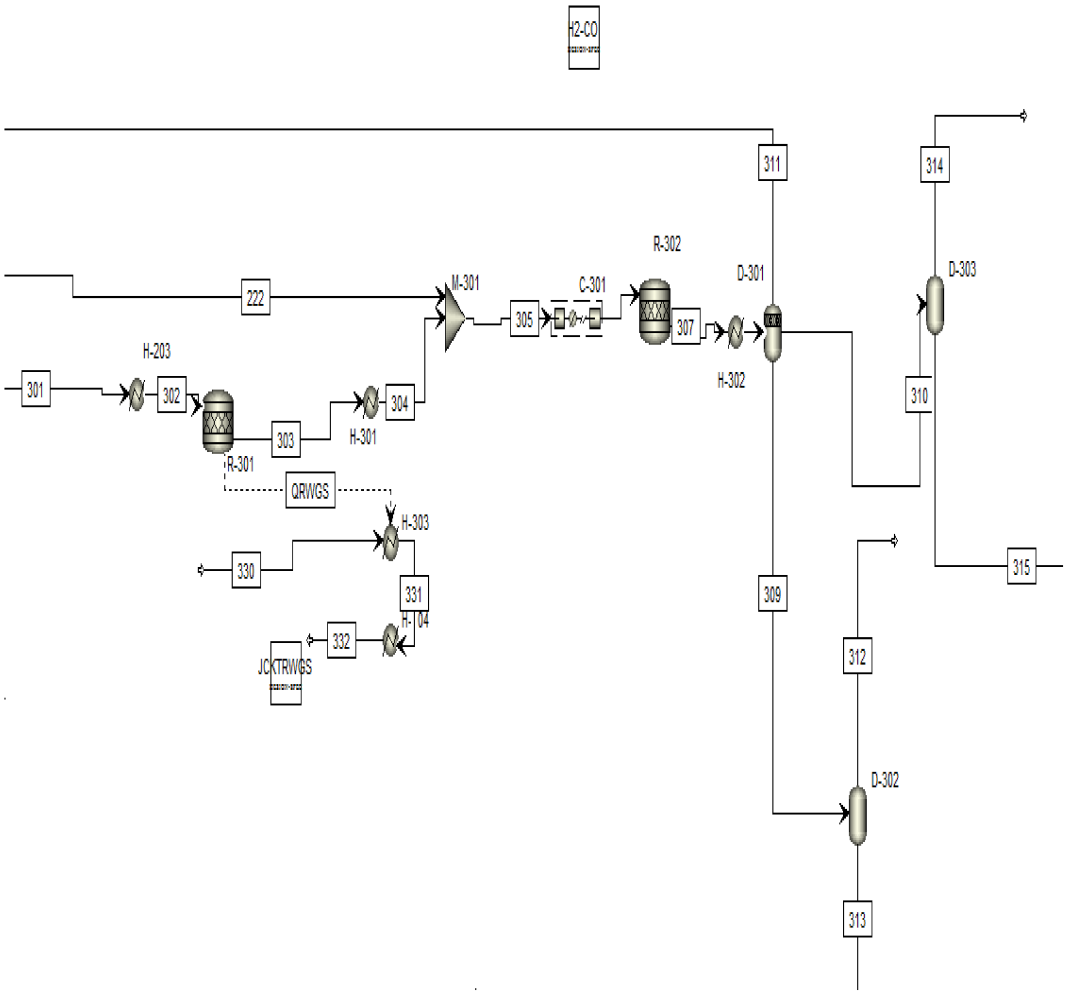

FIGURE 3.7: Snapshot of the RWGS and FT unit

As shown in the equations, both the methanol and methane reaction are exothermic, so higher methanol yields are obtained at lower temperatures and higher pressures, while the RWGS is endothermic. Thermodynamic evaluations at atmospheric pressure show that CO_2 conversion in the RWGS reaction is greater with an excess of H_2 flowing. The equilibrium composition changes with the temperature. It is possible to graph the molar distribution of the products with the temperature, as illustrated in figure 3.8

To determine the working conditions of the RWGS reactor, an evaluation of the possible catalysts has been made in order to understand the conversion and the selectivity to CO. Porosoff et al.[41] reported a study of the catalyst used for the conversion of CO_2 into CO, methanol and methane.

The selectivities and conversions of the catalysts are shown in table 3.9. The catalyst selected for the simulation is the NiO/CeO_2; it allows 40% of CO_2 conversion and almost a 100% selectivity to CO, so no methane and methanol were considered as products. Therefore, the working conditions are $600°$C and 1 bar. For modeling purposes a RSTOIC reactor with a fractional conversion of 0,4 of CO_2 was used.

As shown in table 3.9, the H_2/CO_2 ratio entering the reactor has to be equal to 1. For this reason, a PSA system was considered in order to have a high purity H_2

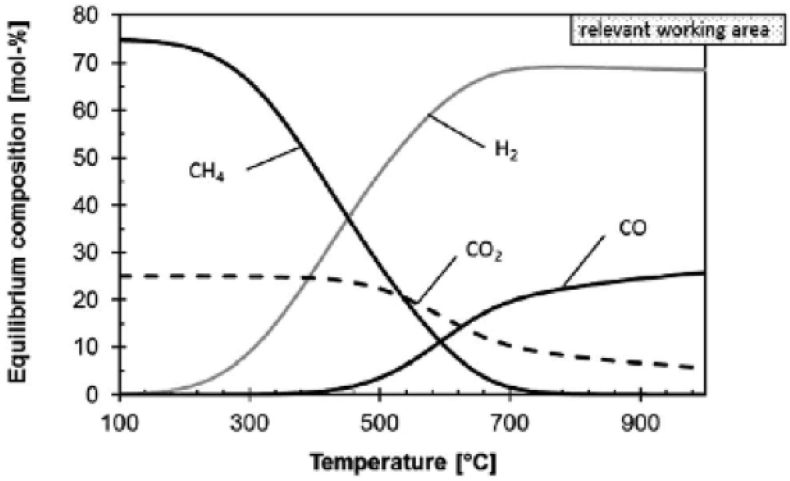

FIGURE 3.8: Influence of temperature on the thermodynamic equilibrium of the RWGS reaction at 1 bar and H_2/CO_2 ratio of 3 ([62])

stream fed to the RWGS. This allows the reduction of the amount of impurities that flow in the process.

Fisher Tropsch

The Fischer Tropsch reactor allows the synthesis of a crude from CO; the CO reacts with hydrogen to produce paraffins, olefins and water [59].

In the Fischer-Tropsch process, CO and H_2 are converted into hydrocarbons (alkanes and alkenes) of various molecular weights according to the equations 3.23 and 3.24 thanks to the presence of a catalyst.

$$(2n+1)H_2 + nCO \leftrightarrow C_nH_{(2n+1)} + nH_2O \tag{3.23}$$

$$2nH_2 + nCO \leftrightarrow C_nH_{2n} + nH_2O \tag{3.24}$$

Along with the Hydrocarbons synthesis, alcohol synthesis (3.25) and coke formation (3.26) take place as side reactions.

$$nCO + 2nH_2 \leftrightarrow H(-CH_2-)_nOH + (n-1)H_2O \tag{3.25}$$

$$2CO \rightarrow C + CO_2 \tag{3.26}$$

For this study the side reactions were not considered due to the catalyst selected because of the high selectivity to alkanes and alkenes. FT conditions are chosen in order to maximize the formation of higher molecular weight hydrocarbon, which form a higher value product ([63]).

The products and the hydrocarbons produced by this process vary with the H_2/CO ratio.

One of the main characteristic of FT synthesis is the liberation of large amounts of heat from the highly exothermic synthesis reactions [64]. The FT process, is analogous to the polymerization process, hence it shows a variety of reaction steps, such as chain propagation, chain branching, olefins and paraffins desorption, methanation and olefin secondary reactions of double bond shift and hydrogenation [64].

TABLE 3.9: Summary of reaction conditions with conversion and selectivity to CO for RWGS catalysts [41]

Catalyst	H_2:CO_2 ratio	Temperature (C)	Pressure (MPa)	Conversion (%)	Selectivity (%)
NiO/CeO_2	1:1	700	0.1	~40	~100
Cu/Al_2O_3	1:9	500	N/A	~60	N/A
Co/MCF-17	3:1	200-300	0.55	~5	~90
Pt-Co/MCF-17	3:1	200-300	0.55	~5	~99
Cu/SiO_2	1:1	600	0.1	5.3	N/A
Cu/K/SiO_2	1:1	600	0.1	12.8	N/A
Cu-Ni/$\gamma - Al_2O_3$	1:1	600	0.1	28.7	79.7
Cu-Fe/SiO_2	1:1	600	0.1	15	N/A
Li/RhY	3:1	250	3	13.1	86.6
Rh/SiO_2	3:1	200	5	0.52	88.1
Rh/TiO_2	1:1	270	2	7.9	14.5
Fe/TiO_2	1:1	270	2	2.7	73.0
Rh-Fe/TiO_2	1:1	270	2	9.2	28.4
Fe-Mo/$\gamma-$	1:1	600	1	~45	~100
Mo/$\gamma - Al_2O_3$	1:1	600	1	34.2	97
Pd/Al_2O_3	1:1	260	0.1	N/A	78
Pd/CeO_2	1:1	260	0.1	N/A	87
Pd/La_2O_3	1:1	260	0.1	N/A	70
CeO_2-Ga_2O_3	1:1	500	0.1	11.0	N/A
Pt/TiO_2	1.4:1	400	N/A	~30	N/A
Pt/Al_2O_3	1.4:1	400	N/A	~20	N/A
PtCo/CeO_2	3:1	300	0.1	3.3	71.0
Co/CeO_2	3:1	300	0.1	3.8	39.4
PtCo/$\gamma - Al_2O_3$	3:1	300	0.1	5.1	89.4
Co/$\gamma - Al_2O_3$	3:1	300	0.1	3.8	67.0
Mo_2C	3:1	300	0.1	8.7	93.9
Mo_2C	5:1	250	2	17	34
Cu-Mo_2C	5:1	250	2	13	40
Ni-Mo_2C	5:1	250	2	21	29
Co-Mo_2C	5:1	250	2	23	24

The product distribution is mainly affected by the chain growth probability parameter (α), so according to this value the quality and the characteristics of the biocrude differ. In order to produce a diesel fuel this factor should be between 0,85 and 0,9, as shown in figure 3.9 [65].

The FT process is catalytic, so different catalysts have been studied in literature [66], [67]. Usually the catalysts used are based on transition metals of iron, cobalt, nickel and ruthenium. The FT catalyst development has largely been focused on the preference for high molecular weight linear alkanes and diesel fuels production.

The activity depend on the H_2 adsorption capacity and on the reducibility of the other metal oxide components [67]. Between the metals mentioned, Ruthenium is one of the most active catalyst for the FT process operating at low temperature. It allows the production of long chain hydrocarbons without the need of any promoters. However, in industrial applications other catalysts are preferred due to its elevated cost [68]. Iron and Cobalt are thus the most suitable catalyst for this application. Fe has a very low selectivity to paraffins, promoting the production of olefins; it is convenient from an economic point of view but it deactivates more quickly than the Cobalt-based catalysts. On the other hand, Co has a good selectivity to paraffins,

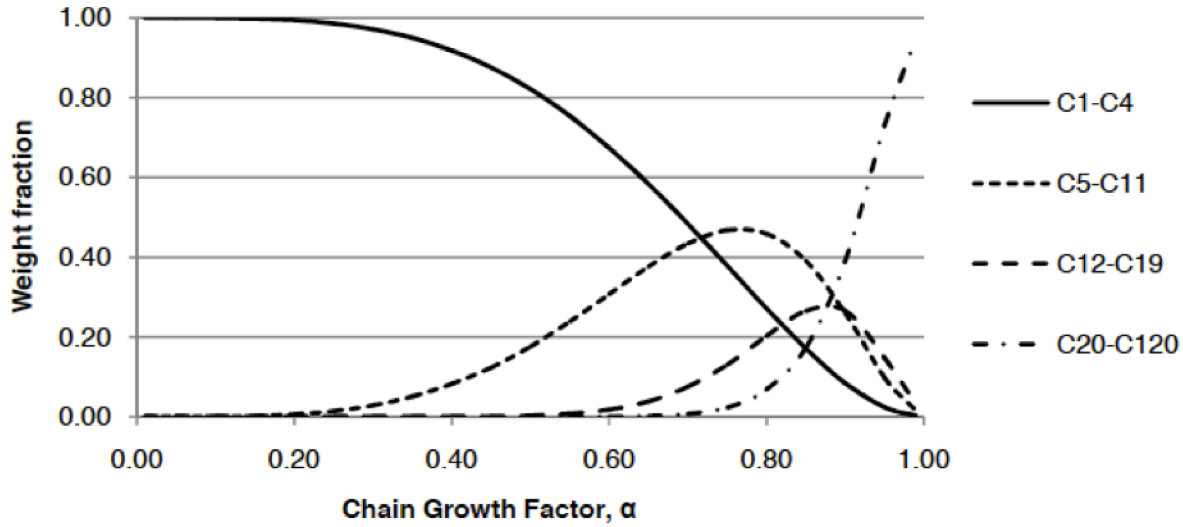

FIGURE 3.9: Fischer-Tropsch hydrocarbons distribution with the growth chain factor [65]

low selectivity to olefins and oxygen, it is more resistant to deactivation, but it is more expensive than Fe [68].

For this study an iron based catalyst was selected [69] due to its higher tolerance to sulfur content [59].

The parameter used to understand the hydrocarbon formation with the FT process is the chain growth factor (α) which can be evaluated with the equation 3.27. Figure 3.9 shows its influence in the distribution.

$$\alpha = (0,2332\frac{y_{CO}}{y_{CO}+y_{H_2}} + 0,633)(1 - 0,0039(T - 533)) \tag{3.27}$$

In equation 3.27 y represents the mole fractions of the compound and T is the temperature of the reactor expressed in Kelvin (K). This correlation is only dependent on H_2 and CO composition in the gas [38]. The methodology for the FT reactor design was based on the method used by Pondini [38]. It is based on a defined temperatures ($220°$), which implies a specific α value. The value of α selected (0.82) is the most suitable for diesel fuel production. The distribution of the different hydrocarbons due to the reactions occurring, and therefore the CO conversion implemented in the software, are based on the hydrocarbon selectivities on a Fe-based catalyst at $220°$ C, 15 bar and 72% conversion of CO found in literature [69]. A detailed calculation of the FT reactor is reported in appendix D. As a result it is obtain a crude which is mainly kerosene (C_{10}-C_{16}) and diesel (C_{17}-C_{22}).

3.2.4 Product separation

Figure 3.10 shows the flowsheet of the product separation unit.

The crude produced in the FT reactor needs to be treated in order to produce valuable bio-fuels. Therefore, a system to split the crude into the various distillates was modeled. Before entering the unit, the FT-Crude is fed to a three phases separator, were the crude is separated from the gas and from the water.

The composition of the FT-Crude allows to understand the distillates that can be produced (fig 3.11). From the graph, it is possible to notice that the main hydrocarbons found are from C_{10} to C_{22} . This is due to the reactor design which,

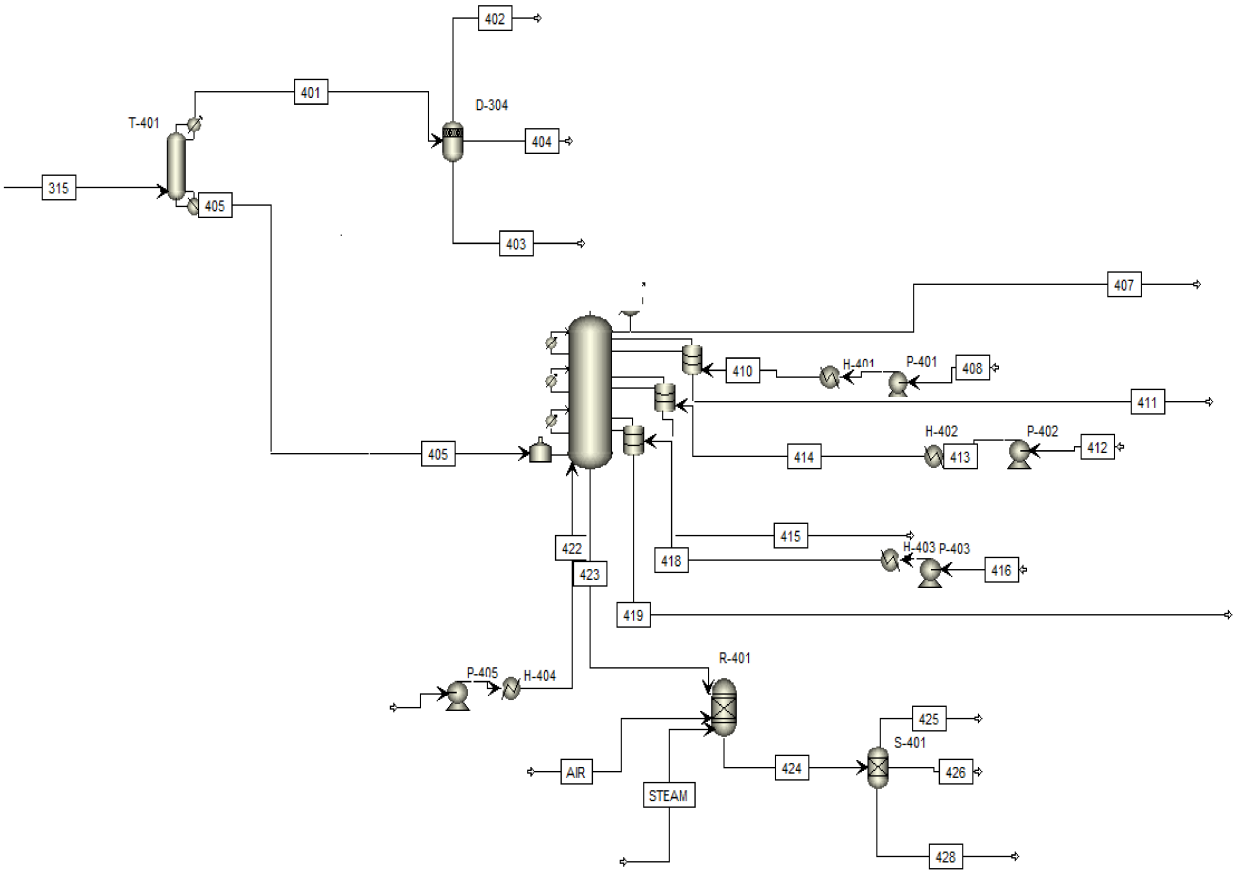

FIGURE 3.10: Snapshot of the product separation unit

as previously said, allows the production of a crude of mostly kerosene and diesel. In fact, depending on the carbon number, each hydrocarbon can be distillate in a specific fraction, for instance hydrocarbons C_{10}-C_{16} are found in the kerosene and C_{17}-C_{22} in the diesel fraction.

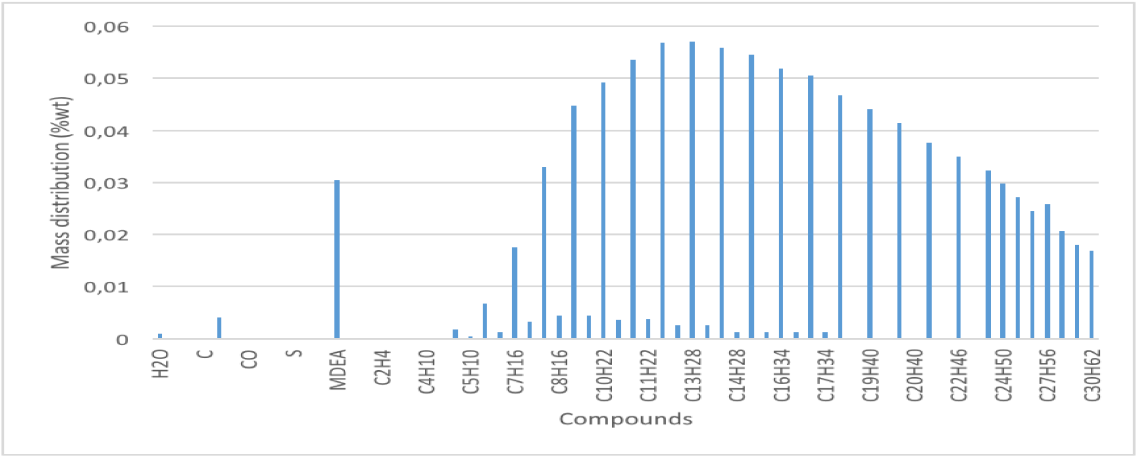

FIGURE 3.11: Hydrocarbons distribution in FT-Crude (%wt)

The separation in multiple distillates is modeled in three steps:

1. Light Naphtha and water separation
2. Production of Heavy Naphtha, Kerosene and diesel
3. FCC for gasoline production from the fractionation column residuum

For each step the appropriate parameters have been evaluated.

Light Naphtha and water separation

In this step a distillation column (T-401) with total condenser and partial reboiler was modeled. A snapshot of the *Light Naphtha and water separation* section is shown in the left top part of figure 3.10. The Distillate to Feed Ratio and the Reflux Ratio were varied until all the Light naphtha hydrocarbons were found in the top stream and the heavier ones remained in the bottom to be fed to the fractionation column. The column was modeled of 25 stages with a Kettle reboiler and a total condenser. After the column a separator was modeled to separate the light naphtha from the water and the off-gas (D-304).

Production of Heavy Naphtha, Kerosene and diesel

In this step a atmospheric fractionation column (T-402) was designed to separate the distillates. The *Production of Heavy Naphtha, Kerosene and diesel* section is shown in figure 3.10. The distillate that can be extracted from the column are based on the carbon number.

- C_1 - C_4: Light Naphtha
- C_5 - C_9: Heavy Naphtha
- C_{10} - C_{16}: Kerosene
- C_{17} - C_{22}: Diesel
- C_{22+}: Waxes

In petroleum refining the boiling points are used to characterize a fraction instead of mass and molar distribution. The curves used to describe the boiling point temperature for % of distillate are the True Boiling Point (TBP) and the ASTM D86 [70]. For modeling purposes, these curves, which were used in the streams specification for the fractionation column, were evaluated from the *Stream Analysis* tool of Aspen Plus®.

Both the fractionation and the FCC unit were simulated on a different Aspen flowsheet due to the characteristics of the distillates. The method to calculate the frictions is to break them into pseudocomponents that have their own Specific Gravity (SG), API Gravity and Molecular weight [42]. The crude fed to the column was then defined as Blend of the different pseudocomponents knowing their mass fraction in the crude. For petroleum fractionation, usually it is specified along with the TBP, the sulfur content curve. In our case the sulfur content was reduced in the AGR Unit to approximately zero, therefore its curve was not taken into account.

The column was modeled as a 25-stages column with a furnace, three strippers and one pump around. The furnace has the aim to partially vaporize the feed. It was located almost at the bottom, at the stage number 22 and at temperature of 370°

that allows the vaporization of ~70% of the feed (data taken from literature [71]) The three strippers allow the removal of the distillates. To model the strippers it was necessary to evaluate the amount of each distillate that was possible to strip and extract from the column: this calculation was easily made knowing the hydrocarbons composition of the distillate and their content in the feed stream. To allow the extraction of the frictions, a stripping vapor stream is necessary for each stripper and also at the bottom of the column. The vapor entering the strippers is at 200°C and 4 bar.

The mass flows of the stripping vapor stream were evaluated knowing the quantity of each distillate that can be stripped in each stripper from the graph 3.12 [71].

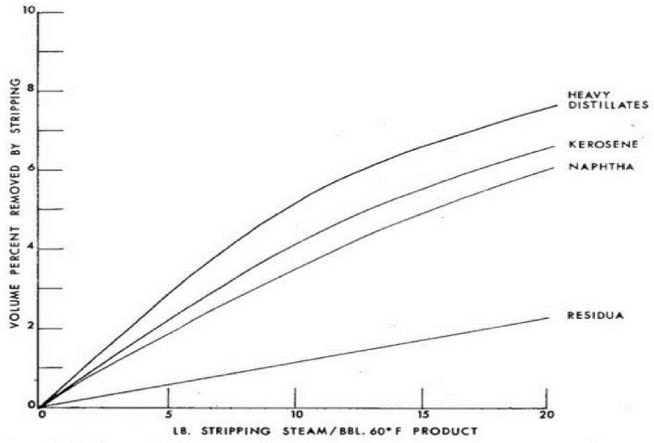

FIGURE 3.12: stripping vapor [71]

The C_{22+} hydrocarbons, the waxes, are found in the bottom stream as residuum to be fed to the FCC step.

Fluid Catalytic Cracking

Fluid Catalytic Cracking (FCC) is a process that allows the cracking of the high hydrocarbons present in the residuum into gas and gasoline. It is used in Petroleum refinery to convert heavy gas oil into more valuable lighter hydrocarbon products. The conversion happens because of the catalytic cracking of the heavy gas oil on the catalytic surface. The catalytic cracking reaction is carried out in a short contact-time vertical reactor called the riser: the reactor is a fluidized bed in which the residence time of the catalyst-hydrocarbon mixture is just for few seconds. A steam stream, normally around 5% of the oil, is fed along with the residuum to allow the conversion [72]. After the reaction, the catalyst needs to be regenerated and this step can happen by combusting the formed coke with air [43]. A schematic representation of the FCC unit is shown in figure 3.13

To model this step, the reactor yields were taken from the literature. The snapshot of the block is shown in figure 3.10. Various studies were made on how the yields change with temperature; the temperature condition chosen for this study was 221°C and 2.9 bar. As a result, the gasoline, gas, coke and residuum yield were inserted in RYIELD (table 3.10)[43].

For the Aspen Plus®modeling, a RYIELD reactor was used with the yields shown in table 3.10.

For modeling purposes, Gasoline, Gas, Coke and residuum were inserted as pseudocomponents in Aspen properties. For each pseudocomponent the appropriate parameters were inserted: for Gas and Coke the molecular weight and the

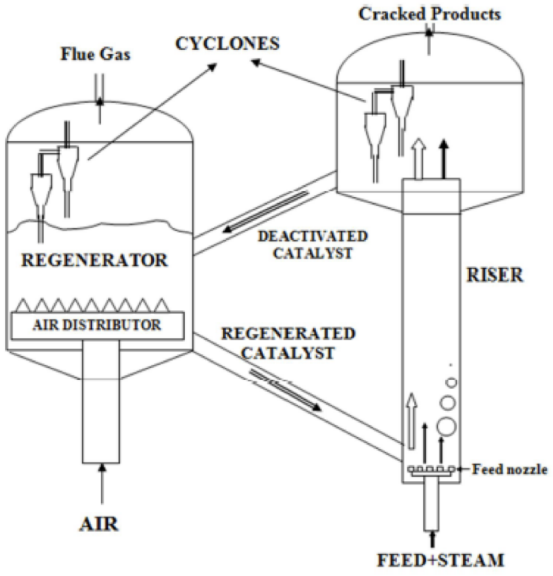

FIGURE 3.13: Schematic representation of FCC Unit [43]

TABLE 3.10: FCC yields al 221°C [43]

Gasoline	0.56
Coke	0.07
Gas	0.18
Residuum	0.18

normal boiling point (NBP) and for Gasoline and residuum the NBP and the API Gravity. In the Yield reactor were fed also the vapor stream needed from the reaction and the air stream for the catalyst regeneration in order to simulate the correct utility needed from the block. Consequently the coke produced in the riser reactor does not exit from the block because it is combusted through air during the regeneration of the catalyst.

3.3 Energy Analysis

The energy analysis was made through the pinch point analysis that allows the understanding of the loads required from the plant. The Energy Analysis tool gives an information on the amount of energy that can be saved, so the amount of heat that can be recovered along the plant. Aspen Energy analyzer is used to calculate the maximum energy recovery of the plant based on the temperature-heat duty profile. Due to the characteristic of the combustible streams exiting from the plant (streams *219* and *230*) a boiler was designed to recover the heat. For modeling purposes the boiler was simulated as a RGIBBS that simulates the complete combustion of the compounds and it was assumed adiabatic working conditions ($Q_{losses} = 0$). Table 3.11 shows the composition of the streams before and after combustion. To control the air to fuel ratio it has been used a *Design Specification*. For modeling purposes it has been designed in order to have a O_2 %wt in the outlet stream of 6%. Furthermore, it has been assumed a preheated air stream at a temperature of 450°C. To recover at maximum the heat load available, the flue gas stream (*502*) is cooled to the pinch point and then to 120°C. Figure 3.14 shows the flowsheet of the utility unit.

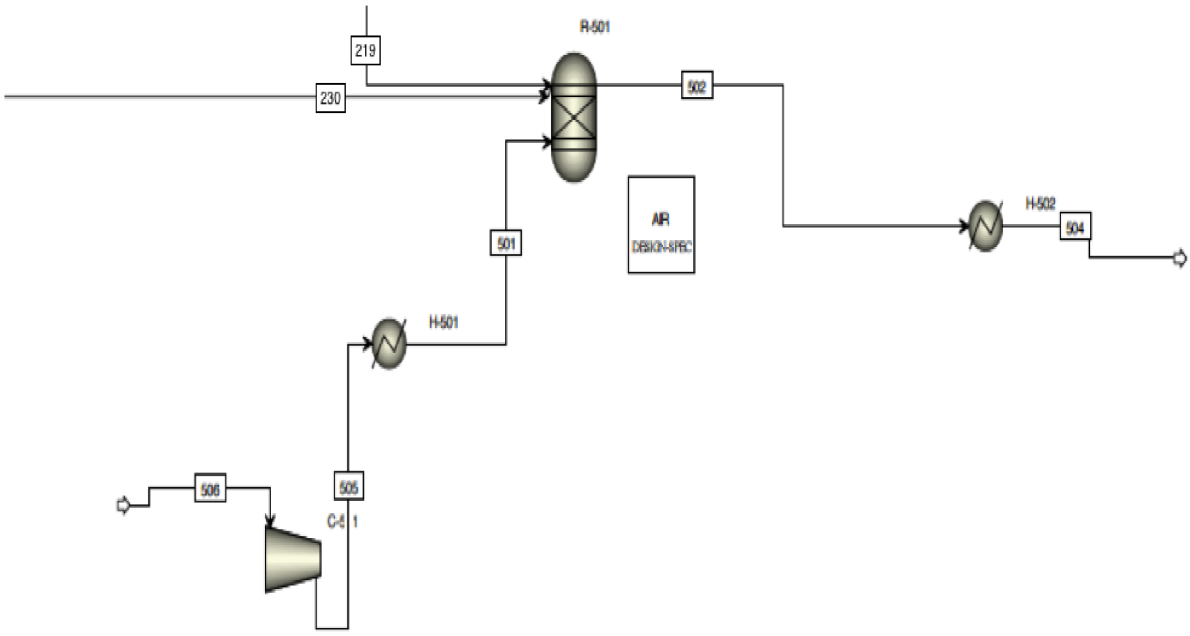

FIGURE 3.14: Snapshot of utility unit

TABLE 3.11: Composition of combustible and combusted streams (%wt)

	219	*230*	*502*
H_2O	1.9	0.2	8.8
H_2	6.9	4.2	0
N_2	12.5	14.1	75.7
CO_2	0.2	0.1	9.6
CO	1.1	34.3	0
CH_4	77.3	38.4	0
O_2	0.1	4.7	6.0

For the endothermic reactors of the plant, for instance the SCWG and the RWGS, the temperature working condition needs to be maintained through a heating jacket. For modeling purposes, the heating jackets were represented as heat exchangers that simulate the heat load required by the reactor to maintain the correct working condition. It has been considered a ΔT of 15°C for the stream crossing the heating jacket. Figure 3.15 shows a snapshot of the Heat Jacket modeled in Aspen plus®.

The overall plant conversion from solid biomass to liquid fuel product is defined on energy basis with biomass to liquid efficiency (BtL) as shown in equation 3.28 (from Ref. [44]).

$$\eta_{BtL} = \frac{q_{HHV,product} m_{product}}{q_{HHV,biomass} m_{biomass}} \tag{3.28}$$

The global plant thermal efficiency can be evaluated through equation 3.29 (from Ref. [44]).

$$\eta_{thermal} = \frac{q_{LHV,products} m_{product}}{q_{LHV,biomass} m_{biomass} + P} \tag{3.29}$$

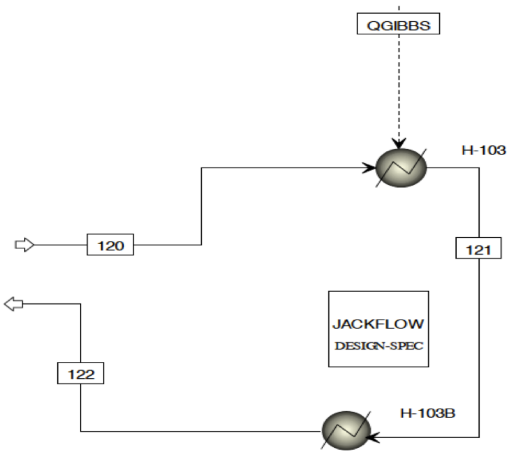

FIGURE 3.15: Snapshot of the modeled Heating Jacket in Aspen plus®for the SCWG reactor

In the equations, q represents the heating values (MJ/kg), m the mass flow (kg/s) and P represents the power consumed by the plant (MW).Tthe efficiency of a fuel conversion to power was not taken into account because the power is purchased offsite (e.g. grid). The vinasse heating value was calculated based on the Boie correlation, as shown in equation 3.1. The heating values of the products were evaluated through Aspen Plus®by simulating complete combustion in a Gibbs reactor. The results obtained were thus compared to the one found in literature (see table 4.3).

The thermal efficiencies values were evaluated after the design of the heat exchanger network which was realized through the tool Aspen Energy Analyzer.

Heat exchanger network

The Aspen Energy analyzer tool gives the recommended design of the heat exchanger network in order to meet the load targets. Thus the solution suggested represents an ideal system not always optimal from an engineering point of view. For this study the simulation was at first ran without restrictions. This means that aspen evaluates the recommended design allowing every combination of streams in order to reach the targets. Secondly, the simulation was run with some restrictions on the areas, therefore the stream combination was allowed only among same section (for instance a stream from unit 1 can give load only to streams of the same unit). The results obtained are shown and commented in chapter 4.

3.4 Techno-economic assessment

The techno-economic assessment attempts to establish the economic feasibility and profitability of the plant. The evaluation was realized based on the methodology used is Ref [73]. It determines the minimum selling price of the final product taking into account operational and capital costs considering a plant lifetime of 20 years. The Total Capital Investment (TCI) was evaluated through several assumptions as shown in table 3.13. It consists of the sum of Fixed Capital Investment (FCI) and Other outlays. The FCI includes the Direct Costs (DC), which were evaluated evaluated as the purchased equipment cost (PEC) of the total units of the plant multiplied by a installation factor, and the indirect costs which depends on the total direct costs. The contingency is thus evaluated as a percentage of the FCI. As illustrated in table

3.13, Other outlays consist of startup costs, working capital, costs of licensing, research and development which depends on O&M costs, DC, FCI and Land cost. The PEC was evaluated in two different ways. For the standard units, for instance vessels, pumps, compressors, the Aspen plus®Economic tool was used. This gives an information of the purchase and installation cost in US dollars. The rest of the units, for instance the SCWG process, the RWGS, the FT, were adapted from literature data (table 3.12). The purchased cost associated to the mixing tank at the beginning of the process (block M-101) was evaluated with the Guthrie method. The costs were brought to the start of construction year (2017) through the Chemical Engineering Plant Cost Index (CEPCI) with equation 3.30.

$$PEC_{2017} = PEC_{Ref.year} \frac{CEPCI_{2017}}{CEPCI_{Refyear}} \tag{3.30}$$

The capacities of the reference were adjusted to the process ones through equation 3.31.

$$PEC_{process} = PEC_{Ref}(Capacity_{process}/Capacity_{Ref})^{\alpha} \tag{3.31}$$

α represents the escalation factor which varies between 0,6 and 1 depending on the equipment type [44].

TABLE 3.12: Capital cost of non-conventional equipment

Equipment	Reference	Escalation factor	Year of Ref.	Capital Cost used (k€)
SCWG	[30]	0,6	2007	202
Cyclone	[74]	0,6	2014	0.71
Ash storage	[35]	0,6	2007	0.005
PSA	[75]	0,55	2016	55
LO-CAT	[35]	0,67	2007	153
RWGS	[76]	0,65		269
FT	[75]	0,75	2016	18
FCC	[77]	0,6	1998	16
Boiler	[78]	0,6	2016	186

The capital costs values reported in 3.12 are referred to Case 1.

A more detailed description of the TCI evaluation is shown in table 3.13.

The operational and maintenance costs (O&M) are divided into fixed and variable: the fixed include the employee salaries and benefits, overhead and insurance.

The variable cost depend on the annual operational time which was set at 8000 hours. This value includes the purchase of the material streams: feedstock (vinasse is considered a waste by-product with no associated purchased cost), solvent and process water (a 10% make-up was assumed for both), utilities and cost related to the replacement of the catalysts. The costs related to the O&M costs are detailed in appendix F. The escalation rate was evaluated based on the changing price of the products between 2000 and 2017 in Finland. As shown in 3.14 it was assumed a straight line depreciation, which consists of computing depreciation and amortization by dividing the difference between an asset's cost and its expected salvage value by the number of years it is expected to be used (equation 3.32). The salvage value of the plant was then assumed equal to zero.

$$StraightLineDepreciation = \frac{PurchasePrice - ApproximateSalvageValue}{EstimatedUsefulLife} \quad (3.32)$$

Table 3.14 shows all the economic assumptions made.

To evaluate the Net Present Value (NPV), the selling prices of each product need to be analyzed which varies through the years as illustrated in the figure 3.16.

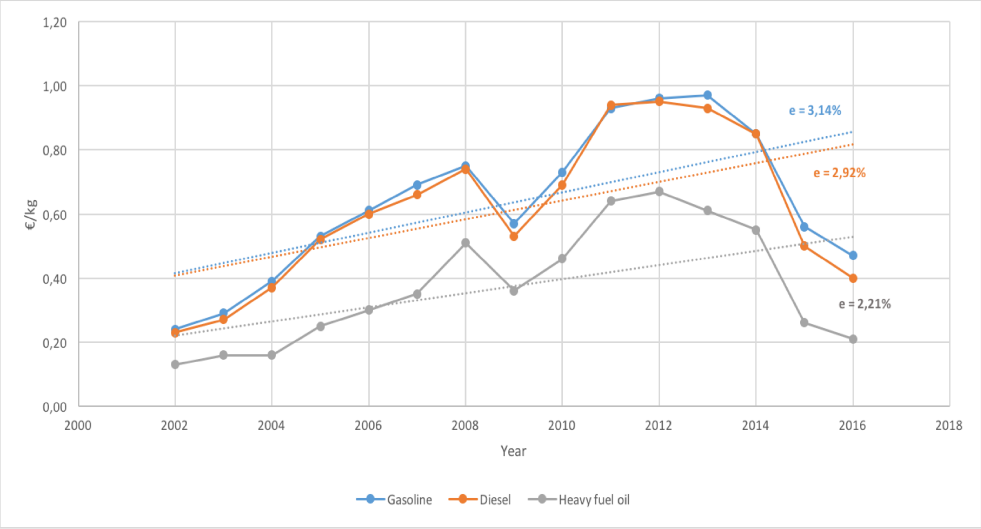

FIGURE 3.16: Prices of the major products over the years in Finland (€/kg) [79]

For the Kerosene and the LPG the prices selected were taken from year 2017 as average in Europe [80], [81].

TABLE 3.13: Steps for the TCI evaluation [73]

Fixed Capital Investment	
Onsite costs	
Purchased equipment cost	PEC
Piping	35 %PEC
Instrumentation and controls	12%PEC
Electrical equipment and material	13%PEC
Offsite costs	
Land	6% PEC
Civil, sxtructural and architectural work	21%PEC
Service facilities	35%PEC
Total direct costs (DC)	Onsite + Offsite
Indirect costs	
Engineering and supervision	8%DC
Construction costs and contractors profit	15%DC
Contingency	15% of Direct+indirect costs
Other outlays	
Startup costs	$\frac{Costoffixed O\&M}{Month} + \frac{Costofvariable O\&M}{6} +$ 2%(FCI-Land)
Working capital	$\frac{Fuelcost}{6} + \frac{Costofvariable O\&M}{Month} +$ Cost of fixed O&M*1.25
Costs of licensing, research and development	2%DC
Total Capital Investment	TCI

TABLE 3.14: Techno economic analysis assumptions

Economic assumptions	
Return on investment	10%
Project life time	20 years
Capacity factor	91%
O&M escalation rate	3% except for electricity (0,34%)
PEC/TCI ratio	0.3
- Case 1	29%
- Case 2	30%
Contingency	15% of Total direct cost, Engineering and supervision and Construction costs
Equity	100%
Average labor cost	36000 euros per year
Number of employees	30
Overhead & insurance	1,5% TCI
Straight line depreciation	
No salvage value	
No fuel cost	
All construction costs are escalated to 1^{st} year operation	

Chapter 4

Results and discussion

4.1 Carbon recovery

Figure 4.1 shows the carbon distribution in the outputs of the plant. Only ~14% of the carbon is recovered in the product, therefore the carbon losses are high. However, ~42% of the carbon is recovered as combustible gas which covers the heating load required by the whole plant, leading to the absence of an external hot utility to the plant. One of the limiting factor for the carbon recovery in the product is the low CO_2 conversion in the RWGS reactor. In fact, as shown in figure 3.9, the catalyst selected allows a conversion of 40%.

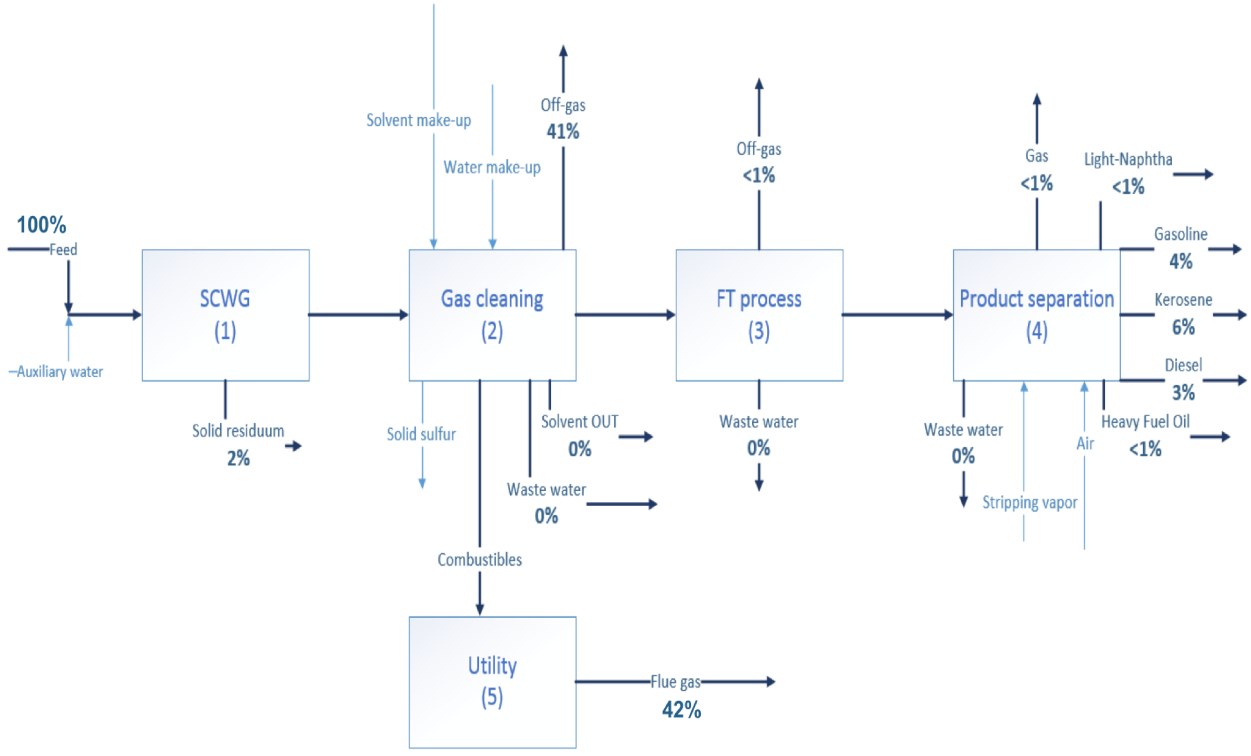

FIGURE 4.1: Carbon partitioning in the plant

All of the combustible gas is used as hot utility. This stream is mainly composed of methane (~45%mol) and hydrogen (~35%mol) if we consider both the stream exiting the PSA system (stream *219*) and the Scrubbing system (stream *230*). This was modeled so that the excess heat load can generate High Pressure steam, and thus partially cover the duty (kW) required by the equipment of the plant (pumps and compressors). As an alternative, the excess methane could be split before entering the boiler and then it could be evaluated as product of the plant (SNG) or it could be

Steam Reformed in order to produce CO, one of the main reactants of the FT process. However this solution would lead to a higher cost of the electricity utility which in this case is partially covered by the HP steam generated. With the design selected for this study, the plant is self sufficient. This means that the heat recovered from the combustible gas is sufficient to cover the heat demand required by the plant and no external utility is needed.

The off-gas is ~41% of the carbon which exits the plant as CO_2 mainly (~70%mol) with a minor content of water (~18%mol) and H_2S (~4%mol). The carbon recovery is limited by the presence of H_2S: their solubilities are different but similar, therefore the more CO_2 we manage to recover, the more H_2S ends in the stream going to the RWGS step.

The 2% of carbon going in the solid residuum stream shown in the diagram (4.1) is the non-reacted carbon from the feedstock. In fact it was made as assumption that 98% of the carbon entering the SCWG step reacts to form the syngas, and the rest is assumed to leave the plant as solid residuum with the ashes. Sensitivity analysis conducted throughout the design of gas cleaning process units enabled the near elimination of carbon losses in the waste water or solvent recovery streams. For this reason they both were thought to be recycled with the evaluation of a periodical replacement of the make-up due to the impurities content. The carbon contained in the FT crude is then split into the different fractions where, as illustrated in the diagram 4.1, the kerosene is the main product. To have a more efficient description of the carbon partitioning within the products is necessary to analyze the product characteristics.

4.2 Product characteristics

The objective of the thesis is to produce transportation liquid fuels, therefore the product distribution should be evaluated. As shown in figure 4.2 the major product obtained from the plant is the Kerosene, which is around 40% of the FT crude. Furthermore, it is possible to notice that still a valuable percentage of the crude is fractioned as Diesel (~22%) and gasoline (~28%), which are also the most valuables in terms of consumption. This characteristic is mainly caused by the catalyst of the FT process and the α parameter which affects the hydrocarbons distribution.

As explained in the chapter 3 chapter the way to evaluate the characteristic of a distillate is through the TBP curves.

The graph 4.3 shows the Temperature Boiling Point curves for each product. It is possible to notice that heavier fractions, and therefore the heavier hydrocarbons, have a higher TBP curve and thus the temperature necessary to extract a certain distillate percentage is higher.

Consequently, it is possible to compare the TBP of each fraction with the ones found in literature for the petroleum crude [71] shown in figures 4.4, 4.5, 4.6. The graphs show the percentage of distillate that can be extracted at a specific temperature.

The difference found between the curves of the model and the one of the Literature are due to the different crude fed to the fractionation unit. In fact, the values reported in literature are referred to the Petroleum crude which has different characteristics than the FT crude. In each graph (4.4, 4.5, 4.6), the blu line represent the value reported in literature for the Petroleum crude. It is possible to notice that the TBP literature curves are higher than the ones evaluated for this study. This is mainly caused by to the higher presence of impurities in the streams, for instance sulfur and

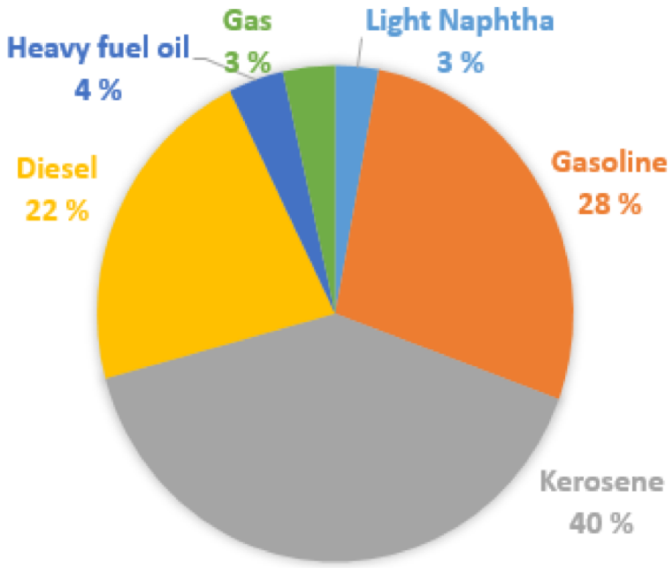

FIGURE 4.2: Product distribution

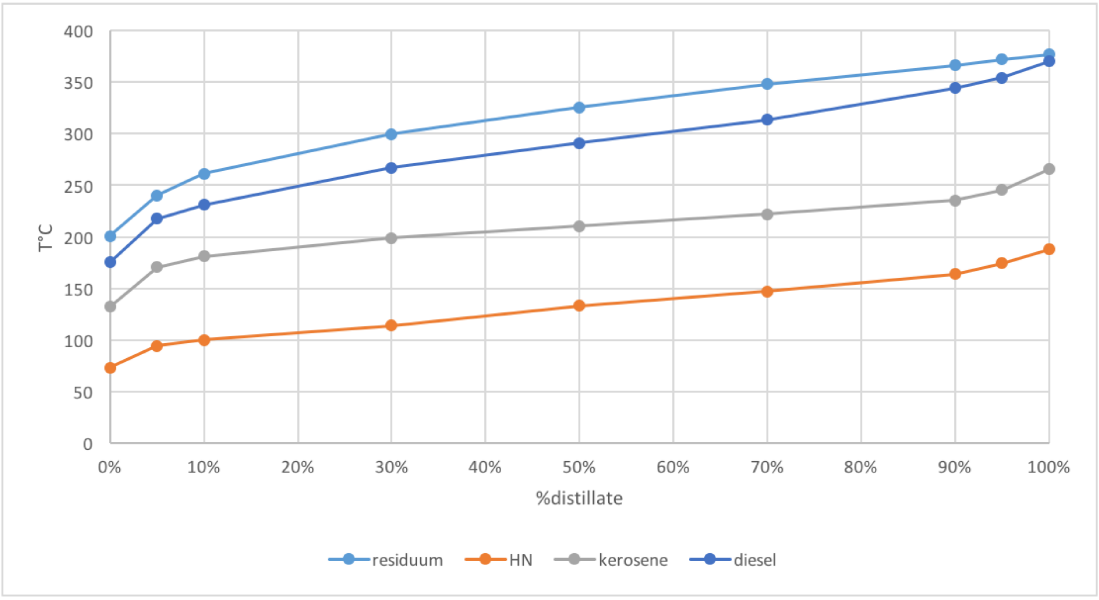

FIGURE 4.3: TBP curves of the fractions

oxygen, which affect the boiling point. For example, in figure 4.5 is shown that a 90% distillate of Petroleum crude can be extracted at ~270°C, while for the kerosene obtained from this study the value is lower (~240°C). Therefore for the Petroleum fractions a higher load is required to obtain the same percentage of distillate.

4.3 Energy analysis

4.3.1 Thermal performance assessment

The grand composite curve (figure 4.7) from the pinch analysis illustrates the maximum heat recovery and minimum utility demand (table 4.1). In the figure the upper

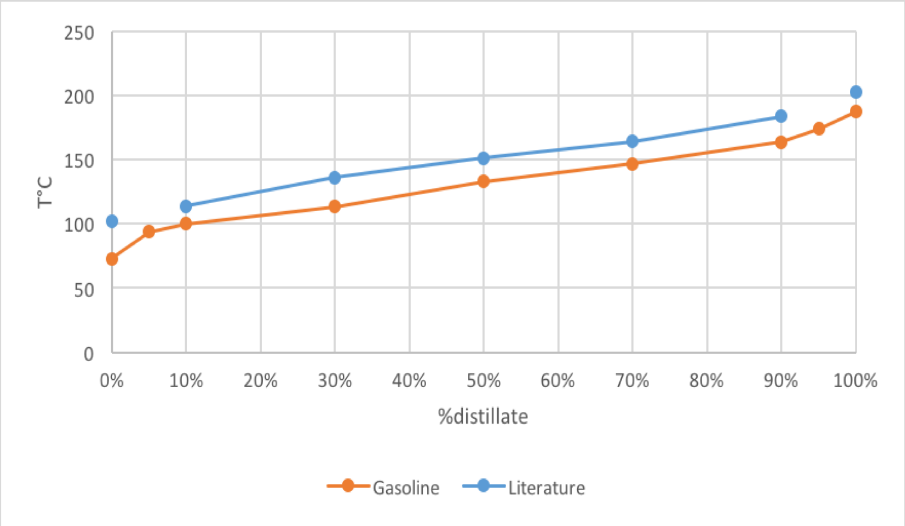

FIGURE 4.4: TBP of gasoline from simulation VS from literature [71]

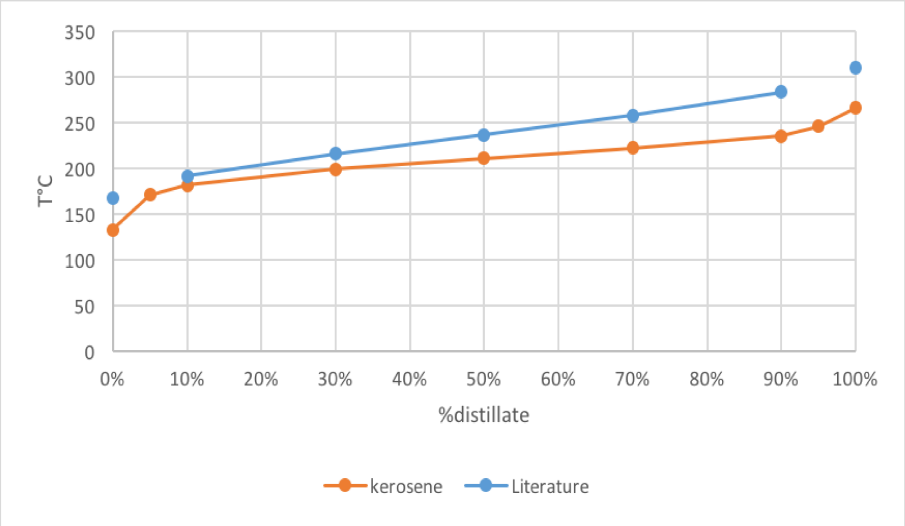

FIGURE 4.5: TBP of Kerosene from simulation VS from literature[71]

curve represents the flue gas from the Utility unit. The other curves (highlighted in the box in figure 4.7) represent multiple streams. It is relevant to notice that the main heat load, besides the flue gas, is given from the Syngas, and the major demand comes from the feedstock pre heating. The heat exchanger network was designed with Aspen Energy Analyzer and, as a result, two different scenarios were selected. With this configurations, it is possible to cover all the heat load required, therefore no external hot utility is needed. On the other hands, the cooling load is high and thus a large amount of cold utility is required. What emerged from the Aspen Energy Analyzer tool is that Cooling water is sufficient, and there is no need for a refrigerant. At the same time it is possible to produce a certain amount of High Pressure (HP) steam due to the high temperature of the Syngas.

As illustrated in the chapter 3, the HHV of the feedstock on dry basis was evaluated through the Boie correlation. From that the HHV on wet, on dry-ash free basis were calculated and the LHV of the biomass were calculated. To evaluate the heating value of the product it was used on Aspen Plus a RGIBBS reactor working at 25°C and 1 bar to simulate complete combustion. The heating values calculated are

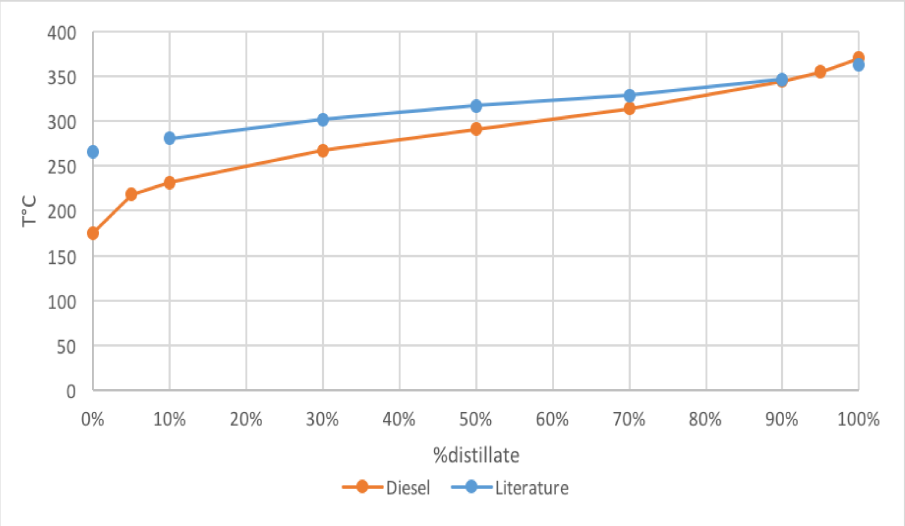

FIGURE 4.6: TBP of Diesel from simulation VS from literature[71]

TABLE 4.1: Target loads of the plant

Heating load	MW	0
Cooling load	MW	7.82

shown in table 4.2. The heating values shown for the stream named *Product* represent an average between the heating values of the different products.

TABLE 4.2: Heating values of Biomass and Product

Biomass		**HHV**	**LHV**
Wet basis	MJ/kg	7.45	5.68
Dry basis	MJ/kg	14.66	13.53
Dry ash-free basis	MJ/kg	20.99	19.38
Product		**HHV**	**LHV**
	MJ/kg	44.05	41.02

Table 4.3 shows the comparison between the heating values of the different products evaluated with Aspen plus®and the values reported in the literature [79]. In the table only the main products are present; the residuum and the light naphtha were neglected because their low amount in the product (as shown in figure 4.2).

The thermal efficiencies of the plant were evaluated after the design of the heat exchanger networks.

Heat exchanger networks

The heat exchanger networks design are reported in Appendix E. In the first case, illustrated in figure E.1, the configuration requires the use of 33 units among which nine use external utilities.

The first solution has limitation from a practical point of view. This because the energy integration is realized between streams of different sections of the plant. Therefore a second simulation was run with some restrictions on the areas, therefore the stream combination was allowed only among same section (for instance a stream

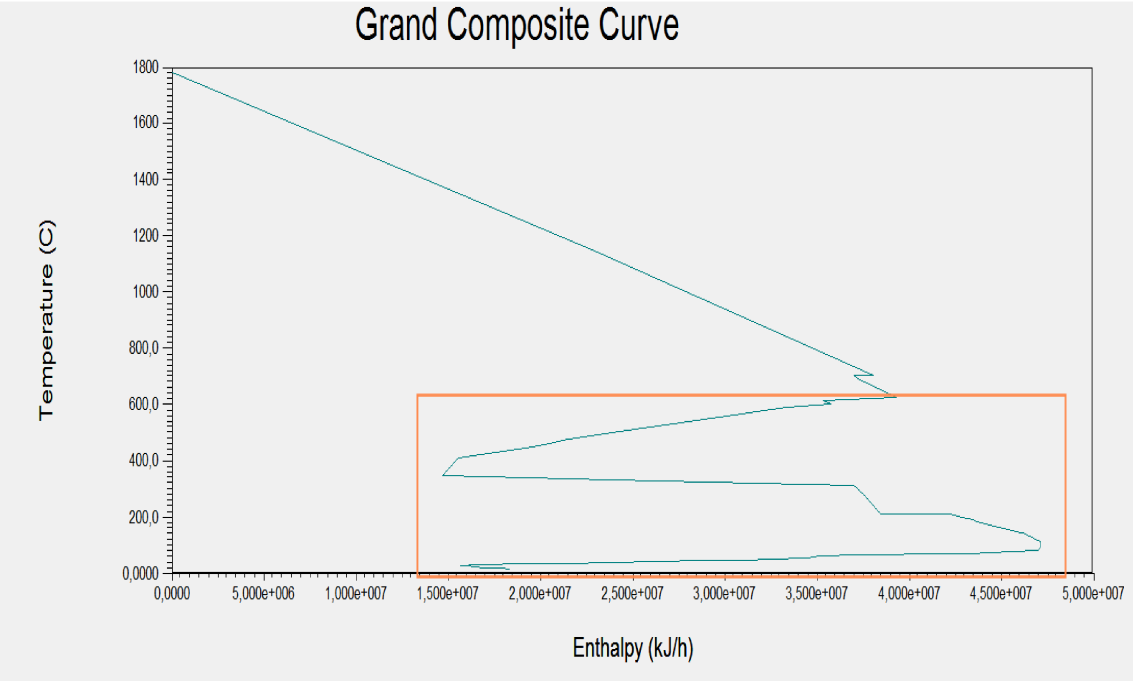

FIGURE 4.7: Grand composite curve

TABLE 4.3: Lower heating values from Aspen Plus®vs values from literature [79] for the main products

Product	LHV_{Aspen}	$LHV_{Literature}$
	MJ/kg	MJ/kg
Gasoline	43.2	41.9
Kerosene	42.6	43.3
Diesel	42.7	42.9

from unit 1 can give load only to streams of the same unit). As a result, in this case 34 units are required leading to a higher capital cost of the network. Figure E.2 shows the heat exchanger network of the second scenario.

The process streams that require the major amount of load are the hot syngas (*109 to 110*) and the feedstock stream that need to be pre heated (*104 to 105*). It is possible to notice (figure E.1) that in the first configuration the syngas should go through ten exchangers to meet the requirements, and stream *104 to 105* through eight exchangers. This makes the first configuration less feasible from an industrial point of view respect to the second case. In fact, in figure E.2 it shown that the syngas should cross six exchangers and stream *104 to 105* four. Hence the amount of units needed from these streams is lower than in the first case. This represents a more realizable configuration on a practical point of view, even though it should be optimize to reduce more the amount of heat exchangers for each stream. On the other hand, the second case leads to a lower production of high pressure steam, therefore the electricity required from external units is higher. This leads to a higher operational cost compared to case 1 (see section *Techno economic assessment results*).

At this point, the efficiency values were evaluated. Results are shown in table 4.5. They refer two different cases based on the two heat exchanger networks evaluated for the study (see section *Heat exchanger network*).

TABLE 4.4: Case1 vs Case 2

	Case 1	Case 2
Capital cost (M€)	51	77
Units	33	34
Number of syngas exchangers	10	6
Number of exchangers for feedstock preheating	8	4
HP steam production	Higher	Lower

TABLE 4.5: Thermal efficiencies (on biomass wet basis) results

η_{BtL}	16.97%
$\eta_{Thermal-Case1}$	20.72%
$\eta_{Thermal-Case2}$	20.72%

The low efficiency values are mainly due to the low recovery of the carbon into the product (~14%). If, for instance, we compare this result to a Hydrothermal liquefaction of lignocellulose residues we can see that the thermal results found from Magdeldin et al. [82] are higher: the thermal efficiency of the plant is around 30%. The efficiency obtained are significantly lower than the one reported in 2.5, although it is important to notice that those efficencies were associated with the SCWG of biomass. In this study, the product obtained from the SCWG process block has been further treated for liquid fuel production. Therefore it necessary to compare the results in table 4.5 also with biomass to liquid production processes. Trippe et al. [47] studied the biomass to liquid conversion via Dimethyl Ether (DME) and via FT synthesis from a syngas obtained through conventional gasification. The energy efficiency associated to this process ranged around 38%. The value is higher than the ones in table 4.5; one reason could be because of the working conditions of the supercritical water gasification system who require a great energy load. Moreover, in this study a RWGS reactor was designed before the FT process block differently from the work of Trippe et al. [47]; this step requires a significant energy load due to the high temperature working condition. Zhu et al. [83] made a techno-economic analysis for the thermochemical conversion of biomass to liquid fuels. They evaluated several pathways for fuel production from biomass and made a comparison among the results obtained (table 4.6).

TABLE 4.6: Thermal efficiencies reported in ref. [83] for different biomass to liquid pathways

Ethanol via Mixed Alcohols	41-45%
Methanol to Gasoline	44-46%
FT diesel	40-46%
Ethanol via acetic acid	55-58%
HTL	63%
Fast pyrolysis	64%

What emerges from the work of Zhu et al. [83] is that the processes with higher overall conversion, for instance methanol and DME, have better thermal efficiency than lower conversion synthesis cases, such as FT diesel. However, all the cases

in table 4.6 show a higher thermal efficiency than the one evaluated for this study. Many factor could be the cause of this result, first of all the low carbon recovery into the product. Secondly could be the complexity of the plant and the high energy demand due to the high pressure and high temperature working conditions for more than just one block.

4.4 Techno economic assessment results

The annual costs associated to each case are reported in table 4.7. From this table it is possible to notice that the cost related to the second case, the restricted one, is higher than the other. This is due to a higher number of exchangers and also to the lower amount of HP steam generated and therefore the higher power demand of the plant.

TABLE 4.7: Costs associated to the two cases

Case 1		
TCI	M€	51.5
Fixed O&M	M€/year	3.5
Variable O&M	M€/year	4.7
Case 2		
TCI	M€	77
Fixed O&M	M€/year	3.5
Variable O&M	M€/year	5.1

The external power required is indeed lower in case 1 than in case 2 due to the HP steam generation. Mid results are shown in table 4.8.

TABLE 4.8: Power demand of the plant

Case 1		
Power consumed	MW	2,03
HP steam	MW	-1,88
Power required	MW	0,14
Case 2		
Power consumed	MW	2,03
HP steam	MW	-1,26
Power required	MW	0,76

With the value of the amount of fuel produced every year, it was possible to evaluate its minimum selling price to reach the break even point. Results are shown in table 4.9.

The cost contribution (%) to total product cost is shown in figure 4.8 and 4.9. The first (4.8) allows to understand the contribution of each unit to the product cost. The second one (4.9) illustrates how much the capital cost and the operative costs effect the minimum selling price of the product.

TABLE 4.9: Minimum Selling Price (MSP)

Case 1		
Total Price per kg of product	€/kg	4.28
Total Price per bbl of product	€/bbl	584.4
Total Price per MWh of product	€/MWh	360.2
Case 2		
Total Price per kg of product	€/kg	5.72
Total Price per bbl of product	€/bbl	780.72
Total Price per MWh of product	€/MWh	481.25

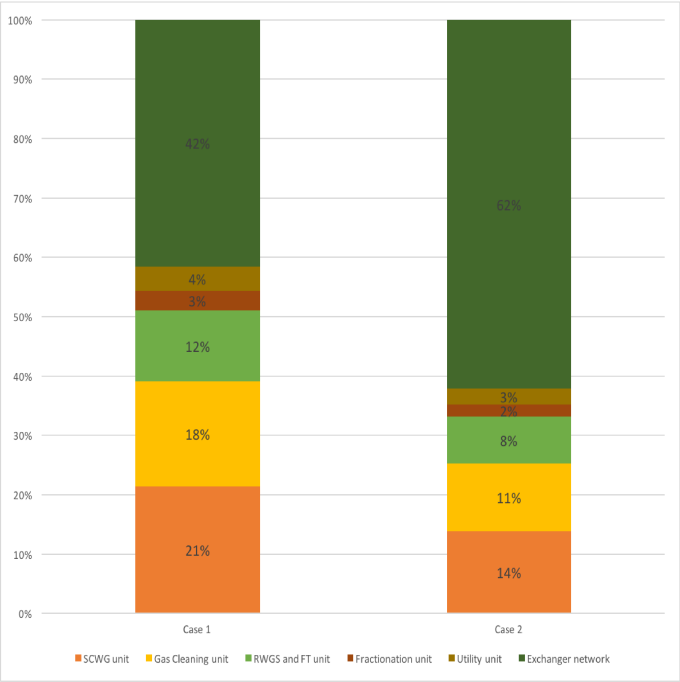

FIGURE 4.8: Cost contribution of each unit (%) to total product cost

The graph 4.8 shows that the major cost contribution to the Purchased equipment cost is given by the heat exchanger network (~42% for case 1 and ~62% for case 2). Secondly to that, the principal cost related to the purchased equipment is due to the SCWG unit. Therefore, although hydrothermal treatment offers efficient heat recovery compared to losses in evaporative process, the cost associated to the heat recovery is significantly high. Figure 4.9 highlights that in both cases the major contribution to the production cost is the capital carrying charges. This is due to the high cost of the units and the especially to the heat exchanger network, which affects the capital cost due to the difference in number of units. It is possible to compare the MSP obtained with the values found in literature for other processes of biomass conversion into liquid fuels (table 4.10).

The values reported in table 4.10 refer respectively to a Hydrothermal Liquefaction of lignocellulose residues and a fischer tropsch for liquid fuels production rescaled to year 2017. It is clear that the production cost related to the cases of this study are much higher than the others. This is due mostly to the low recovery of

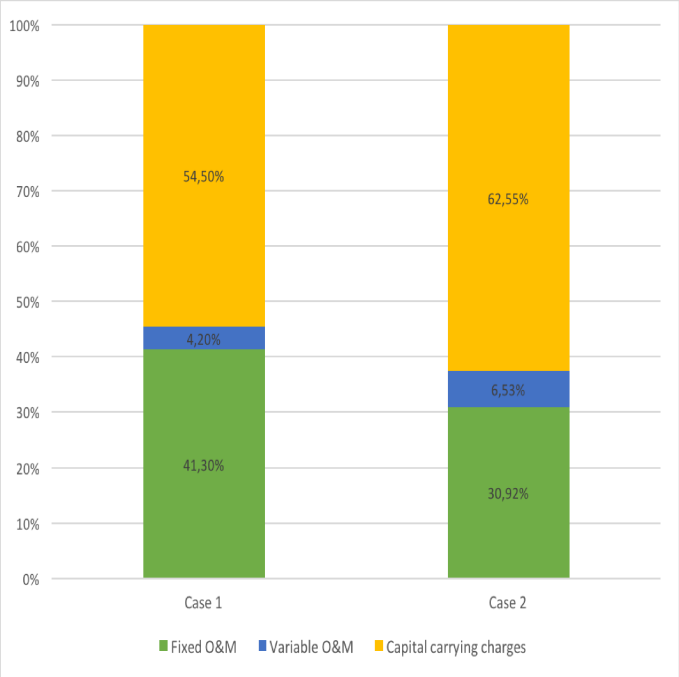

FIGURE 4.9: Cost contribution of capital cost and the operative costs (%) to MSP

TABLE 4.10: MSP comparison

Process	€/MWh	Ref.
Case 1	360	-
Case 2	481	-
HTL	191	[44]
FT fuels	74	[45]

carbon into liquid fuel. One other reason could be the high cost associated to the heat exchanger network. The solution found from aspen energy analyzer tool represents the recommended design and thus the ideal network. Only with through an optimization the process could lead to the production of a competitive product on the market.

The Net Present value of the plant was evaluated knowing the prices of each product in 2016 and their escalation rates from 2000. For both cases the incomes related to the products are lower than the total expenses. A sensitivity analysis was made to understand the amount of income necessary to breakeven. As a result, the incomes related to the process should be 7 times higher than the actual situation for Case 1 and around 9 times for Case 2. Table 4.11 shows a comparison between the current incomes related to the process and the incomes needed to breakeven.

4.5 Conclusions

In conclusion, what emerges from this study is that vinasse has a good potential for the production of hydrogen through the use of supercritical water. However, the production of liquid fuel through the Fischer Tropsch process is limited by the low carbon recovery into fuel (only ~14%). As analyzed, this limit is mainly caused by

TABLE 4.11: Current incomes related to the process vs incomes needed to breakeven

	Current incomes	Incomes needed to breakeven
	€/year	€/year
Case 1	1.332.351	9.425.443
Case 2	1.332.351	12.591.915

the presence of a high sulfur content which affects the solubility of CO_2 in water. One possible solution could be the pretreatment of the biomass before entering the SCWG reactor to remove the sulfur content and thus to reduce to the minimum the synthesis of H_2S. This solution, however, could effect the thermal analysis. The process modeled is thermally self sufficient but the use of external utility to cover the power demand is needed. It was possible to reach this self-sufficiency condition thanks to the presence of a high amount of combustibles which are recovered from the acid gas removal step. Hence, a different method for the sulfur removal could lead to a lower heat recovery and consequently to the need of an external hot utility. At last, the production costs related to this process (in both case 1 and 2) are higher than the costs associated to other processes for conversion of biomass into liquid fuels.

The goal of the future studies is certainly the reduction of the carbon losses and the improvements of the current technologies. The conversion of waste biomass for biofuels production by applying supercritical fluids will play a significant role in industry development because of its sustainability and its environmental-friendly characteristics.

Bibliography

[1] "Monthly Energy Review", *U.S. Energy Information Administration's (EIA)*,

[2] *Statistics Explained*. [Online]. Available: http://ec.europa.eu/eurostat/statistics-explained/index.php/File:Infographic_REN-2004-2015.png(Accessed:2017-08-08).

[3] *2030 Energy Strategy - European Commission*. [Online]. Available: https://ec.europa.eu/energy/en/topics/energy-strategy-and-energy-union/2030-energy-strategy(Accessed:2017-05-23).

[4] S. V. Vassilev, D. Baxter, L. K. Andersen, and C. G. Vassileva, "An overview of the chemical composition of biomass", *Fuel*, no. 5, pp. 913–933,

[5] V. Kirubakaran, V. Sivaramakrishnan, R. Nalini, T. Sekar, P. Subramanian, and M. Premalatha, "A review on gasification of biomass", *ScienceDirect*,

[6] M García-Jarana, J Sánchez-Oneto, J. Portela, and E. Martinez de la Ossa, *Chapter 10 - Supercritical Water Gasification of Organic Wastes for Energy Generation*. Dec. 2014.

[7] *About Sugar | International Sugar Organization*. [Online]. Available: https://www.isosugar.org/sugarsector/sugar(Accessed:2017-10-07).

[8] B. S. Moraes, M. Zaiat, and A. Bonomi, "Anaerobic digestion of vinasse from sugarcane ethanol production in Brazil: Challenges and perspectives", *Renewable and Sustainable Energy Reviews*, pp. 888–903,

[9] *How molasses is made - manufacture, making, history, used, processing, structure, industry, machine, History*. [Online]. Available: http://www.madehow.com/Volume-5/Molasses.html(Accessed:2017-08-06).

[10] C. Baez-Smith, "Anaerobic Digestion of Vinasse for the Production Of Methane in the Sugar Cane Distillery", *2006 SPRI Conference on Sugar Processing*,

[11] Elda I España-Gamboa, Javier O Mijangos-Cortés, Galdy Hernández-Zárate, Jorge A Domínguez Maldonado, and Liliana M Alzate-Gaviria, "Vinasses-Characterization-and-treatments", *Biotechnology for Biofuels*,

[12] A. Robertiello, "Upgrading of agricultural and agro-industrial wastes: The treatment of distillery effluents (vinasses) in Italy", *Agricultural Wastes*, no. 5, pp. 387–395,

[13] V. Anikeev and M. Fan, *Supercritical Fluid Technology for Energy and Environmental Applications*. 2013.

[14] K. Byrappa and Masahiro Yoshimura, "Hydrothermal Technology - Principles and Applications", in *Handbook of Hydrothermal Technology*, 2013th ed., Elsevier.

[15] C. Hognon, F. Delrue, J. Texier, M. Grateau, S. Thiery, H. Miller, and A. Roubaud, "Comparison of pyrolysis and hydrothermal liquefaction of Chlamydomonas reinhardtii. Growth studies on the recovered hydrothermal aqueous phase", *Biomass and Bioenergy*, pp. 23–31,

[16] Mohamed Magdeldin, Thomas Kohl, Cataldo De Blasio, Mika Järvinen, Song Won Park, and Reinaldo Giudici, "The BioSCWG Project: Understanding the Trade-Offs in the Process and Thermal Design of Hydrogen and Synthetic Natural Gas Production", *Energies 2016*,

[17] *Le-Chateler's principle- The effect of change in temperature*. [Online]. Available: http://www.citycollegiate.com/chemical_equilibrium8.htm(Accessed: 2017-08-06).

[18] F. Safari, A. Tavasoli, A. Ataei, and J.-K. Choi, "Hydrogen and syngas production from gasification of lignocellulosic biomass in supercritical water media", *International Journal of Recycling of Organic Waste in Agriculture*, no. 2, pp. 121–125,

[19] *Chemical Process Optimization Software - Chemical Process Design | Aspen Plus*. [Online]. Available: http://www.aspentech.com/products/engineering/aspen-plus/(Accessed:2017-08-05).

[20] M. K. Dowd, S. L. Johansen, L. Cantarella, and P. J. Reilly, "Low Molecular Weight Organic Composition of Ethanol Stillage from Sugarcane Molasses, Citrus Waste, and Sweet Whey", *Journal of Agricultural and Food Chemistry*, no. 2, pp. 283–288,

[21] M. Akram, C. K. Tan, R. Garwood, and S. M. Thai, "Vinasse – A potential biofuel – Cofiring with coal in a fluidised bed combustor", *Fuel*, pp. 1006–1015,

[22] M. J. Dirbeba, A. Brink, N. DeMartini, D. Lindberg, and M. Hupa, "Sugarcane vinasse CO2 gasification and release of ash-forming matters in CO2 and N2 atmospheres", *Bioresource Technology*, pp. 606–614,

[23] C. L.A.B and P. Brossard, "Experiences on vinasse disposal: Part III: combustion of vinasse-# 6 fuel oil emulsions", *Brazilian Journal of Chemical Engineering*, no. 1,

[24] A. Magnano, "Supercritical Water Gasification (SCWG) of Black Liquor: Thermodynamic Analysis and Experimental Tests in a Plug Flow Reactor", PhD thesis, Politecnico di torino, Jul. 2015.

[25] *Phase Diagram for Water | CK-12 Foundation*. [Online]. Available: https://www.ck12.org/book/CK-12-Chemistry-Concepts-Intermediate/section/13.20/(Accessed:2017-08-06).

[26] *NIST Chemistry WebBook*. [Online]. Available: http://webbook.nist.gov/chemistry/(Accessed:2017-08-06).

[27] O. Yakaboylu, J. Harinck, G. K. Smit, and W. de Jong, "Supercritical Water Gasification of Biomass: A Literature and Technology Overview", *Energies*, vol. 8, no. 2, 2015.

[28] L.-P. D, J. M. Prado, T.-M. P, T. Forster-Carneiro, M. A. A. Meireles, L.-P. D, J. M. Prado, T.-M. P, T. Forster-Carneiro, and M. A. A. Meireles, "Supercritical Water Gasification of Biomass for Hydrogen Production: Variable of the Process", en, *Food and Public Health*, no. 3, pp. 92–101,

[29] J. Louw, C. E. Schwarz, J. H. Knoetze, and A. J. Burger, "Thermodynamic modelling of supercritical water gasification: Investigating the effect of biomass composition to aid in the selection of appropriate feedstock material", *Bioresource Technology*, pp. 11–23,

[30] E. Gasafi, M.-Y. Reinecke, A. Kruse, and L. Schebek, "Economic analysis of sewage sludge gasification in supercritical water for hydrogen production", *Biomass and Bioenergy*, no. 12, pp. 1085–1096,

[31] Y. Lu, L. Guo, X. Zhang, and Q. Yan, "Thermodynamic modeling and analysis of biomass gasification for hydrogen production in supercritical water", *Chemical Engineering Journal*, 2007.

[32] M. Aziz, "Integrated supercritical water gasification and a combined cycle for microalgal utilization", *Energy Conversion and Management*, 2015.

[33] E. Gasafi, L. Meyer, and L. Schebek, "Exergetic efficiency and options for improving sewage sludge gasification in supercritical water", en, *International Journal of Energy Research*, no. 4, pp. 346–363,

[34] Y. Calzavara, C. Joussot-Dubien, G. Boissonnet, and S. Sarrade, "Evaluation of biomass gasification in supercritical water process for hydrogen production", *Energy Conversion and Management*, no. 4, pp. 615–631,

[35] R. M. Swanson, A. Platon, J. A. Satrio, and R. C. Brown, "Techno-economic analysis of biomass-to-liquids production based on gasification", *Techno-economic Comparison of Biomass-to-Biofuels Pathways*, S11–S19,

[36] *Selecting-Amines-for-Sweetening-Units.pdf*, 2006. [Online]. Available: `https://bre.com/PDF/Selecting-Amines-for-Sweetening-Units.pdf(Accessed: 2017-05-24)`.

[37] S. Saeidi, M. K. Nikoo, A. Mirvakili, S. Bahrani, N. A. S. Amin, and M. R. Rahimpour, "Recent advances in reactors for low-temperature Fischer-Tropsch synthesis: Process intensification perspective", *Reviews in Chemical Engineering*,

[38] M. Pondini and M. Ebert, "Process synthesis and design of low temperature Fischer-Tropsch crude production from biomass derived syngas", PhD thesis, Master's thesis, Chalmers University of Technology, Göteborg, Sweden.

[39] L. P. Dancuart and A. P. Steynberg, "Fischer-Tropsch Based GTL Technology: A New Process?", *Studies in Surface Science and Catalysis*, Fischer-Tropsch Synthesis, Catalyst and Catalysis, pp. 379–399,

[40] S. Saeidi, S. Najari, F. Fazlollahi, M. K. Nikoo, F. Sefidkon, J. J. Klemeš, and L. L. Baxter, "Mechanisms and kinetics of CO2 hydrogenation to value-added products: A detailed review on current status and future trends", *Renewable and Sustainable Energy Reviews*, pp. 1292–1311,

[41] M. D. Porosoff, B. Yan, and J. G. Chen, "Catalytic reduction of CO_2 by H_2 for synthesis of CO, methanol and hydrocarbons: Challenges and opportunities", en, *Energy Environ. Sci.*, no. 1, pp. 62–73,

[42] P. T. Juma Haydary, "Steady-state and dynamic simulation of crude oil distillation using ASPEN Plus and ASPEN dynamics", *2009*,

[43] D. R. A. Mahfud, "Modeling of a Fluid Catalytic Cracking (FCC) Riser Reactor", *Department of Chemical Engineering- Sabrattah Zawia University*,

[44] M. Magdeldin, T. Kohl, and M. Järvinen, "Techno-economic assessment of the by-products contribution from non-catalytic hydrothermal liquefaction of lignocellulose residues", *Energy*,

[45] K. S. Ng and J. Sadhukhan, "Techno-economic performance analysis of bio-oil based Fischer-Tropsch and CHP synthesis platform", *Biomass and Bioenergy*, no. 7, pp. 3218–3234,

[46] M. K. Hrncic, G. Kravanja, and Z. Knez, "Hydrothermal treatment of biomass for energy and chemicals hydrothermal treatment of biomass for energy and chemicals", *Energy*, 2016.

[47] F. Trippe, M. Fröhling, F. Schultmann, R. Stahl, E. Henrich, and A. Dalai, "Comprehensive techno-economic assessment of dimethyl ether (DME) synthesis and fischer–tropsch synthesis as alternative process steps within biomass-to-liquid production", *Fuel Processing Technology*, pp. 577–586, Supplement C Feb. 1, 2013.

[48] J. C. Meerman, M Knoope, A Ramírez, W. C. Turkenburg, and A. P. C. Faaij, "The techno-economic potential of integrated gasification co-generation facilities with ccs", *Energy Procedia*, 2013.

[49] *Benefits of Multi-Solvent NRTL Models in Aspen Plus | Solution | Aqueous Solution*. [Online]. Available: https://www.scribd.com/document/257172217/Benefits-of-Multi-Solvent-NRTL-Models-in-Aspen-Plus(Accessed: 2017-08-19).

[50] *Green Fuels Technology - Biofuels Author= | Carlos Ricardo Soccol |*.

[51] "Aspen Physical Property System", Tech. Rep., Feb. 2012. [Online]. Available: http://www.diquima.upm.es/documentos/AspenPhysPropModelsV732-Ref.pdf.

[52] Andrea Mary Siefers, "A novel and cost-effective hydrogen sulfide removal technology using tire derived rubber particles", PhD thesis, Iowa State University.

[53] *Amine Scrubbing Process | Global CCS Institute*. [Online]. Available: https://hub.globalccsinstitute.com/publications/final-report-project-pioneer/amine-scrubbing-process(Accessed:2017-05-24).

[54] Robert N. Maddox, Gilbert J. Mains, and Mahmud A. Rahman, "Reactions of Carbon Dioxide and Hydrogen Sulfide with Some Alkanolamines", *Oklahoma State University*,

[55] Zare Aliabad, H. and Mirzaei, S., "Removal of CO2 and H2s using Aqueous Alkanolamine Solusions", *International Journal of Chemical, Molecular, Nuclear, Materials and Metallurgical Engineering*,

[56] Karim H. Hassan, Zuhair A-A Khammas, and Ameel. M. Rahman, "Zinc Oxide Hydrogen Sulfide Removal Catalyst/ Preparation, Activity Test and Kinetic Study", *Al-Khwarizmi Engineering Journal*,

[57] McKinsey Zicarai, S., "Removal of hydrogen sulfide from biogas using cow-manure compost", *Thesis Presented to the Faculty of the Graduate School of Cornell University*,

[58] *LO-CAT®: A Flexible Hydrogen Sulfide Removal Process*. [Online]. Available: http://www.merichem.com/LO-CAT-Flexible-H2S-Removal-Process(Accessed: 2017-06-25).

[59] P. M. Maitlis and A. d. Klerk, *Greener Fischer-Tropsch Processes for Fuels and Feedstocks*, en. John Wiley & Sons, Jan. 2013.

[60] "Hydrogen Recovery by Pressure Swing Adsorption", Linde Group, Tech. Rep.

[61] B. Fredric, H. Christian, P. Tobias, and T. Daniel, "Biogas upgrading - Review of commercial technologies", Lund University, Tech. Rep.

[62] Y. A. Daza and J. N. Kuhn, "CO $_2$ conversion by reverse water gas shift catalysis: Comparison of catalysts, mechanisms and their consequences for CO $_2$ conversion to liquid fuels", en, *RSC Adv.*, no. 55, pp. 49 675–49 691,

[63] *Ftsynthesis | netl.doe.gov*. [Online]. Available: `https://www.netl.doe.gov/research/coal/energy-systems/gasification/gasifipedia/ftsynthesis(Accessed:2017-05-23)`.

[64] G. Jiménez-García and R. Maya-Yescas, "Differences between Fisher–Tropsch synthesis of either gasoline or diesel based on changes of entropy and free energy", *International-Mexican Congress on Chemical Reaction Engineering (IMCCRE 2014). Part 2*, pp. 184–190,

[65] Johanna Kihlman, "Catalytic upgrading of biomass gasification gas", Tech. Rep., Apr. 2017.

[66] J. A. Moulijn, M. Makkee, and A. E. v. Diepen, *Chemical Process Technology*. 2001.

[67] I. Chorkendorff and J. W. Niemantsverdriet, *Concepts of Modern Catalysis and Kinetics*. 2003.

[68] Hessam Jahangiri, James Bennett, Parvin Mahjoubi, Karen Wilson, and Sai Gu, "A review of advanced catalyst development for Fischer–Tropsch synthesis of hydrocarbons from biomass derived syn-gas", *Catalysis Science & Technology*,

[69] T. Olewski, B. Todic, L. Nowicki, N. Nikacevic, and D. B. Bukur, "Hydrocarbon selectivity models for iron-based Fischer–Tropsch catalyst", *Chemical Engineering Research and Design*, pp. 1–11,

[70] *NPTEL PHASE -II :Petroleum Refinery Engineering*. [Online]. Available: `http://nptel.ac.in/courses/103102022/evaluation\%20of\%20crude\%20oil/Crude\%20Assay\%20ASTM\%20TBP\%20distillations\%20evaluation\%20of\%20crude\%20oil\%20properties.html(Accessed:2017-08-08)`.

[71] W. R., *Petroleum Refinery Distillation*. 1979.

[72] J. A. Souza, J. V. C. Vargas, J. C. Ordonez, W. P. Martignoni, and O. F. von Meien, "Thermodynamic optimization of fluidized catalytic cracking (FCC) units", *International Journal of Heat and Mass Transfer*, no. 5, pp. 1187–1197,

[73] B. Adrian, T. George, and M. Michael, *Thermal Design & Optimization*. 1996.

[74] A. Giaconia, L. Turchetti, A. Ienna, D. Mazzei, B. Schiavo, O. Scialdone, G. Caputo, and A. Galia, "Conceptual Study of the Coupling of a Biorefinery Process for Hydrothermal Liquefaction of Microalgae with a Concentrating Solar Power Plant", ENEA-Casaccia Research Center, Tech. Rep.

[75] Y. Jiang and D. Bhattacharyya, "Techno-Economic Analysis of a Novel Indirect Coal–Biomass to Liquids Plant Integrated with a Combined Cycle Plant and CO2 Capture and Storage", *Industrial & Engineering Chemistry Research*, no. 6, pp. 1677–1689,

[76] F. G. Albrecht, D. H. König, N. Baucks, and R.-U. Dietrich, "A standardized methodology for the techno-economic evaluation of alternative fuels – A case study", Apr. 2017.

[77] S. A. El-Temtamy and T. S. Gendy, "Economic evaluation and sensitivity analysis of some fuel oil upgrading processes", *Egyptian Journal of Petroleum*, no. 4, pp. 397–407,

[78] I. V.Ion, G. Ciocea, and F. Popescu, "Waste heat recovery technologies from heating boiler flue gas", "DUNAREA DE JOS" UNIV ERSITY OF GALATI, Tech. Rep.

[79] "Energy in Finland", Statistics Finland, Tech. Rep.

[80] *IATA - Price Analysis*. [Online]. Available: http://www.iata.org/publications/economics/fuel-monitor/Pages/price-analysis.aspx(Accessed: 2017-09-06).

[81] *LPG prices around the world, 04-Sep-2017 | GlobalPetrolPrices.com*. [Online]. Available: http://www.globalpetrolprices.com/lpg_prices/(Accessed: 2017-09-06).

[82] M. Magdeldin, T. Kohl, and M. Järvinen, "Techno-economic Assessment of Integrated Hydrothermal Liquefaction and Combined Heat and Power Production from Lignocellulose Residues", *Journal of Sustainable Development of Energy, Water and Environment Systems*,

[83] Y. Zhu, S. Tjokro Rahardjo, C Valkenburg, L. J. Snowden-Swan, S. Jones, and M. Machinal, "Techno-economic analysis for the thermochemical conversion of biomass to liquid fuels", U.S. Department of Energy, Tech. Rep., 2011.

[84] *Lightnin Store - A310 Impellers*. [Online]. Available: http://store.lightninmixers.com/catalog/parts/impellers/a310?page=7(Accessed:2017-08-05).

[85] E. L. Paul, V. Atiemo-Obeng, and S. M. Kresta, *Handbook of Industrial Mixing: Science and Practice*. 2003.

[86] E. C. Tan, M. Talmadge, A. Dutta, J. Hensley, L. J. Snowden-Swan, D. Humbird, J. Schaidle, and M. Biddy, "Conceptual process design and economics for the production of high-octane gasoline blendstock via indirect liquefaction of biomass through methanol/dimethyl ether intermediates", *Biofuels, Bioprod. Bioref.*, no. 1, pp. 17–35, Jan. 1, 2016.

[87] N. Inc., "Equipment design and cost estimation for small modular biomass systems, synthesis gas cleanup, and oxygen separation equipment, task 1: Cost estimates of small modular systems", National Renewable Energy Laboratory, Tech. Rep., 2006.

Appendix A

Agitated tank

For the solid-liquid mixing system some simplified calculation can be carried out. At first the type of impeller has to be chosen for example the LIGHTNIN A310 (dimensions selected by catalog [84]). Based on that and on the physical properties of the feedstock, the diameter and the rotation speed can be evaluated through equations given from the literature [85].

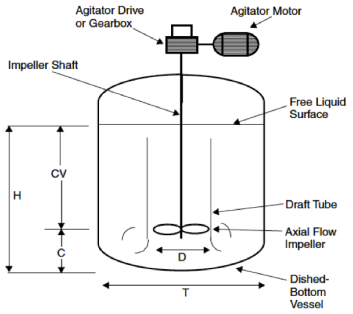

FIGURE A.1: Mixer design [85]

Therefore it is possible to evaluate the dimensions of the tank with equations A.1, A.2 and A.3.

$$T = 2,4 * D \tag{A.1}$$

$$C = \frac{T}{4} \tag{A.2}$$

$$H = T * 1,3 \tag{A.3}$$

The rps required for a solid-liquid mixing can be evaluated through equation A.4 [85].

$$N_{js} = Sv^{0,1}[\frac{g_c(\rho_s - \rho_l)}{\rho_l}]^{0,45} X^{0,13} d_p^{0,2} D^{-0,85} \tag{A.4}$$

In equation A.4, D is the impeller diameter, d_p is the mass-mean particle diameter, X is the mass ratio of suspended solids to liquid x 100 (kg solid/kg liquid) and S the dimensionless number which is a function of impeller type (6,9 for the impeller selected). v is the kinematic viscosity of the liquid (m^2/s); g_c is the gravitational acceleration constant; ρ_s and ρ_l the density of the solid and the density of liquid (kg/m^3) [85].

Appendix B

Plant Flowsheet and equipment table

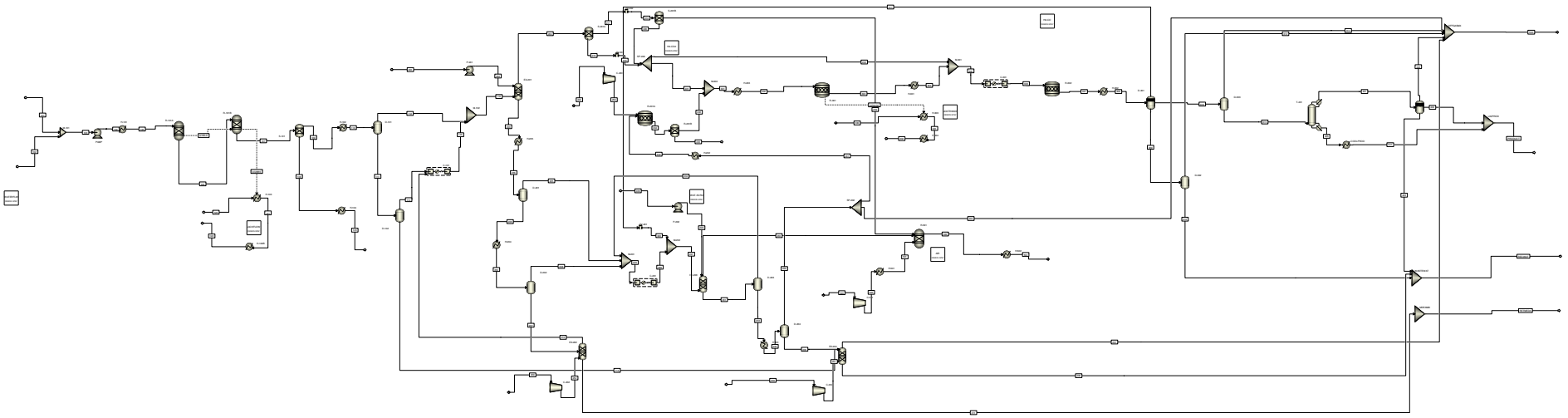

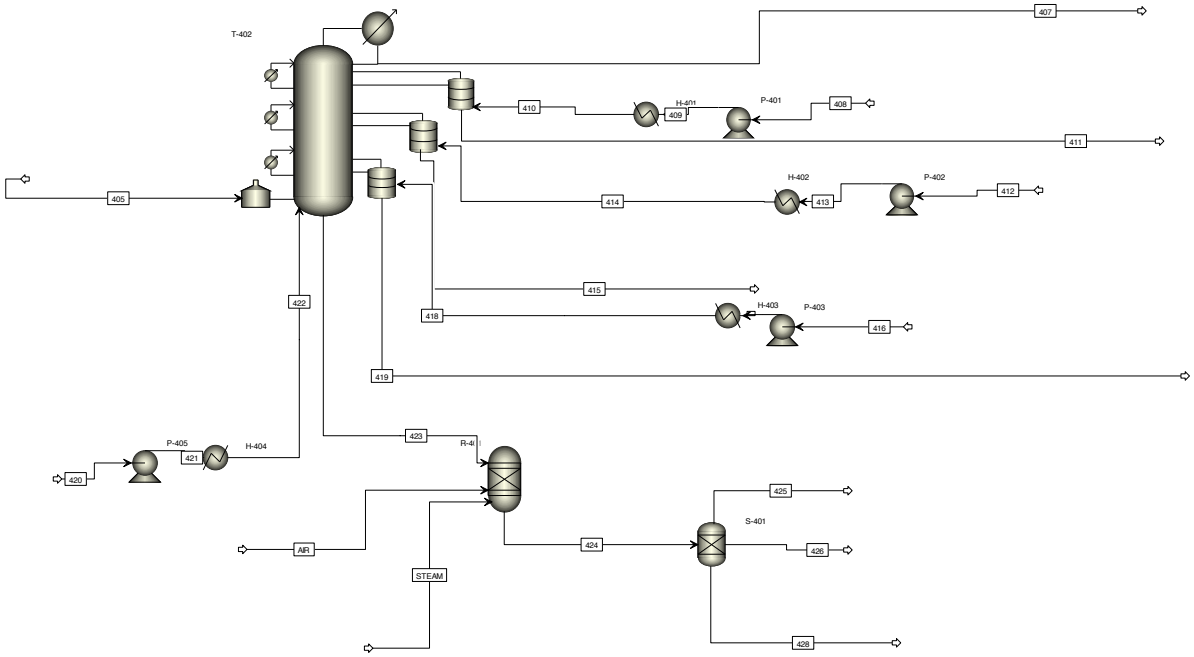
T-402
407
410
H-401
409
P-401
408
411
405
414
H-402
413
P-402
412
415
422
418
H-403
P-403
416
419
423
P-405
421
H-404
420
R-401
425
S-401
AIR
424
426
STEAM
428

TABLE B.1: Plant equipments (Unit 1-2)

Unit 1	
M-101	Feedstock mixer
PUMP	Pump
H-101	Feedstock preheater
R-101A/B	SCWG reactor
H-103A/B	SCWG reactor heating jacket
S-101	Solid separator
H-104	Solid cooler
H-102	Syngas cooler
D-101	Flash for water removal
D-102	Flash for water purification
M-102	Mixer
Unit 2	
P-201	Pump
P-202	Pump
EX-201	MDEA adsorber
D-201	Flash
D-202	Flash
D-203	Flash
D-204	Flash
H-201	Heater
H-202	Cooler
H-203	Heater
H-204	Heater
H-205	Cooler
EX-202	Gas desorber
EX-203	Gas desorber
EX-204	Gas desorber
C-201	Compressor
C-202	Compressor
C-203	Compressor
C-204	Compressor
M-201	Mixer
M-202	Mixer
M-203	Mixer
TV-201	Trottling valve
TV-202	Trottling valve
TV-203	Trottling valve
SP-201	Split
SP-202	Split
SP-203	Split
R-201A/B	LO-CAT reactor
S-101A/B	PSA system

TABLE B.2: Plant equipments (Unit 3-5)

Unit 3	
R-301	RWGS reactor
R-302	FT reactor
H-301	Cooler
H-302	Cooler
H-303/H-304	RWGS reactor heating jacket
C-301	Compressor
M-301	Mixer
D-301	Flash for FT-crude separation
D-302	Flash
D-303	Flash
Unit 4	
T-401	Distillation column for Light naphta separation
T-402	Fractionation column
D-304	Flash
P-401	Pump
P-402	Pump
P-403	Pump
P-404	Pump
P-405	Pump
H-401	Heater
H-402	Heater
H-403	Heater
H-404	Heater
R-401	FCC reactor
S-401	Product separator
Unit 5	
C-501	Compressor
H-501	Heater
H-502	Cooler
R-501	Boiler

Appendix C

Amine scrubbing stages evaluation

This process block was at first modeled on excel in order to find the ideal number of stages for the acid gas removal and subsequently implemented o Aspen Plus.

The first assumption made is:

- H_2S removal: 99%
- CO_2 removal: 90%
- Removal of 0.4 mol of Acid gas per mol of amine
- Solvent at 30% of MDEA

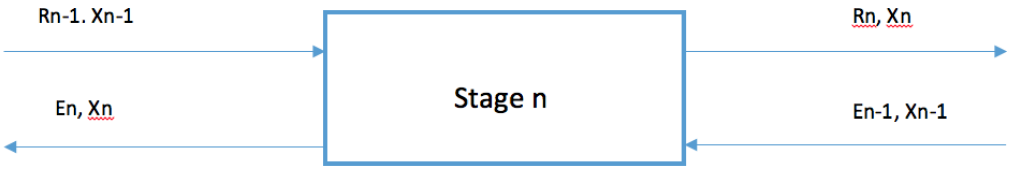

FIGURE C.1: Schematic representation of stage n of amine scrubbing

The calculation was iterative by assuming a certain amount of solvent and verifying the content of acid gas after each stage.

Stage 1			R1	R2	E1	En	w/w
SOLVENT	kg/h	0		3841,679191	88231,7558	84390,0766	0,96
CO2	kg/h	3963,234		162,3760373	-233,9474	3566,9106	0,0405
H2S	kg/h	42,74777		1,926541517	1,4991	42,3203	0,0005
Flow rate	**kg/h**	**4005,98177**		**4005,98177**	**87999,30754**	**87999,30754**	
					Extraction NOT verified		
Stage 2			R2	R3	E2	E1	w/w
SOLVENT	kg/h	3841,679191	4016,563486		88406,6401	88231,7558	1,00
CO2	kg/h	162,3760373	-10,6499573		-406,9734	-233,9474	-0,0027
H2S	kg/h	1,926541517	0,0682417		-0,3592	1,4991	1,70E-05
Flow rate	**kg/h**	**4005,98177**	**4005,98177**		**87999,30754**	**87999,30754**	
					Extraction NOT verified		
Stage 3			R3	R4	E3	E2	w/w
			0				
SOLVENT	kg/h	4016,563486	4024,524722		88414,6014	88406,64013	1,00
CO2	kg/h	-10,64995733	-18,5265986		-414,8500	-406,9733573	-0,0046
H2S	kg/h	0,0682417	-0,01635346		-0,4438	-0,3592	-4,08E-06
Flow rate	**kg/h**	**4005,98177**	**4005,98177**		**87999,30754**	**87999,30754**	
					Extraction verified		
Stage 4			R4	R5	E4	E3	w/w
SOLVENT	kg/h	4024,524722	4024,88714		88414,9638	88414,60137	1,00
CO2	kg/h	-18,52659863	-18,885166		-415,2086	-414,8499986	-0,0047
H2S	kg/h	-0,016353457	-0,02020447		-0,4477	-0,4438	-5,04E-06
Flow rate	**kg/h**	**4005,98177**	**4005,98177**		**87999,30754**	**87999,30754**	
					Extraction verified		

FIGURE C.2: Schematic representation of stage n of amine scrubbing

Appendix D

Calculations for the FT reactor

For the FT reactions usually the reactor works with a temperature range between 200 and $400°$C. It was though evaluated the value and it was selected the optimal temperature in order to have a chain growth factor of 0,82 which is the most suitable for a diesel fuel production as illustrated in the table 3.9.

TABLE D.1: alpha values with temperature

Temperature [C]	α [-]
200	0,88
210	0,85
220	**0,82**
240	0,77
260	0,71
280	0,65
300	0,60
320	0,54
340	0,49
360	0,43
380	0,38
400	0,32

The main assumption made in this calculation are shown in table D.2

TABLE D.2: Main assumptions for FT conversions calculation

H_2/CO	-	2
α	-	0.82
P	bar	15
T	°C	220
c	-	0.25
CO conversion	-	0.72

The conversions of CO into paraffins and olefins were evaluated with some equations. It is first possible to determine the molar (M_n) and mass (W_n) distribution (illustrated in D.1 and D.2) with equations D.1 and D.2.

$$M_n = \alpha^{n-1}(1-\alpha) \tag{D.1}$$

TABLE D.3: Hydrocarbon selectivities on a Fe-based catalyst at 220°C and 15 bar and 72% conversion of CO [69]

S_{C5+}	67,5%
S_{C2-4}	25,2%
S_{C1}	7,3%

$$W_n = \alpha^{n-1}(1-\alpha)^2 n \tag{D.2}$$

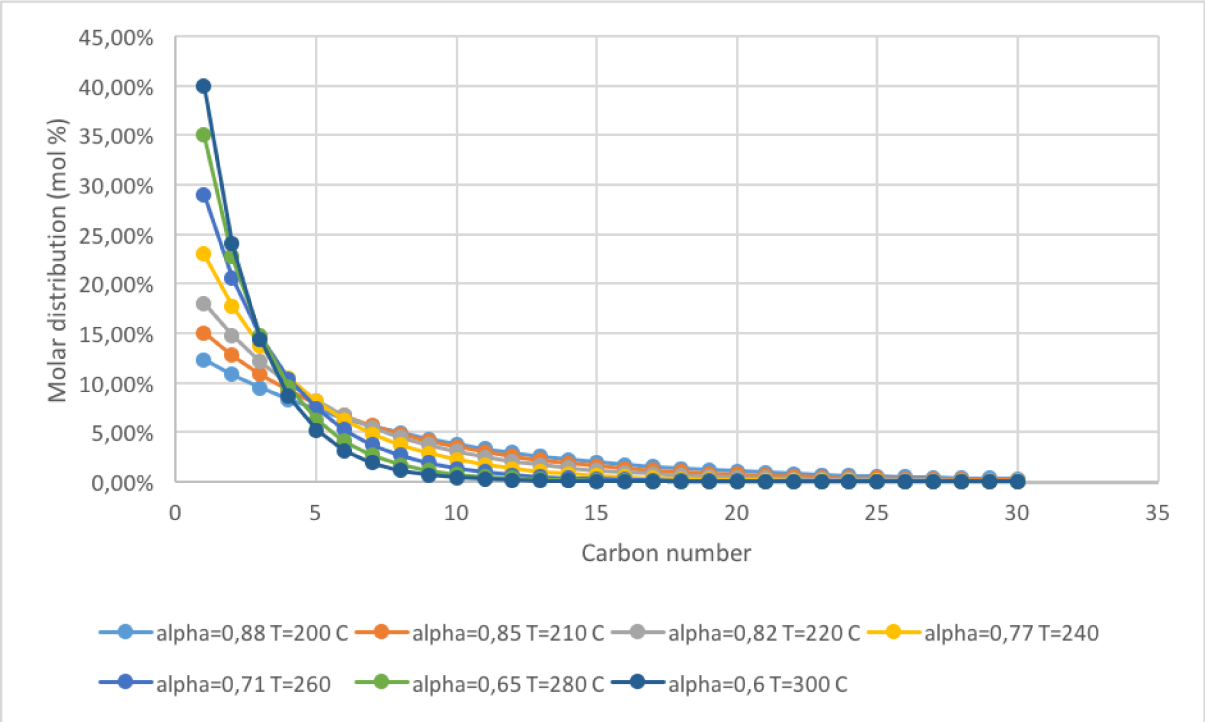

FIGURE D.1: Molar distribution (mol%) of hydrocarbon at different FT working conditions

In the graphs (D.1 and D.2), it is shown that for higher temperatures, and thus lower values of the chain growth factor, short chain hydrocarbons are mainly obtained while at lower temperature the greater amount of long-chained hydrocarbons is produced. It is possible to evaluate the Olefin to Paraffin ratio (O/P) for each carbon numbers. This parameter depend on the carbon number and on a constant value (c) which varies between 0,19 and 0,49 [38].

$$\frac{O}{P} = e^{-cn} \tag{D.3}$$

The W_n value is thus adjusted based on the effective selectivities of the catalyst illustrated in table D.3.

As first step the selectivity of higher hydrocarbons should be evaluated as

$$\sum_{n=5}^{50} W_n \tag{D.4}$$

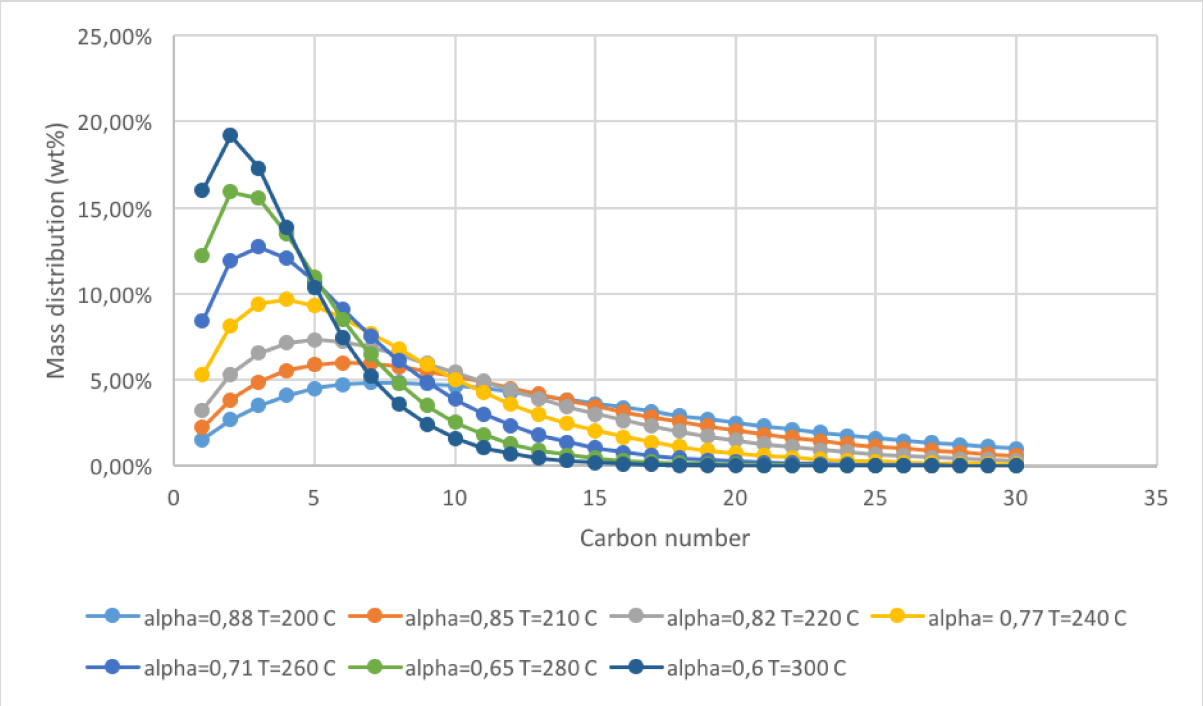

FIGURE D.2: Mass distribution (wt%) of hydrocarbon at different FT working conditions

Consequently the selectivity of C_{1-4} is calculated as $S_{C_{1-4}}$ = 1 - $S_{C_{5+}}$. The weight distribution is thus calculated by rescaling the values.

$$W_n = \frac{S_{Cn}}{\sum_{n=1}^{4} S_{Cn}} S_{C_{1-4}} \tag{D.5}$$

The selectivity is based on the carbon content, so the atom carbon content for each hydrocarbon is relevant: M_{Cn} = 12n

Consequently, the M_{Ctot} can be evaluated as

$$M_{Ctot} = \frac{1}{\sum_n \frac{W_n}{M_{Cn}}} \tag{D.6}$$

Therefore,

$$M_{ncalc} = \frac{W_n}{M_{Ctot}} \tag{D.7}$$

With the Mn_{calc} values, it is possible to calculate the amount of CO converted for each reaction:

$$CO_{conv,n} = \frac{CO_{in}}{\sum_{n=1}^{50} nM_{ncalc}} nM_{ncalc} \tag{D.8}$$

At this point of the calculation, it is possible to determine the percentage of CO converted into olefin and paraffin per each carbon number knowing the O/P ratio. For this calculation it was chosen a medium value for the constant c (c=0,25).

$$\%P = \frac{1}{1 + \frac{O}{P}} \tag{D.9}$$

$$\%O = 1 - \%P \tag{D.10}$$

Therefore, the flow of CO converted in paraffin and olefin are respectively the flow of CO converted times the percentage of olefin and paraffin per each carbon. The conversion value that was inserted in the RSTOIC used for the simulation is therefore the ratio between the amount of CO converted as explained divided by the flow of CO entering the reactor. Figure D.3 shows the main calculation for this block.

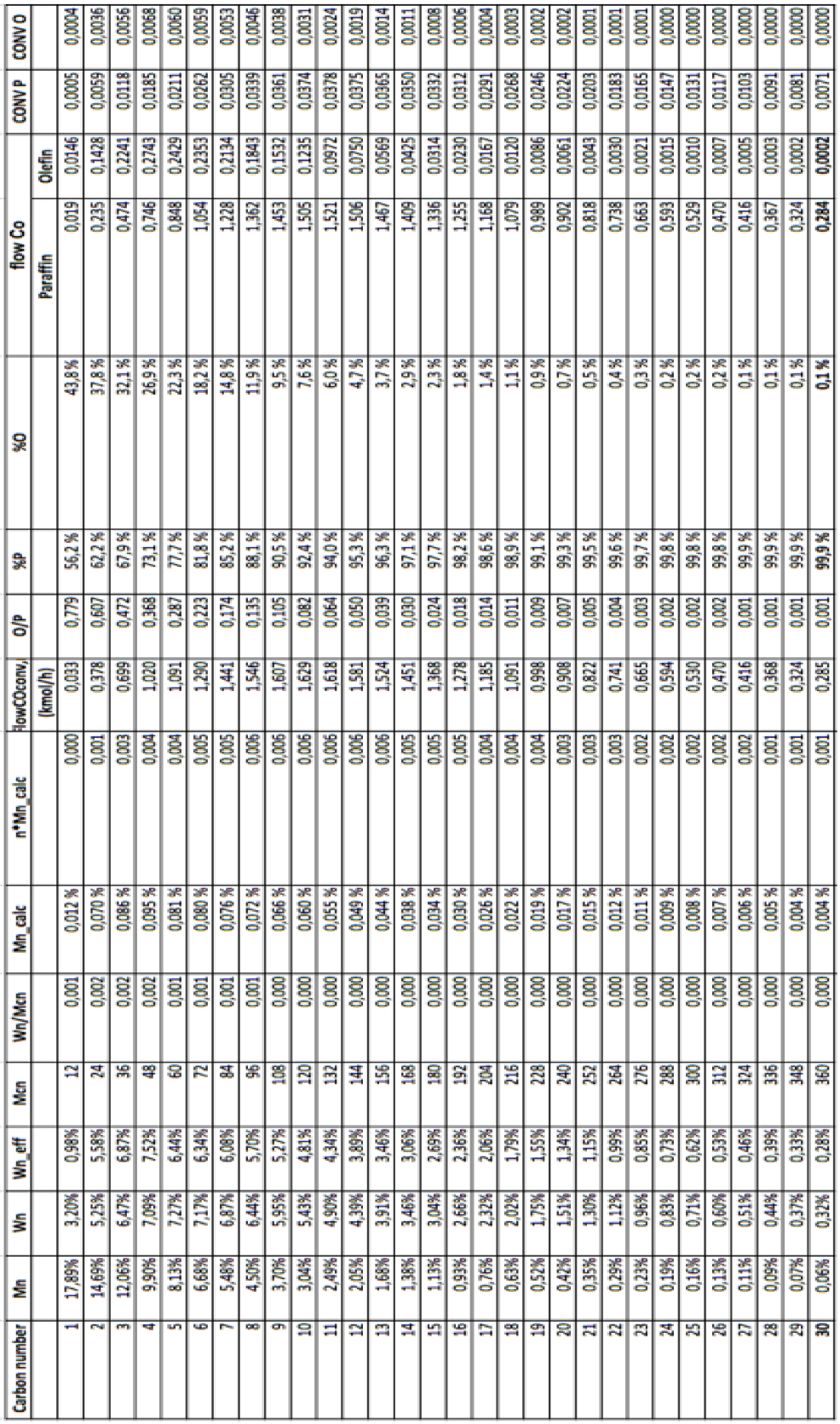

Carbon number	Mn	Wn	Wn_eff	Mcn	Wn/Mcn	Mn_calc	n*Mn_calc	FlowCOconv, (kmol/h)	O/P	%P	%O	flow Co		CONV P	CONV O
												Paraffin	Olefin		
1	17,89%	3,20%	0,98%	12	0,001	0,012 %	0,000	0,033	0,779	56,2 %	43,8 %	0,019	0,0146	0,0005	0,0004
2	14,69%	5,25%	5,58%	24	0,002	0,070 %	0,001	0,378	0,607	62,2 %	37,8 %	0,235	0,1428	0,0059	0,0036
3	12,06%	6,47%	6,87%	36	0,002	0,086 %	0,003	0,699	0,472	67,9 %	32,1 %	0,474	0,2241	0,0118	0,0056
4	9,90%	7,09%	7,52%	48	0,002	0,095 %	0,004	1,020	0,368	73,1 %	26,9 %	0,746	0,2743	0,0185	0,0068
5	8,13%	7,27%	6,44%	60	0,001	0,081 %	0,004	1,091	0,287	77,7 %	22,3 %	0,848	0,2429	0,0211	0,0060
6	6,68%	7,17%	6,34%	72	0,001	0,080 %	0,005	1,290	0,223	81,8 %	18,2 %	1,054	0,2353	0,0262	0,0059
7	5,48%	6,87%	6,08%	84	0,001	0,076 %	0,005	1,441	0,174	85,2 %	14,8 %	1,228	0,2134	0,0305	0,0053
8	4,50%	6,44%	5,70%	96	0,001	0,072 %	0,006	1,546	0,135	88,1 %	11,9 %	1,362	0,1843	0,0339	0,0046
9	3,70%	5,95%	5,27%	108	0,000	0,066 %	0,006	1,607	0,105	90,5 %	9,5 %	1,453	0,1532	0,0361	0,0038
10	3,04%	5,43%	4,81%	120	0,000	0,060 %	0,006	1,629	0,082	92,4 %	7,6 %	1,505	0,1235	0,0374	0,0031
11	2,49%	4,90%	4,34%	132	0,000	0,055 %	0,006	1,618	0,064	94,0 %	6,0 %	1,521	0,0972	0,0378	0,0024
12	2,05%	4,39%	3,89%	144	0,000	0,049 %	0,006	1,581	0,050	95,3 %	4,7 %	1,506	0,0750	0,0375	0,0019
13	1,68%	3,91%	3,46%	156	0,000	0,044 %	0,006	1,524	0,039	96,3 %	3,7 %	1,467	0,0569	0,0365	0,0014
14	1,38%	3,46%	3,06%	168	0,000	0,038 %	0,005	1,451	0,030	97,1 %	2,9 %	1,409	0,0425	0,0350	0,0011
15	1,13%	3,04%	2,69%	180	0,000	0,034 %	0,005	1,368	0,024	97,7 %	2,3 %	1,336	0,0314	0,0332	0,0008
16	0,93%	2,66%	2,36%	192	0,000	0,030 %	0,005	1,278	0,018	98,2 %	1,8 %	1,255	0,0230	0,0312	0,0006
17	0,76%	2,32%	2,06%	204	0,000	0,026 %	0,004	1,185	0,014	98,6 %	1,4 %	1,168	0,0167	0,0291	0,0004
18	0,63%	2,02%	1,79%	216	0,000	0,022 %	0,004	1,091	0,011	98,9 %	1,1 %	1,079	0,0120	0,0268	0,0003
19	0,52%	1,75%	1,55%	228	0,000	0,019 %	0,004	0,998	0,009	99,1 %	0,9 %	0,989	0,0086	0,0246	0,0002
20	0,42%	1,51%	1,34%	240	0,000	0,017 %	0,003	0,908	0,007	99,3 %	0,7 %	0,902	0,0061	0,0224	0,0002
21	0,35%	1,30%	1,15%	252	0,000	0,015 %	0,003	0,822	0,005	99,5 %	0,5 %	0,818	0,0043	0,0203	0,0001
22	0,29%	1,12%	0,99%	264	0,000	0,012 %	0,003	0,741	0,004	99,6 %	0,4 %	0,738	0,0030	0,0183	0,0001
23	0,23%	0,96%	0,85%	276	0,000	0,011 %	0,002	0,665	0,003	99,7 %	0,3 %	0,663	0,0021	0,0165	0,0001
24	0,19%	0,83%	0,73%	288	0,000	0,009 %	0,002	0,594	0,002	99,8 %	0,2 %	0,593	0,0015	0,0147	0,0000
25	0,16%	0,71%	0,62%	300	0,000	0,008 %	0,002	0,530	0,002	99,8 %	0,2 %	0,529	0,0010	0,0131	0,0000
26	0,13%	0,60%	0,53%	312	0,000	0,007 %	0,002	0,470	0,002	99,8 %	0,2 %	0,470	0,0007	0,0117	0,0000
27	0,11%	0,51%	0,46%	324	0,000	0,006 %	0,002	0,416	0,001	99,9 %	0,1 %	0,416	0,0005	0,0103	0,0000
28	0,09%	0,44%	0,39%	336	0,000	0,005 %	0,001	0,368	0,001	99,9 %	0,1 %	0,367	0,0003	0,0091	0,0000
29	0,07%	0,37%	0,33%	348	0,000	0,004 %	0,001	0,324	0,001	99,9 %	0,1 %	0,324	0,0002	0,0081	0,0000
30	0,06%	0,32%	0,28%	360	0,000	0,004 %	0,001	0,285	0,001	99,9 %	0,1 %	0,284	0,0002	0,0071	0,0000

FIGURE D.3: Excel calculations for *CO* conversion into Hydrocarbons in the FT reactor

Appendix E

Heat exchanger networks

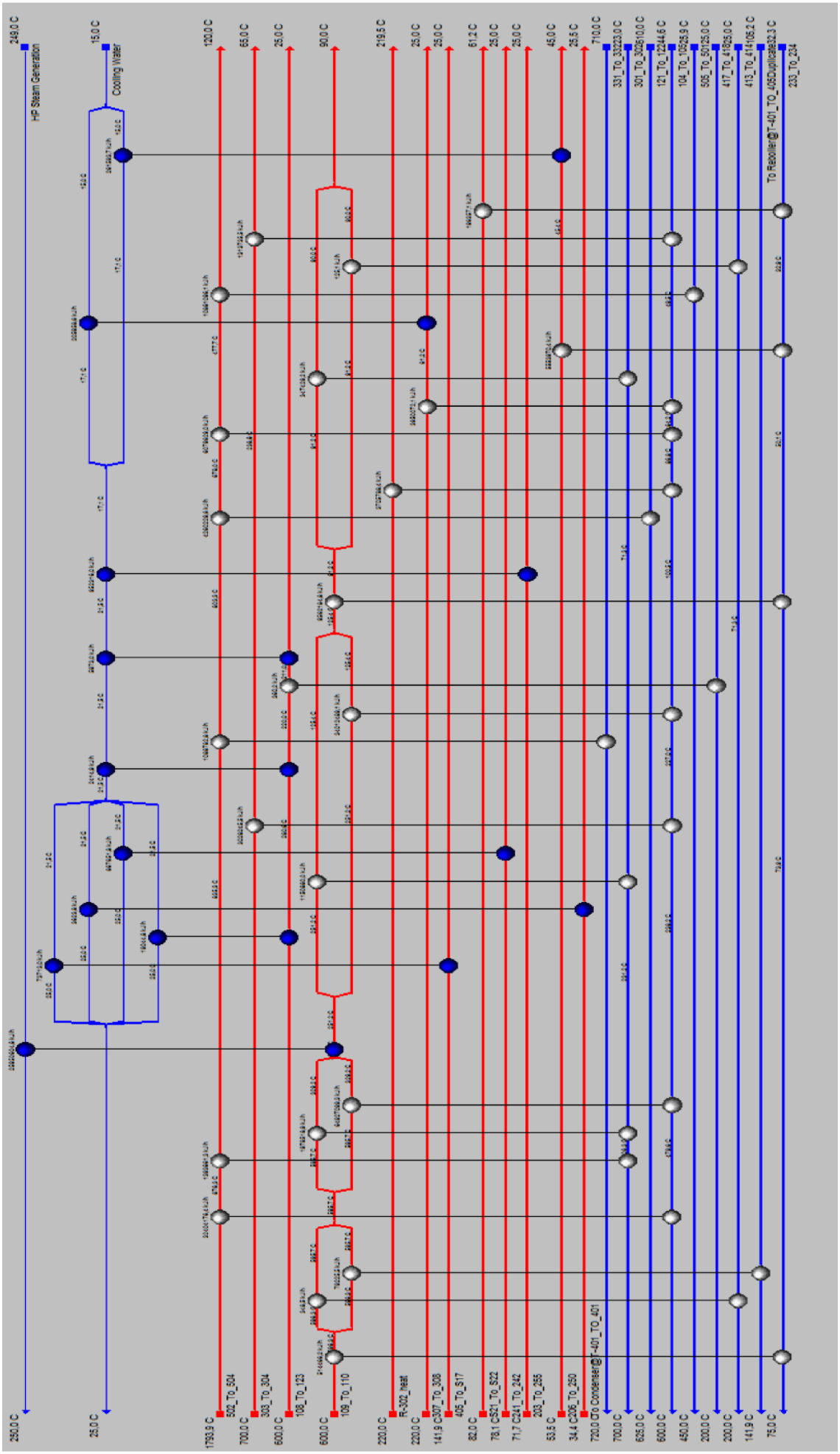

FIGURE E.1: Heat exchanger network-case 1

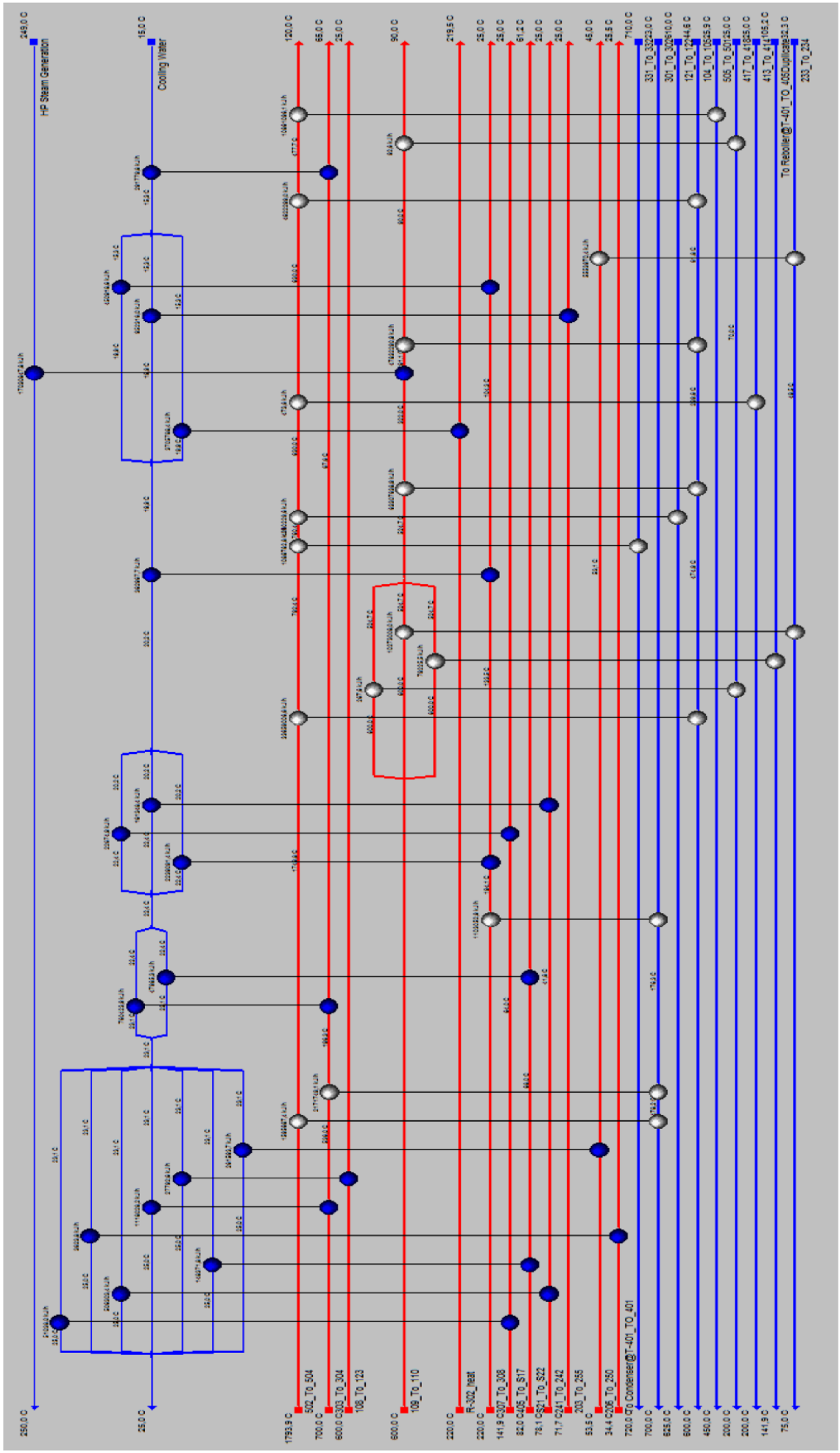

FIGURE E.2: Heat exchanger network-case 2

Appendix F

Calculations of Operative and Maintenance costs

TABLE F.1: Operative and Maintenance costs

Annual Fixed O&M		
Working hours	h/year	8000
Capacity factor		91%
Labor position for operating and maintenance		30
Average labor rate	€/year	36000
Overhead expenses	% of Avg Labor	0.5
Personal insurance	% of Avg Labor	0.3
Cost of Plant Maintenance	1,5%TCI	722 k€
Cost of Property Insurance	1,5%TCI	722 k€
Total	k€/year	3.390
Variable O&M		
	k€/year	Reference
MDEA replacement cost	96	[75]
Make-up water	130	[44]
Electric power	99	[44]
FT catalyst replacement	5	[75]
LOCAT catalyst	22	[86]
RWGS catalyst	40	-
PSA packing replacement	0.006	[35]
FCC catalyst replacement	5	[87]
Total Utilities and Chemicals cost	**4679**	

For the MDEA replacement cost it was assumed 5% of replacing solvent per year due to the recycle. The replacement of the RWGS catalyst was evaluated as 15% of the capital cost associated to the RWGS reactor divided by the working hours per year.